

**London  
South Bank  
University**

EST 1892

# **CFD investigations on Multiphase Flow in Well-Control Operations**

**Ahmed Mostafa Elsayed Mohamed Borg**

<https://orcid.org/0009-0000-0171-3246>

A thesis submitted in partial fulfilment of

the requirements for the award of

Doctor of Philosophy

Lead Supervisor (LSBU): Prof Saurav Goel

Associate Supervisor (LSBU): Dr Elsa Aristodemou and Dr Maria  
Centeno

Associate Supervisor (Egypt): Prof Attia Mahmoud Attia

Academic Year: 2018-2024

School of Engineering

London South Bank University

© LSBU 2024. All rights reserved. No part of this publication may be reproduced without the written permission of the copyright owner.

## **Declaration**

I declare that the thesis has been composed by myself with the fabulous support of my supervisors. The thesis is submitted for examination in consideration for the award of a degree of Doctor of Philosophy at London South Bank University (LSBU). I would like to emphasise that it is my effort and that the work has not to be submitted for any other degree or professional qualification. Furthermore, I took reasonable care to ensure that the work is original and to the best of my knowledge, does not breach copyright law and has not been taken from other sources except where such work has been cited and acknowledged within the text.

## Acknowledgements

At the outset, I'd like to acknowledge that this research work is a unique partnership initiative between two amazing Universities, LSBU in the UK and The British University in Egypt based at Egypt. Through years of efforts and amazing guidance from many individuals, I've been benefitted from the quality of supervision, the resource pool, and timely inputs.

I would like to begin this acknowledgement by thanking **Prof. Saurav Goel** for supervising me and for the opportunity to work in his working group. Through him, I received many interesting insights into High performance computing, computational fluid dynamics and, thanks to his support; I was able to acquire a well-founded knowledge base. He has supported this work in many ways, not least in organizational and human terms.

I would like to thank **Dr. Elsa Aristodemou** for her kind support in completing this work. She was the reason I got accepted at LSBU to begin my research work. I would also like to thank **Dr. Maria Centeno** and **Prof. Attia Mahmoud Attia** as associate supervisors for their outstanding supervision and unlimited support throughout my PhD. Furthermore, I would like to thank all employees of the chair for the good and friendly working atmosphere, which I always appreciated.

My special thanks go to my family, for their love, help, understanding and continuous encouragement; they were always a great support for me and gave me the necessary drive to complete this work

I am indebted to many people who have influenced and inspired me in my research but my thanks, indebtedness is directed first, and always to God for all his graces, without the power he gave me, the accomplishment of this work would have been certainly impossible.

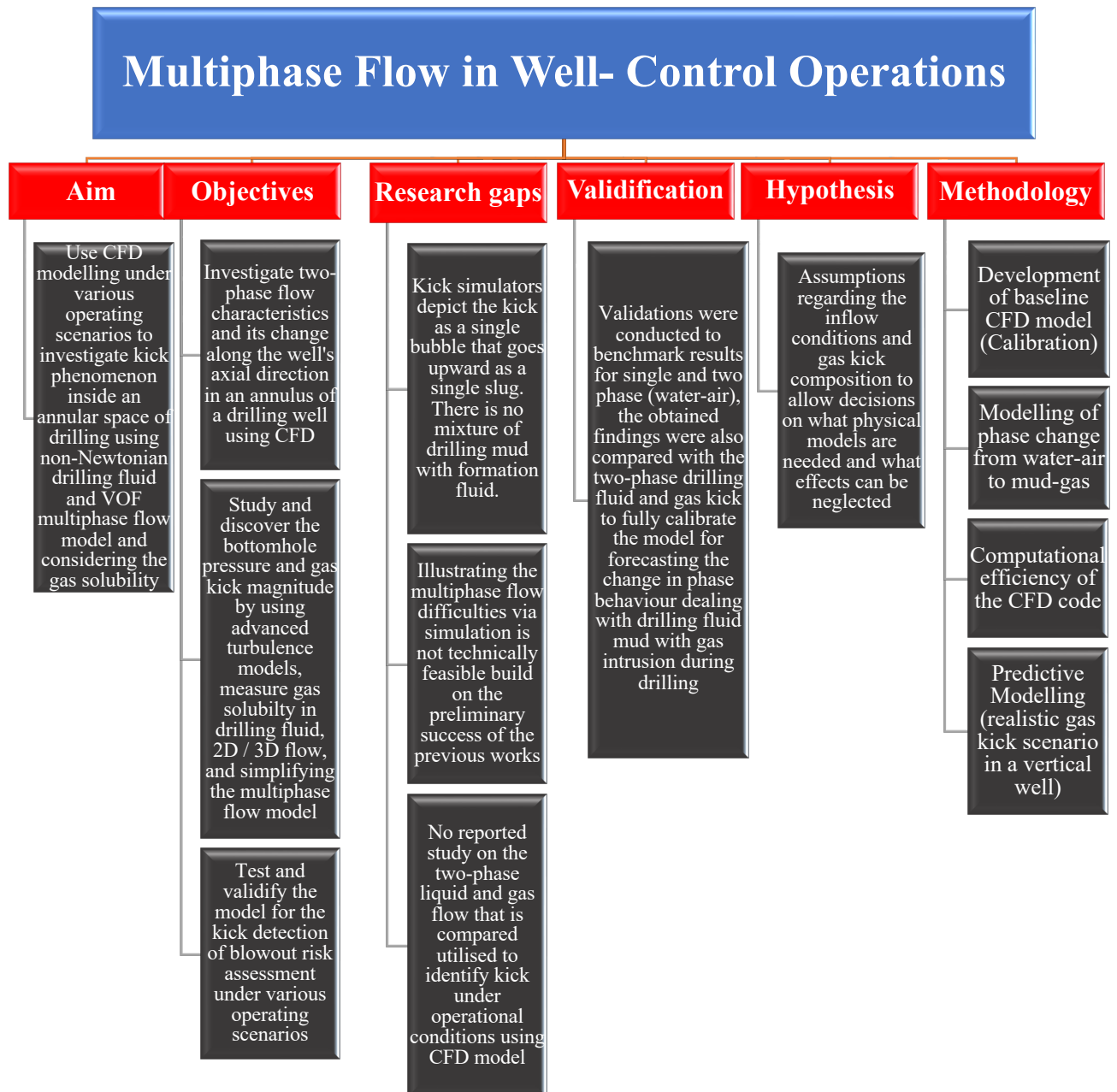
Finally, I would like to express my gratitude to my friends and colleagues who helped me technically and mentally throughout my work period.

## Abstract

Multiphase flow problem encountered during well control involves managing the circulating drilling fluid within the wells and avoiding kicks and blowouts as these can lead to loss of life and damage to the large-scale facilities. BP Deepwater Horizon disaster on April 20, 2010, is an iconic example of how destructive, costly, and deadly blowouts can be with eleven died workers in the explosion. Ninety-four crew members were rescued by lifeboat or helicopter, 17 of whom were treated for injuries. Since the Macondo explosion, kick detection has emerged as a primary concern. Around 172 million gallons of gas-saturated oil leaked during the 87-day rupture, which occurred at a depth of 1522 meters into the Gulf of Mexico. Modern days computational tools and simulation offer great opportunities to perform predictive simulations to improve the extant understanding of the intricacies associated with these problems. As such the current methodologies to model “kick” phenomena are limited by the assumption that only one gas bubble exists in the annulus that gradually rises after shut-in. This assumption over-simplifies the fluid flow models to satisfy the volumetric well control leading to erroneous pressure loss calculations. This thesis provides a comprehensive review of the work carried out in this important direction of research over the past 30 years outlining the progress on simulating multiphase fluid flow for well control operations. It then addresses the issue of multiphase fluid flow by proposing novel way to model this problem using computational fluid dynamics with assist of high-performance computing (HPC) system. Gas kick solubility in drilling fluid was considered in conjunction with the  $k-\epsilon$  realizable turbulence model. Two-dimensional and three-dimensional flow simulations, integrated with a volume of fraction multiphase model, were conducted. These simulations aimed to predict and model both bottomhole pressure and gas kick magnitude. This comprehensive approach reflects a thorough consideration of fluid dynamics and multiphase interactions, providing a more accurate representation of the drilling process.

Flow simulations, incorporating two and three-dimensional models, were conducted to predict bottomhole pressure and gas kick magnitude. New fluid flow models, accounting for fluid miscibility and non-Newtonian properties, aimed at realistic kick treatment. This improved early kick identification, crucial for preventing gas blowouts. Gas ingress scenarios were analysed, focusing on phase interface precision between drilling fluid and gas. Temporal and spatial changes in wellbore flow patterns during gas inrush were discussed, considering rising gas density and solubility effects on flow appearance. The models closely matched experimental results, leading to enhanced understanding of gas kick formation and growth during drilling. The study also highlighted a shift in wellbore composition, with liquid fraction decreasing from 25% to under 9%, and gas void fraction increasing from 75% to over 91%, indicating a transition from liquid to gas dominance.

## Graphical summary of the thesis



## Table of contents

<b>1.</b>	<b>INTRODUCTION .....</b>	<b>2</b>
1.1.	BACKGROUND .....	2
1.2.	RESEARCH MOTIVATION .....	4
1.3.	NEED FOR IMPROVED UNDERSTANDING OF THE MULTIPHASE FLOW SIMULATION: .....	7
1.4.	RESEARCH AIMS AND OBJECTIVES: .....	8
1.5.	CHAPTER PLAN .....	9
<b>2.</b>	<b>THEORETICAL SECTION: THEORETICAL BASIS OF THE MULTIPHASE FLUID FLOWS .....</b>	<b>12</b>
2.1.	RELEVANT PARAMETERS ASSOCIATED WITH MULTIPHASE FLUID FLOW: .....	12
2.2.	FUNDAMENTAL FLUID FLOW EQUATIONS .....	17
2.2.1.	<i>Navier Stokes</i> .....	17
<b>2.3</b>	<b>DIMENSIONLESS NUMBERS .....</b>	<b>20</b>
2.4.	APPROACHES OF MULTIPHASE FLOW MODELLING: .....	25
2.4.1.	<i>Turbulence models</i> .....	28
2.4.2.	<i>Multiphase flow models:</i> .....	31
2.4.3.	<i>Principle of Flow Patterns for Two-Phase Flow (Gas–Liquid)</i> .....	46
2.5.	EARLY KICK DETECTION (EKD) .....	48
<b>3.</b>	<b>MULTIPHASE FLOW MODEL FOR DIFFERENT OPERATION CONDITIONS .....</b>	<b>53</b>
3.1.	TWO PHASES FLOW .....	53
3.2.	THREE PHASES FLOW .....	58
3.3.	MANAGED PRESSURE DRILLING (MPD) .....	60
3.4.	UNDERBALANCE DRILLING (UBD) .....	64
3.5.	GAS KICK SOLUBILITY .....	65
3.6.	EARLY KICK DETECTION (EKD) SIMULATION .....	71
3.7.	SUMMARY OF THE CHAPTER .....	75
<b>4.</b>	<b>MODELLING SIMULATION METHODOLOGY AND VALIDATION.....</b>	<b>81</b>
4.1.	RESEARCH METHODOLOGY .....	81
4.2.	MODELLING APPROACH .....	82
4.3.	SIMULATION TOOL .....	83
4.4.	MODELLING MULTIPHASE FLOWS .....	84
4.4.1.	<i>Modelling Geometry</i> .....	85
4.4.2.	<i>Defining the Simulation Topology</i> .....	86
4.4.3.	<i>Meshing</i> .....	86
4.4.4.	<i>Solver</i> .....	87
4.4.5.	<i>CFD Tools</i> .....	87
4.4.6.	<i>Analysis</i> .....	88
4.4.7.	<i>Volume of Fluid (VOF) Method</i> .....	88
4.5.	MODELLING AND VALIDATION CASES .....	89
4.5.1.	<i>Validation procedure and experimental data acquisition</i> .....	89
4.6.	DEVELOPMENT OF CFD MODEL TO MIMIC THE EXPERIMENTAL DATASETS .....	93
4.6.1.	<i>CFD model of Single phase in a pipe and annulus</i> .....	94
4.6.2.	<i>CFD model of two-phase (gas–liquid) flow through pipeline</i> .....	94
<b>5.</b>	<b>MODELLING A GAS KICK-DRILLING FLUID MODEL FOR CALIBRATION PURPOSES .....</b>	<b>98</b>

5.1.	PROBLEM DEFINITION .....	98
5.2.	DEVELOPMENT OF THE BASELINE CFD MODEL .....	98
5.2.1.	<i>Predictive modelling and simulation of drilling fluids with gas kick .....</i>	98
5.2.2.	<i>Baseline CFD model of two-phase (gas–liquid) flow through pipeline .....</i>	99
5.2.3.	<i>Investigating two-phase flow (Mud / Gas) and understanding gas-kick dynamics .....</i>	101
5.2.4.	<i>Sensitivity analysis .....</i>	102
5.2.5.	<i>Model Geometry .....</i>	103
5.3.	MODELLING OF PHASE CHANGE FROM WATER-AIR TO MUD-GAS .....	104
5.4.	COMPUTATIONAL EFFICIENCY USING PARALLEL PROCESSING ARCHITECTURE .....	105
<b>6.</b>	<b>PREDICTIVE MODELLING OF REALISTIC GAS KICK IN A VERTICAL WELL.....</b>	<b>109</b>
6.1.	PROBLEM DEFINITION .....	109
6.2.	CFD ASSUMPTIONS FOR COMPLEX FLOW GEOMETRIES .....	109
6.3.	MODEL SETUP SIMULATION OF GAS-KICK SCENARIOS .....	111
6.3.1.	<i>Model Geometry Setup &amp; Representation of the Drill Bit.....</i>	111
6.3.2.	<i>Boundary Condition &amp; Kick-Gas Inlet Condition &amp; position .....</i>	113
6.3.3.	<i>Multiphase fluid flow physics model .....</i>	117
6.3.4.	<i>Turbulence Modelling &amp; Grid Considerations .....</i>	119
6.3.5.	<i>Pressure condition for a realistic gas kick scenario .....</i>	121
6.3.6.	<i>Mud Circulation and influence of rotation .....</i>	123
6.4.	MODELLING OF GAS DISSOLUTION .....	125
6.5.	LOCATION OF KICK ENTRANCE SENSITIVITY ANALYSIS .....	129
6.5.1.	<i>Lateral kick .....</i>	130
6.5.2.	<i>Bottom-Hole Kick Scenario – Multiple Fractures .....</i>	132
6.6.	THREE-DIMENSION MODELLING .....	135
6.7.	TURBULENCE MODELS SENSITIVITY ANALYSIS .....	138
<b>7.</b>	<b>RESULTS AND DISCUSSION.....</b>	<b>144</b>
7.1.	TWO-PHASE FLOW ANALYSIS .....	144
7.1.1.	VELOCITY DATA .....	145
7.1.2.	VOID FRACTION .....	148
7.2.	ANALYSIS OF DYNAMIC BEHAVIOUR OF TWO-PHASE FLOW PATTERNS IN VERTICAL WELLBORES .....	149
<b>8.</b>	<b>CONCLUSION.....</b>	<b>153</b>
8.1.	OUTLOOK AND RECOMMENDATIONS FOR FUTURE WORK .....	154
8.2.	CONTRIBUTION TO KNOWLEDGE .....	156

## Nomenclature

<b>BHP</b>	Bottom Hole Pressure
<b>CBHP</b>	Constant bottom-hole pressure
<b>CFD</b>	Computational Fluid Dynamics
<b>DFM</b>	Drift Flux Model
<b>ECD</b>	Equivalent Circulation Density
<b>EKD</b>	Early kick Detection
<b>EOS</b>	Equation of State
<b>GTL</b>	Gas to Liquid
<b>G-L</b>	Gas-Liquid Phase
<b>HPC</b>	High-Performance Computing
<b>HPHT</b>	High-Pressure, High-Temperature
<b>ID</b>	Inner Diameter
<b>OBM</b>	Oil based Mud
<b>OD</b>	Outer Diameter
<b>PVT</b>	Pressure-Volume-Temperature
<b>RANS</b>	Reynolds Averaged Navier–Stokes
<b>RSM</b>	Reynolds Stress Model
<b>SBM</b>	Synthetic based mud
<b>SST</b>	Shear Stress Transport
<b>VOF</b>	Volume of Fluids Technique
<b>WHP</b>	Well head Pressure
<b>WBM</b>	Water Based Mud
<b>1-D/2-D/ 3-D</b>	one dimensional/two dimensional/three dimensional



## List of Figures

<b>Fig. 1.1</b> Schematic for vertical drilling well with gas kick and multiphase flow .....	3
<b>Fig. 1.2</b> Effect of gas kick on mud pit and the mud circulation system. ....	6
<b>Fig. 1.3</b> Thesis Outline & Research Workflow. ....	9
<b>Fig. 2.1</b> Correlation of the Rise Velocity of Cylindrical Bubbles[23].....	26
<b>Fig. 2.2</b> Model Relationship and Hierarchy.....	29
<b>Fig. 2.3</b> Multiphase Flow Model Categories, STARCCM+ .....	34
<b>Fig. 2.4</b> Euler-Euler Modelling Approach.....	36
<b>Fig. 2.5</b> Volume Fractions on a Discrete Mesh (a) True Interface; (b) Volume Fractions [37].....	38
<b>Fig. 2.6</b> Classification of Gas-Liquid Flows.....	48
<b>Fig. 2.7</b> Types of Drilling Mud used in drilling process.....	51
<b>Fig. 2.8</b> Early Kick Detection modelling parameters in well control process .....	53
<b>Fig. 2.9</b> EKD Multiphase Modelling Parameters .....	53
<b>Fig. 3.1</b> Schematic View of CBHP MPD set up during influx removal.....	62
<b>Fig. 3.2</b> Integrated schematic of automatic intelligent gas kick condition detection.....	64
<b>Fig. 4.1.</b> Demonstration of computational domain (a) schematic draw for the pipeline with dimensions implemented using CFD with number of cells 4,500,000; (b) annular pipe with dimensions implemented using CFD with number of cells 1,500,000; (c) schematic draw for the annuli on x-y plane. ....	90
<b>Fig. 4.2</b> The geometry of two-phase (gas–liquid) flow through pipeline (a) schematic draw for the pipeline on x-y plane showing water and air inlet configuration; (b) Inlet flow geometry in constructed CFD model; (c) Schematic of the air-water mixing chamber used in the experiment.....	92
<b>Fig. 4.3</b> Comparison of simulated pressure gradient with experimental data (a) through pipeline; (b) through annuli. ....	94
<b>Fig. 4.4</b> Effect of superficial liquid velocity on axial liquid velocity for constant $V_L = 5$ m/s and variable $V_g$ (a) $V_g = 0.25$ m/s; (b) $V_g = 0.5$ m/s; (c) $V_g = 0.8$ m/s. ....	96
<b>Fig. 4.5</b> Effect of different interface forces on gas volume fraction for constant $V_L = 5$ m/s and variable $V_g$ (a) $V_g = 0.25$ m/s; (b) $V_g = 0.5$ m/s; (c) $V_g = 0.8$ m/s. ....	97
<b>Fig. 5.1</b> Model 2-D geometry (a) 2-D pipe geometry of the modelled domain; (b) Orthogonal mesh for annular geometry for a 3-D geometry domain section used in CFD.....	104

<b>Fig. 5.2</b> Different gas volume fraction for a two-phase flow at the beginning of the pipe used to inject both fluids (a) Water-Air; (b) Mud-Methane. ....	106
<b>Fig. 5.3</b> (a) The effect of superficial gas velocity on axial liquid velocity, and (b) The effect of different interface forces on Gas Void Fraction.....	106
<b>Fig. 5.4</b> The effect of number of cores on: (a) time step for 5 minutes simulation; (b) speedup simulation for 50 timestep.....	108
<b>Fig. 5.5</b> Scaling performance of bond order potentials on two HPCs (high-performance computing) ( <a href="http://www.archer.ac.uk/">http://www.archer.ac.uk/</a> ) .....	108
<b>Fig. 6.1</b> CFD model geometry with dimensions used to simulate the kick during drilling process...	114
<b>Fig. 6.2</b> Venturi pipe showing working principle of a draw gas into the mud stream.....	115
<b>Fig. 6.3</b> Pressure (Pa) during Mud circulation.....	116
<b>Fig. 6.4</b> Pressure profile during mud circulation. ....	117
<b>Fig. 6.5</b> Boundary condition for gas inlet in STARCCM+ constructed model. ....	118
<b>Fig. 6.6(a)</b> STARCCM+ available multiphase models, and (b) selected multiphase models and the available optional models.....	120
<b>Fig. 6.7</b> Mesh of constructed CFD model used after grid independency study using 2-D at STARCCM+. ....	121
<b>Fig. 6.8</b> STARCCM+ available Turbulence models.....	123
<b>Fig. 6.9</b> Hydrostatic pressure, pore pressure, overburden stress, and effective stress in a borehole at the true vertical depth.....	125
<b>Fig. 6.10</b> Velocity vector with drill bit rotation 100 rpm (a) only mud, and (b) during gas kick.....	126
<b>Fig. 6.11</b> CFD model with gas solubility (a) Phase distribution, (b) Computed interface Area per volume, and (c) Convective Courant Number based on isosurface between two-phases.....	130
<b>Fig. 6.12</b> Single fracture model sketch. ....	132
<b>Fig. 6.13</b> CFD model (a) Total pressure mud circulation, (b) Total pressure gas kick, (c) Contours of velocity magnitude (d) Contour of turbulent kinetic energy, and (e) Contours of gas volume fraction. ....	133
<b>Fig. 6.14</b> Bottom-hole scenario multiple fractures model sketch .....	135
<b>Fig. 6.15</b> Phase distribution along the annulus after the flow has stabilized (a) Injecting gas from bottom two side inlets, (b) Injecting gas from bottom one middle inlet. ....	136

---

<b>Fig. 6.16</b> Phase distribution (a) Total pressure injecting gas from bottom, (b) Total pressure gas kick. .....	137
<b>Fig. 6.17</b> CFD model used after grid independency study using 3-D at STARCCM+ (a) Geometry of constructed 3-D model, (b) Mesh of constructed 3-D model, and (c) CSA mesh 3-D model.....	138
<b>Fig. 6.18</b> 3-D model during gas kick (a) Phase distribution, (b) Velocity vector with drill bit rotation 100 rpm. ....	140
<b>Fig. 6.19</b> Volume fraction of gas kick at top of model at different turbulent models. ....	142
<b>Fig. 6.20</b> Volume fraction of gas kick at bottom of model at different turbulent models. ....	143
<b>Fig. 6.21</b> Residuals during simulation at different turbulent models.....	143
<b>Fig. 6.22</b> CFL during simulation at different turbulent models.....	143
<b>Fig. 7.1</b> Histogram of 4 constructed model simulating two phase flow in annulus (a) Axial mixture velocity, (b) Radial mixture velocity. ....	146
<b>Fig. 7.2</b> Phase distribution of each model simulating two phase flow in annulus.....	179
<b>Fig. 7.3</b> Comparison of volume of fraction in each contour individual segment position after the gas reach the outlet of the model (0.35 seconds). ....	152

## List of tables

<b>Table 2.1</b> Forces acting on a fluid element .....	17
<b>Table 2.2</b> Dimensionless Groups in Fluid Mechanics.....	20
<b>Table 2.3</b> Comparison between two fluid and drift flux model approaches .....	47
<b>Table 2.4</b> Classification of Gas-Liquid Flows (STARCCM+).....	49
<b>Table 3.1</b> The three components of a complete simulation model.....	56
<b>Table 3.2</b> Ability of models used in the simulation study to qualitatively represent dynamics in given scenario .....	56
<b>Table 3.3</b> Literature Review Summary .....	75
<b>Table 4.1</b> Range of parameters considered for the baseline model development. ....	<b>Error! Bookmark not defined.</b>
<b>Table 5.1</b> Structural and fluid model including drilling fluid and Methane gas.	<b>Error! Bookmark not defined.</b>
<b>Table 5.2</b> Grid independence verification .....	75
<b>Table 5.3</b> Factors affecting gas bubble flow and dependency on other parameters.....	93
<b>Table 5.4</b> The effect of number of cores on time step for 5 minutes simulation .....	99
<b>Table 5.5</b> The effect of number of cores on speedup simulation for 50 timestep .....	100
<b>Table 6.1</b> Drilling Mud and gas kick Properties .....	102
<b>Table 6.2</b> Turbulence models sensitivity.....	106
<b>Table 7.1</b> Inlet condition for 4 compared cases.....	<b>Error! Bookmark not defined.</b>
<b>Table 7.2</b> Volume of fraction analysis at each position across the annulus.....	117

## **Publication**

Paper communicated to Geoenergy Science and Engineering titled “Gas-Kick in Vertical Well Investigated using Computational Fluid Dynamics” (under review as on 10<sup>th</sup> Jan 2024)

# CHAPTER 1

## Introduction

### Outline of the chapter

This chapter presents the preamble to the thesis motivation, its aims and objectives in light of the blowout risk assessment model based on kick detection and consequences as functions of the incident and failure of well control barriers.

#### 1. Introduction

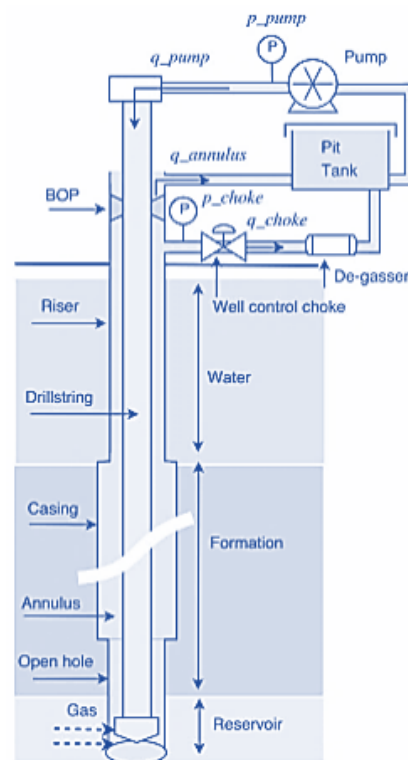
There are several issues faced by the drilling sector especially those related to high pressure, high temperature wells in offshore drilling, dynamic well control in particularly dealing with kick phenomena which is both financially and environmentally damaging. In general, well control during drilling phase is governed by a phenomenon known as multiphase flow, the investigation of which forms the core objective of this PhD work. This thesis offers a thriving collection of new discoveries concerning gas kick during drilling operations investigated using high performance CFD models, hitherto unreported in the literature. The thesis used innovative computational simulations with advanced computational tools such as robust material specifications and a modified turbulence model to aid in the capture of critical data such as bottomhole pressure and gas kick magnitude as a novel insight into the kick phenomena.

#### *1.1. Background*

Over the last century, fossil fuels have contributed to global economic progress. Extraction of non-renewable energy in the form of fluids from earth's bed continues to be a key driver to meet the energy demands. It generates 85% of global energy demand, making earth mining of

fossils a dominant energy source. In 2020, 3325.8 million tonnes of oil equivalent were produced [1]. To drill more securely and dependably deeper into a reservoir of high pressure and high temperature (HPHT), well drilling technology has been improving. According to Augustine [2], this transition raises drilling costs and threatens rig safety. Consequently, any efforts for lowering drilling costs might influence safe drilling in an unknown gas kick scenario [3, 4].

Control of the drilling operation poses multiple challenges and one of such well known challenge is the “kick” phenomena [5, 6]. Gas blowout incidents can be caused by ineffective kick mitigation plans [7, 8]. Conventionally, a gas kicks in the drilling process, as illustrated in **Fig. 1.1**, is defined as an unplanned and uncontrollable movement of reservoir gas inside the well [9].



**Fig. 1.1** Schematic for vertical drilling well with gas kick and multiphase flow [9].

When the hydrostatic pressure of the drilling fluid falls below the formation pressure at the well's bottom, gas ingress occurs, which is a common occurrence in HPHT gas reservoirs. This causes compressed bubbles of gas, which could dissolve in the drilling fluid, leading to a flow into the well annulus. Gas-kicks tend to be most harmful since gas lowers the wellbore pressure faster than liquids and confined at the surface becomes difficult. In turn this causes blowouts, accidents, environmental damage, and casualties beside the excessive cost and risk involved to relief and repairs. Consequently, it's imperative to remove formation fluids from the wellbore as soon as they start to displace the drilling fluid. Due to the presence of a complex multiphase zone, designing a practical hydraulic model to solve a well control issue is a challenging procedure. At the initial phase of a kick, it is extremely hard to identify gas influx in most situations. High-pressure, high-temperature (HPHT) reservoirs frequently experience gas kick during drilling because the hydrostatic pressure exerted by the mud column is insufficient to overcome pore pressure in the formation at the well's bottom [10]. The low gas dissolution into the mud and undissolved gas start to expand and accelerate, so the kick develops and increase. Well-control operations are emergency measures to handle unpredictable influx and its consequences [9]. During the last few years, common techniques like "wait and weight" and the "drillers" approach have been used to eliminate formation fluids from the wellbore. Kick detection techniques are frequently overly sluggish and imprecise. It might take some time for a kick to be noticed at the surface. A significant volume of gas might leak into the wellbore at this period, creating a potentially dangerous situation. To avoid human life loss and destruction of drilling facilities, the early prediction of the kick is crucial, as well as the ability to circulate the kicked fluid out of the hole [8, 11].

### *1.2.Research motivation*

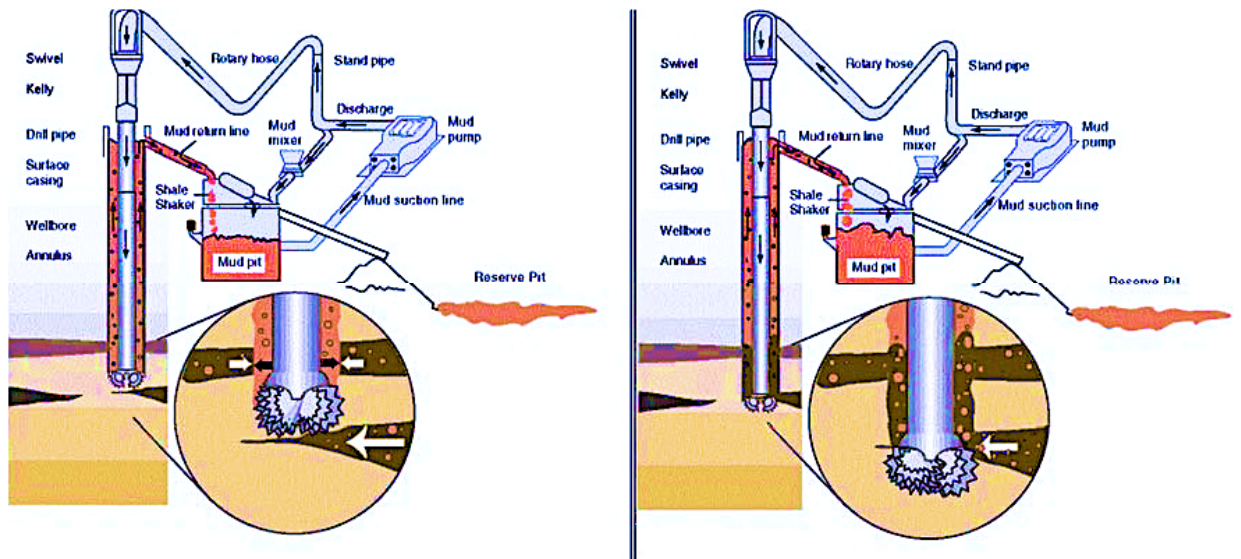
The kick has the potential to grow and increase their volume as the gas expand and rapidly move to the surface because of this dissolved and undissolved gas movement, which also



includes expansion and degassing (low gas solubility into drilling fluids). Such kicks can become blowouts, which are very costly both financially and environmentally and, most significantly, may result in loss of life if identified too late. The spectacular BP Deepwater Horizon disaster in 2010 is an iconic example of how destructive, costly and deadly blowouts can be [12]. Among other underlying reasons, several investigative studies point to the necessity of more advanced Early Kick Detection (EKD) technology [12]. Regretfully, because of the increased dependence on surface detection technologies which have reaction time issues limited progress has been accomplished. Within the industry, there is a general agreement to investigate a bottom-up strategy that enables early detection and tracking of kicks at various places along the wellbore.

Since the Macondo explosion on April 20, 2010, kick detection has emerged as a primary concern. Around 172 million gallons of gas-saturated oil leaked during the 87-day rupture, which occurred at a depth of 1522 metres into the Gulf of Mexico [13]. As to the Macondo blowout investigation report, changes in mud flowrate and pressure due to a kick were noted during the riser's passage [10, 14]. Accurate and clear identification of the kick before it passed through the riser may have prevented the loss of eleven personnels. Clearly, more work is required to be done around kick detection utilising surface-based variables that are already in use.

This instance demonstrates Early Kick Detection (EKD) of inflow gas kick in the HPHT well and plays a vital role to control and cease further blowouts [15]. Pressure at the well head and choke, increase in mud tanks, flow of mud whether into or out of the well, and pressure volume temperature of the mud used are some of the major elements taken into consideration for tracking Early Kick Detection throughout the drilling process, as shown in **Fig. 1.2** [10].



**Fig. 1.2** Effect of gas kick on mud pit and the mud circulation system [10].

These variables are also helpful in determining gas kick scenarios and assessing reservoir pore pressure, bottom hole pressure (BHP), and the properties of new mud that is used for improved well control and mitigation. Drilling mud is displaced in the well annulus by gas influx increasing mud flow in mud tanks, the first of the standards for determining and detecting a gas kick is the measurement of this increase in mud volume [16]. When deciding whether to start well control procedures in situations when tiny mistakes in judgement might cause a blowout, the operator takes these signs into account as a whole and applies its knowledge and experience. Enforcing well control procedures, however, also causes drilling delays and higher drilling costs. To avoid a potential blowout, the operator must thus evaluate the costs involved in taking preventative action against the benefits of doing so. To better respond to gas kicks, well control can benefit from an understanding of how the gas kick affects the various mud flow characteristics. [3, 4].

Precise estimation of the pressure change resulting from gas kick in wells that are originally filled with fluid is important for both operation security and technical design. Until now,

experimental, and numerical modelling approaches are used to study the flow pattern during drilling operations.

As on today, the typical way for detecting kicks is by monitoring of the balance of drilling mud and variations in pit volume. Typically, indirect flow measurements are derived by dividing the pump's volumetric displacement by the total number of pump strokes. This approach is not entirely precise, and it has the disadvantage of allowing small kicks to go unrecognized since they are detected afterwards. When a kick is identified, remedial action is performed to take back control of the well. When the well is closed, a kick killing procedure is initiated. While deciding, the driller is under a lot of anxiety. Inaccuracies in the design of the killing approach may result in formation damage or well blowout. Due to the ineffective kick detection method, a large amount of gas still exists inside the wellbore and must be removed before it can be safely circulated out. Despite substantial advances in well control, little study has been conducted on multiphase flow dynamics during a gas-kick. A wide range of kick simulators can reproduce various kick sizes and intensities for every situation. For the purpose of forecasting pressure profiles during the kick removal circulation, simulators have been extremely useful. Many kick simulators depict the kick as a single bubble that goes upward as a single slug. There is no mixture of drilling mud with formation fluid. While these simulators are useful for predicting pressure profiles during well control operations, they are inadequate for describing multiphase flow processes. It is possible to model the movement of each phase, the development and deformation of the phase interface, and phase interactions such the solubility of gas in liquid.

### *1.3. Need for improved understanding of the multiphase flow simulation:*

Accurate predictions of the fluid properties linked to hydrodynamics and flow have been sought after in the petroleum and natural gas industry using a variety of various

methodologies. However, due to issues with simulating the concentration of a dispersed phase, calculating drag and lift forces as well as relative motion between phases, and the requirement to consider particles with a variety of shapes, size and densities, computational fluid dynamics (CFD) is frequently explored to be the only practical option for creating precise solutions to difficult multiphase flow problems [17, 18].

To fully simulate the thermo-hydraulic parameters and analyse flow assurance problems, CFD could potentially be used. The number of experiments can be decreased by using CFD, but it is crucial to remember that CFD does not totally replace experimental analysis. This is because of the input data's ambiguity, which needs a time-consuming validation and confirmation process and eventually reduces the efficiency of the mathematical model.

Forecasting the related nonuniform pressure distribution if the vacancy fraction distribution throughout the pipe is known. A function of void fraction is the two-phase density, hydraulic, frictional, and momentum pressure decreases are added together to form the total pressure drop. The frictional pressure drop is specifically reliant on the two-phase density among these three components of pressure drop. Thus, good two-phase density prediction is required for accurate pressure drop prediction. It is necessary to forecast the gas void percent with accuracy to anticipate the two-phase density.

#### *1.4. Research aims and objectives:*

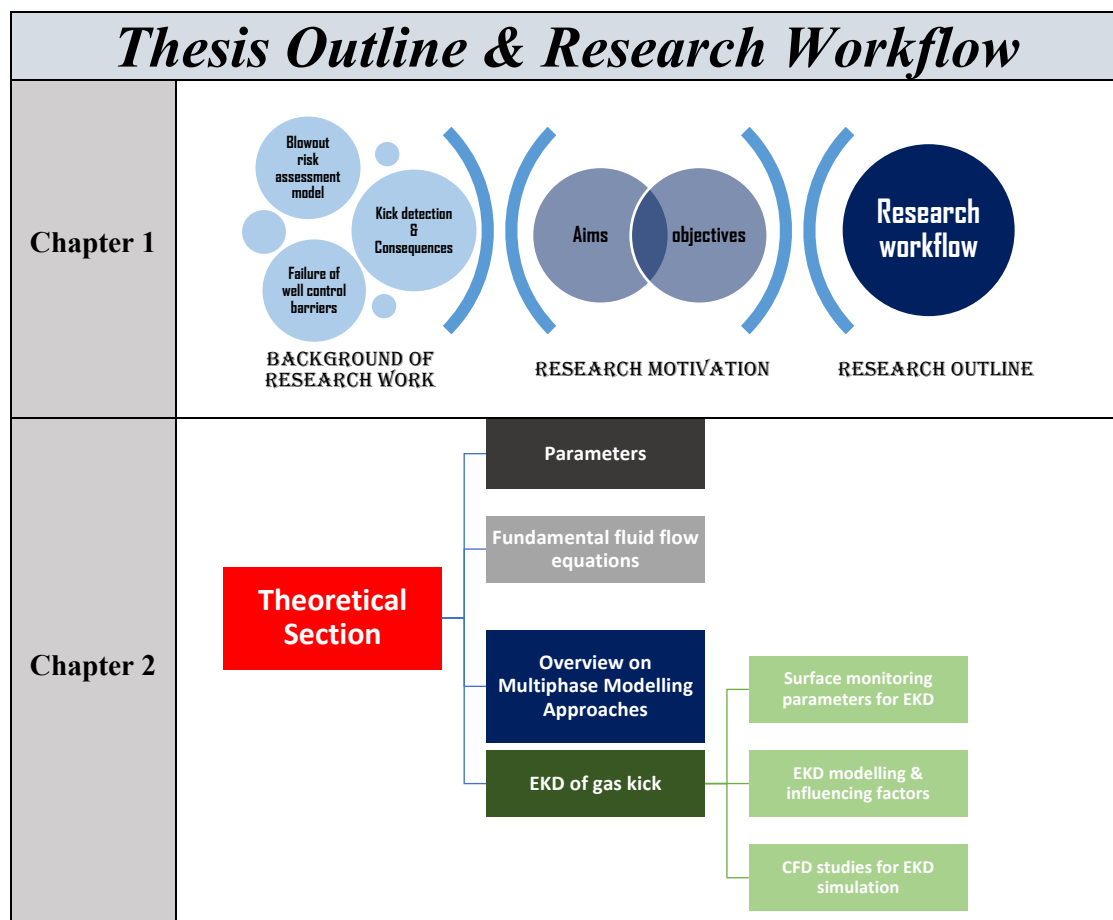
The aim of this research is to use CFD modelling under various operating scenarios to investigate kick phenomenon inside an annular space of drilling using non-Newtonian drilling fluid, VOF multiphase flow model and considering the gas solubility in the mud.

The main objectives of this research are:

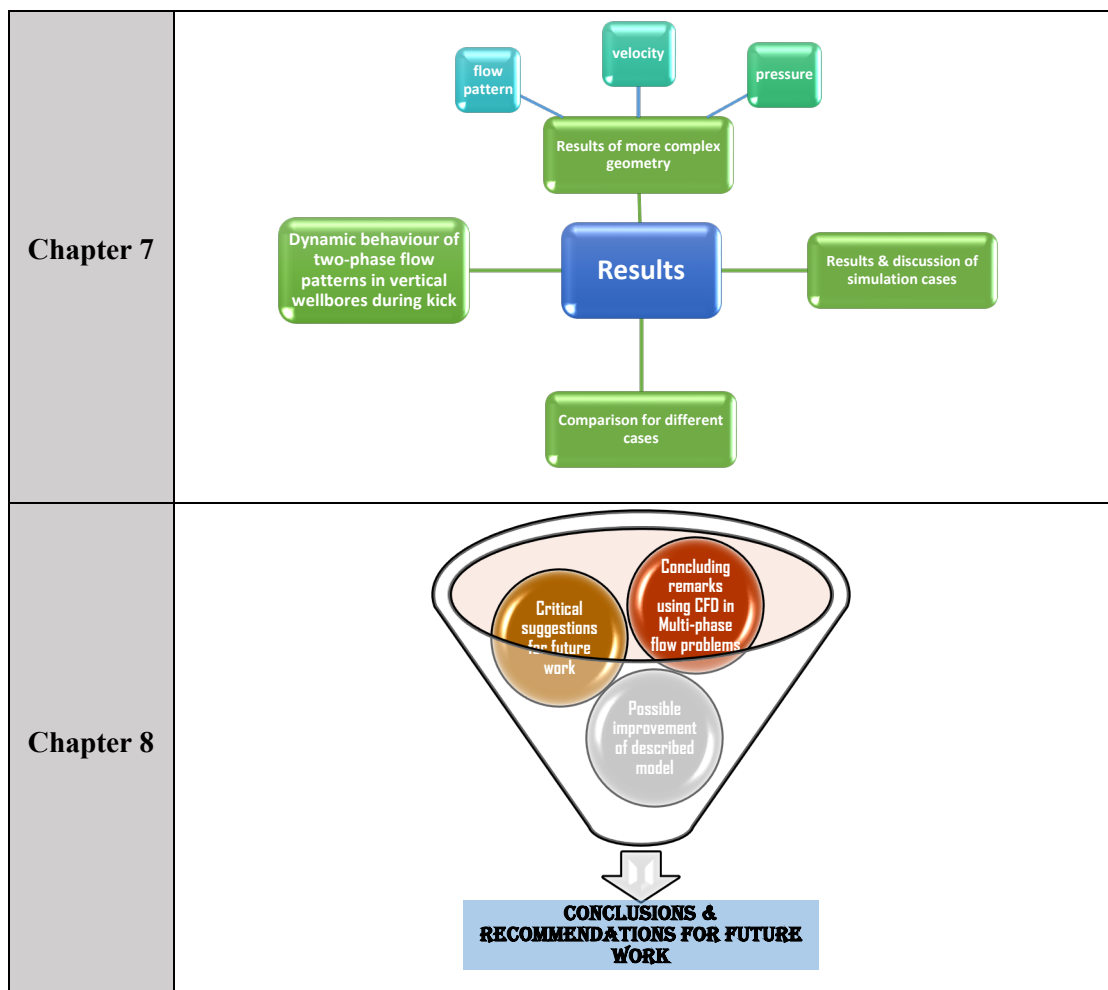
- Investigate two-phase flow characteristics and its change along the well's axial direction in an annulus of a drilling well using CFD.
- Study and discover the bottomhole pressure and gas kick magnitude by using advanced turbulence models, measure gas solubility in drilling fluid, 2D / 3D flow, and simplifying the multiphase flow model.
- Test and validate the model for the kick detection of blowout risk assessment under various operating scenarios.

### 1.5. Chapter plan

With a better visual, the plan of work carried out in this thesis are depicted by **Fig.1.3**.



<p><b>Chapter 3</b></p>	<pre> graph LR     LR[Literature review] --&gt; WCC[Well control at different operation conditions]     WCC --&gt; T3[Two &amp; Three phases well control]     WCC --&gt; MPU[MPD &amp; UBD]     WCC --&gt; GSOB[Gas solubility in OBM &amp; WBM]     WCC --&gt; EKD[EKD]         </pre>
<p><b>Chapter 4</b></p>	<pre> graph LR     MS[Modelling Simulation Methodology &amp; Validation] --- MA[Modelling Approach]     MS --- ST[Simulation Tool]     MA --- VPE[Validation procedures &amp; Experimental data acquisition]     ST --- VPE     VPE --- SP[Single phase data sets (water)]     VPE --- TP[Two-phase (air-water)]         </pre>
<p><b>Chapter 5</b></p>	<pre> graph LR     MS[Modelling Simulation (Calibration)] --&gt; DC[Development of baseline CFD model]     DC --&gt; BCFD[Baseline CFD model of two-phase (gas-liquid) flow through pipeline]     DC --&gt; I2P[Investigating two-phase flow drilling fluid &amp; gas in annulus]     DC --&gt; SA[Sensitivity analysis at drilling conditions]     SA --&gt; UGD[Understanding gas-kick dynamics.]     SA --&gt; MPCM[Modelling of phase change from water-air to mud-gas]     MPCM --- CE[Computational efficiency of the CFD code]         </pre>
<p><b>Chapter 6</b></p>	<pre> graph TD     PM[Predictive Modelling (realistic gas kick scenario in a vertical well)] --- SA[Sensitivity analysis]     PM --- SA2[Simplified assumptions]     PM --- MGD[Modelling of Gas Dissolution]     PM --- PSC[Pressure scenario for a gas kick]     PM --- CFC[CFD for complex flow geometries]     PM --- MSS[Model setup simulation of gas-kick scenarios]     MSS --- BC[Boundary Condition &amp; Kick-Gas Inlet Condition &amp; position]     MSS --- MGS[Model Geometry Setup &amp; Representation of Drill Bit]     MSS --- MFM[Multiphase Flow Model]     MSS --- TMC[Turbulence Modelling &amp; Grid Considerations]     MSS --- PS[Pressure Situation]     MSS --- MCI[Mud Circulation &amp; Influence of Rotation]         </pre>



**Fig. 1.1** Thesis Outline & Research Workflow.

## CHAPTER 2

### Literature review

#### Outline of the chapter

A critical review of theoretical basis of the multiphase fluid flow introducing the solid knowledge of the previously reported approaches in the Multi-Phase Flow Modelling is made.

#### **2. Theoretical Section: Theoretical basis of the multiphase fluid flows (two and three phase flows)**

The determination of a flow-pattern image is crucial work in simulating two-phase or three-phase flow in pipe or annular geometries in the field of drilling engineering. Historically, flow shape characterization has been utilised for evaluating drilling and production performance because flow architecture impacts physical phenomena such as mass, heat exchange, and pressure drop. However, the capability to establish down an experimental model for the two-phase flow condition of a gas-kick can be extremely difficult and expensive. Due to the harmful effects of gas kick and the high-pressure situations required to mimic bottom-hole conditions, an accurate conceptual and computational model is needed for this flow situation as an alternative.

##### *2.1.Relevant parameters associated with multiphase fluid flow:*

The following parameters are necessary to describe the gas-liquid-solid multiphase flow[19, 20]:

- Mass flow rate (G):



The quantity of fluid passing across the cross-section in a unit of time is known as the mass flow rate.  $G_g$ ,  $G_l$  and  $G_s$ , reflect the gas, liquid, and solid mass flow rates respectively.

$$G = G_g + G_l + G_s \quad (1)$$

- Volumetric flow rate (Q):

The volume of fluid that moves across a cross section in a particular period of time is known as the volumetric flow rate.  $Q_g$ ,  $Q_l$  and  $Q_s$ , reflect the gas, liquid, and solid volume flow rates respectively.

$$Q = Q_g + Q_l + Q_s \quad (2)$$

- Mean velocity:

$$V_g = \frac{Q_g}{A_g} \quad (3)$$

$$V_l = \frac{Q_l}{A_l} \quad (4)$$

$$V_s = \frac{Q_s}{A_s} \quad (5)$$

In the equation, the following variables are defined:  $V_g$  as the actual velocity of the gas phase in m/s,  $A_g$  as the cross-sectional area of gas flow in  $m^2$ ,  $v_l$  as the actual velocity of the liquid phase in m/s,  $A_l$  as the cross-sectional area of liquid flow in  $m^2$ ,  $V_s$  as the actual velocity of the solid phase in m/s, and  $A_s$  as the cross-sectional area of solid flow in  $m^2$ .

- Superficial flow velocities for the gas and liquid phases:

Superficial velocities of gas and liquid phases refer to the volumetric flux of each phase, representing the volumetric flow rate per unit area. Essentially, superficial

velocity signifies the velocity within the entire cross-sectional area, assuming that the entire area is occupied by a single phase.

$$V_{ag} = \frac{Q_g}{A} \quad (6)$$

$$V_{al} = \frac{Q_l}{A} \quad (7)$$

$$V_{as} = \frac{Q_s}{A} \quad (8)$$

In the equation, the following variables are defined:  $v_{ag}$  as the superficial velocity of the gas phase in m/s;  $A$  as the flow cross-sectional area in  $m^2$ ;  $v_{al}$  as the superficial velocity of the liquid phase in m/s, and  $v_{as}$  as the superficial velocity of the solid phase in m/s.

- Velocity of mixture:

This represents the relationship between the cross-sectional area and the total volume of mixture passing through it in a specific period of time:

$$v_H = \frac{Q_g + Q_l + Q_s}{A} = V_{ag} + V_{al} + V_{as} \quad (9)$$

where  $v_H$  is the velocity of mixture, m/s.

- The gas phase drift velocity:

As the density of the gas phase decreases, the velocity difference between the gas and the mixture increases, causing a significant deviation between the actual velocity of the gas phase and that of the liquid phase or gas-liquid mixture. This difference in velocity is referred to as the gas phase drift velocity.

$$\Delta v = v_g - v_H \quad (10)$$

In the equation,  $\Delta v$  represents the drift velocity in m/s, and  $v_H$  denotes the average velocity of the mixture in m/s.

The Drift Slip ratio (**S**) is defined as the ratio of the actual velocity of the gas phase to the actual velocity of the mixture:

$$S = \frac{v_g}{v_H} \quad (11)$$

- Slip velocity for solid phase:

In the scenario of liquid-solid two-phase flow within a wellbore or pipe, slippage arises from the velocity disparity between each phase. Additionally, variations in solid phase concentration occur at different locations due to the retention effect of the solid phase. The average slip velocity can be quantified as follows:

$$v_{sH} = v_H - v_s \quad (12)$$

- Mass fraction( $x_i$ ):

The mass fraction is determined by the proportion of the mass of a single phase to the total mass of the mixture flowing through the cross-section per unit of time. This relationship can be articulated as follows:

$$x_i = \frac{G_i}{G} = \frac{G_i}{G_g + G_l + G_s} \quad (13)$$

- Volume fraction( $\beta_i$ ):

The volume fraction is characterized as the ratio of the volume occupied by a single phase to the total volume of the mixture flowing through the cross-section per unit of time. This ratio can be articulated as follows:

$$\beta_i = \frac{Q_i}{Q} = \frac{Q_i}{Q_g + Q_l + Q_s} \quad (14)$$

- Actual gas volume fraction( $\phi$ ):

The actual gas volume fraction is determined by the ratio of the area occupied by a specific phase to the entire cross-sectional area as the mixture traverses the cross-section. In the context of gas-liquid-solid multiphase flow, an illustration is the ratio of the area occupied by the gas phase to the entire cross-sectional area, referred to as the actual gas volume fraction. This ratio can be expressed as follows:

$$\phi = \frac{A_g}{A} = \frac{A_g}{A_g + A_l + A_s} \quad (15)$$

- Flowing density( $\rho'$ ):

The mass to volume ratio of the mixture passing through the cross section in a particular amount of time is known as the flowing density:

$$\rho' = \frac{G}{Q} \quad (16)$$

- Phase volume fraction ( $E_k$ ):

The phase volume fraction signifies the proportion of the volume of a single phase to the total volume or the area occupied by that phase to the entire cross-sectional area. This metric serves as an indicator of phase distribution characteristics and can be mathematically defined as follows:

$$E_k = \frac{V_k}{V} = \frac{A_d}{A} \quad (17)$$

In the equation, the following variables are defined:  $V$  as the volume of the mixture in  $m^3$ ,  $V_k$  as the volume of one phase in  $m^3$ , and  $A_d$  as the cross-sectional area of one phase in  $m^2$ .

## 2.2. Fundamental fluid flow equations

### 2.2.1. Navier Stokes

The Navier-Stokes equations are the governing formulas used in continuum mechanics to represent fluid movement. The conservation of mass, momentum, and energy for a single phase is described by this particular set of formulas [14, 21]. Examining single-phase flow reveals that the motion of a fluid is instigated by forces acting on the fluid element. Broadly, these forces can be classified into three categories based on their proportionality to spatial dimensions: volume forces, surface forces, and line forces, as illustrated in Table 2.1.

**Table 2.1:**  
Forces influencing a motion of a fluid.

Volume forces	Surface forces	Line forces
Gravity force Inertia force Buoyancy force	Pressure force Viscosity force	Surface tension force

The equation of motion can alternatively be formulated in the following terms: Inertial forces equal the sum of pressure forces, viscous forces, and external forces. **(18)**

Furthermore, the continuity principle asserts that mass remains conserved unless it exits the domain. The preservation of mass, devoid of any sources or sinks, is expressed as:

$$\frac{\partial \rho}{\partial t} + \nabla \cdot \rho \mathbf{v} = 0 \quad (19)$$

Considering the fluid as a continuum and applying Newton's second law of motion, along with the assumption that the stress state in the fluid comprises a pressure term and a viscous term, leads to the derivation of the equation of motion for a fluid element:

$$\rho \left( \frac{d\mathbf{v}}{dt} \right) = \nabla \cdot \boldsymbol{\sigma} + \mathbf{F} \quad (20)$$

where  $\boldsymbol{\sigma}$  represents the stress tensor, while  $\mathbf{F}$  incorporates the effects of body forces in the system.

This equation articulates the conservation of momentum, signifying that the cumulative impact of all forces acting on a fluid element equals its temporal change in momentum. The alteration in the flow, whether acceleration or deceleration, is contingent upon the force applied, being proportionate to the mass of the fluid element. Essentially, this embodies the principle of conservation of momentum, a manifestation of Newton's second law.

The time derivative of the fluid velocity is expressed as:

$$(d\mathbf{v}/dt) = (\partial\mathbf{v}/\partial t) + \mathbf{v} \cdot \nabla\mathbf{v} \quad (21)$$

The stress tensor can be decomposed into two components: the pressure ( $\mathbf{p}$ ) multiplied by the identity matrix ( $\mathbf{I}$ ), along with the deviatoric stress tensor ( $\mathbf{T}$ ).

$$\sigma_{ij} = \begin{bmatrix} \sigma_{xx} & \tau_{xy} & \tau_{xz} \\ \tau_{yx} & \sigma_{yy} & \tau_{yz} \\ \tau_{yz} & \tau_{zy} & \sigma_{zz} \end{bmatrix} = - \begin{bmatrix} p & 0 & 0 \\ 0 & p & 0 \\ 0 & 0 & p \end{bmatrix} + \begin{bmatrix} \sigma_{xx} + p & \tau_{xy} & \tau_{xz} \\ \tau_{yx} & \sigma_{yy} + p & \tau_{yz} \\ \tau_{yz} & \tau_{zy} & \sigma_{zz} + p \end{bmatrix} = -p \mathbf{I} + \mathbf{T} \quad (22)$$

Revising the equation of motion results in the following generalized form:

$$(d\mathbf{v}/dt) = -\nabla p + \nabla\mathbf{T} + \mathbf{F} \quad (23)$$

This equation still lacks details regarding the unknown stress tensor  $\mathbf{T}$ . To address this, a constitutive law is required to characterize the viscous stress state in the fluid, offering insight into the fluid's viscous behaviour or rheology. For Newtonian fluids, a linear relationship exists between the applied stress and resulting strain, rendering the fluid viscosity a constant.

$$\rho ((\partial\mathbf{v})/\partial t + \mathbf{v} \cdot \nabla\mathbf{v}) = -\nabla p + \nabla \cdot (\mu (\nabla\mathbf{v} + (\nabla\mathbf{v})^T) - 2/3\mu (\nabla \cdot \mathbf{v}) \mathbf{I}) + \rho \mathbf{g} \quad (24)$$

In compressible flow, an equation of state and the formulation of energy conservation are essential. The ideal gas law is frequently employed as an equation of state, although the specific relationship chosen depends on the nature of the fluid and the prevailing operating conditions.

Conservation of energy is expressed as:

$$\rho \frac{dh}{dt} = \frac{dp}{dt} + \nabla \cdot (k \nabla T) + \Phi \quad (25)$$

In the equation, (**h**) denotes enthalpy, (**k**) represents the heat conduction coefficient, (**T**) stands for temperature, and (**Φ**) is a function representing the dissipation of energy resulting from viscous effects. [22].

These three equations together is known as the Navier-Stokes equations, forming the core of fluid flow modelling. Once the velocity field is determined, other variables of interest, such as pressure or temperature, can be derived. In specific flow scenarios, simplifications may enable an analytical solution of the equations. However, solving the complete Navier-Stokes equations is achievable only through numerical methods. These equations have the capability to describe the motion of each phase in intricate detail, accounting for every drop, bubble, and the surrounding fluid across various spatial and temporal scales. Yet, the computational power required for such a direct numerical simulation exceeds the present capabilities for many common flow scenarios due to their complexity.

The application of Navier-Stokes equations is feasible for each phase individually up to an interface but not across it. At the interface, special treatment is required to accommodate abrupt changes in variables and to define the exchange of mass, momentum, and energy between phases. Various approaches have been proposed to address the diverse spectrum of multiphase flow across different scales. These approaches typically involve solving the Navier-Stokes equations along with additional models and assumptions specific to the flow conditions. Handling turbulence, particularly when both phases are turbulent, poses a considerable computational challenge. Therefore, simplifications are essential in realistic models for most multiphase flows. Achieving reasonable simplifications in the governing equations relies on a comprehensive understanding of the flow and an investigation into the

dominant forces and mechanisms involved [14, 21]. Engineers typically begin looking into a flow by characterising it using dimensionless numbers.

### 2.3. Dimensionless Numbers

By formulating the forces included in the Navier-Stokes equations individually and establishing their relationships, non-dimensional groups known as dimensionless numbers in fluid mechanics can be derived. The utilization of these dimensionless numbers facilitates the categorization of flow problems and aids in the identification of dominant forces that play a more significant role in the system.

Dimensionless numbers have been used for many decades to simplify fluid flow modelling. It is advisable in engineering practice to analyze the flow problem by examining its dominant forces and fundamental relationships before establishing a computational model. This analysis serves as the groundwork for a well-founded modelling approach, a step that is sometimes overlooked as computational modelling tools and computing capabilities become more readily accessible.

Using the six fundamental forces in fluid mechanics, the subsequent five distinct dimensionless groups can be deduced. A comprehensive explanation, along with the corresponding equations, is provided afterward [14, 21].

**Table 2.2**  
Dimensionless Groups in Fluid Mechanics

<b>Re</b>	<b>Reynolds number</b>	$\frac{\text{inertia force}}{\text{viscous force}}$
<b>Eu</b>	<b>Euler number</b>	$\frac{\text{pressure force}}{\text{inertia force}}$
<b>Fr</b>	<b>Foude number</b>	$\frac{\text{inertia force}}{\text{force of gravity}}$
<b>We</b>	<b>Weber number</b>	$\frac{\text{inertia force}}{\text{surface tension force}}$
<b>Eo</b>	<b>Eotvos number</b>	$\frac{\text{buoancy force}}{\text{surface tension force}}$



The initial three among them are familiar in the context of single-phase flow but also hold significance in characterizing multiphase flow. Additional dimensionless numbers, beyond those outlined in **Table 2.2**, are available in the literature. However, fundamentally, they can be obtained by rearranging the five fundamental groups. For example, combining two or more dimensionless numbers allows the derivation of Archimedes number ( $A_r$ ), Capillary number ( $C_a$ ), inverse viscosity number ( $N_f$ ), Morton number ( $M_o$ ), Ohnesorge number ( $O_h$ ), and Suratman number ( $S_u$ ), as demonstrated below:

$$A_r = \sqrt{\frac{1}{M_o}} Ri \cdot Re^2, \quad (26) \quad C_a = \frac{Fr}{\sqrt[4]{M_o E_o}} = \frac{We}{Re}, \quad (27)$$

$$N_f = \sqrt[4]{\frac{E_o^3}{M_o}} \quad (28) \quad M_o = \frac{E_o We^2}{Re^4} \quad (29)$$

$$O_h = \frac{\sqrt{We}}{Re} \quad (30) \quad S_u = \frac{Re^2}{We} \quad (31)$$

Perhaps the most widely recognized dimensionless number in fluid dynamics is the Reynolds number. It signifies the balance between inertial and viscous forces, essentially quantifying the relationship between a fluid's momentum and its viscosity. Mainly employed to categorize single-phase flow, the Reynolds number distinguishes between turbulent and laminar flow.

$$Re = \frac{F_I}{F_V} = \frac{\rho L U}{\mu} \quad (32)$$

In this context,  $\rho$  denotes the density of the fluid,  $L$  represents the characteristic length,  $U$  is the mean velocity of the fluid, and  $\mu$  stands for the dynamic viscosity of the fluid.

Multiphase flows are commonly regarded as turbulent, although instances of laminar flow can occur when the flow channel is horizontally aligned. In inclined flows, buoyancy introduces an influence, causing the lighter phase to accelerate and induce turbulence. Naturally, the concept of the Reynolds number needs adaptation in multiphase flow. One approach involves utilizing mixture quantities to calculate a mixture Reynolds number, which

is applicable in scenarios of dispersed flow with a low slip velocity. However, in cases of segregated flow where fluid velocities vary significantly, this approach proves insufficient to characterize the flow. In such instances, it becomes necessary to compute the Reynolds number separately for each phase, considering individual phase velocities and properties. Nevertheless, there exists no consensus on the most suitable definition of Reynolds number for multiphase flow, leaving the researcher to choose a definition that aligns best with the specific flow conditions under investigation.

The Euler number signifies the balance between pressure forces and inertia forces, establishing a connection between the local pressure gradient ( $\Delta p$ ) and the kinetic energy of the fluid volume. Its purpose is to characterize losses in the flow, and it is defined as the ratio of the local pressure gradient to the kinetic energy of the fluid volume. An Euler number of one indicates a fully frictionless flow.

$$E_u = \frac{FP}{FI} = \frac{\Delta p}{\rho U^2} \quad (33)$$

The Froude number is used to define various open channel flow regimes. Its definition is the gravity to flow inertia ratio:

$$Fr = \frac{FI}{FG} = \sqrt{\frac{\rho U^2}{\rho g h}} = \frac{U}{\sqrt{g L}} \quad (34)$$

In this equation,  $g$  represents the acceleration due to gravity,  $h$  is the hydraulic depth, and  $L$  is the characteristic length.

The significance of the Froude number arises in scenarios involving fluid flow with a free interface, particularly evident in separated two-phase flow. This parameter serves as a suitable correlating factor for such flows, as those with identical Froude numbers exhibit comparable wave patterns at the phase interface. In the context of the Froude number, open

channel flow is categorized into three types, with the denominator representing the speed of a small surface wave relative to the speed of the bulk fluid, known as wave celerity. Critical flow is characterized by a Froude number equal to 1, Supercritical flow occurs when the Froude number exceeds 1, and Subcritical flow is observed when the Froude number is below 1. In critical flow, the wave celerity matches the bulk flow velocity, resulting in stationary disturbances. Subcritical flow, on the other hand, involves a bulk flow velocity slower than the wave velocity, leading to the transmission of flow disturbances both upstream and downstream. This condition often leads to backwater effects. In supercritical flow, the bulk flow surpasses the surface wave speed, causing disturbances to transmit only downstream. Hydraulic jumps are exclusively possible in supercritical flows.

Utilizing dimensional analysis, the following interpretation of the Froude number is applied, representing the balance between inertia and buoyancy forces:

$$Fr_{gas} = \frac{U_{TB}}{\sqrt{gd \frac{\rho_l - \rho_g}{\rho_l}}} \quad (35)$$

In this equation,  $U_{TB}$  denotes the Taylor bubble velocity,  $\rho_g$  represents the gas density,  $\rho_l$  is the liquid density, and  $d$  stands for the pipe diameter.

The relationship that exists between surface tension ( $\sigma$ ) force and inertial force is known as the Weber number.

$$We = \frac{F_I}{F_S} = \frac{\rho L U^2}{\sigma} \quad (36)$$

Inertia serves as the propelling force leading to the partial disruption of flow structures, but it is opposed by the resistance from interfacial tension. Elevated Weber numbers are linked to an increased inclination for droplet deformation and breakup, particularly in conditions of heightened shear or more intense mixing. The Weber number proves valuable in assessing stable bubble diameters and predicting the tendency for bubble distortion under specific flow

conditions. When surface tension forces prevail, bubbles tend to exhibit a spherical shape, whereas dominance of inertial forces results in a more hemispherical bubble shape.

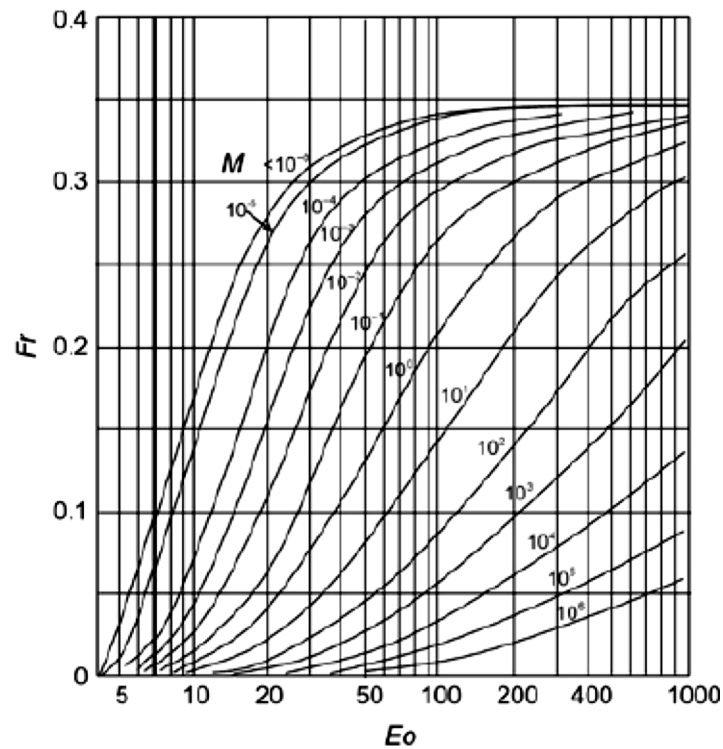
The proportional importance of surface tension and buoyancy is measured by the Eotvos number.

$$Eo = Bo = \frac{FB}{FS} = \frac{(\rho_l - \rho_g)gd^2}{\sigma} \quad (37)$$

A low Eotvos number signifies a pronounced impact of surface tension, leading to a more spherical bubble shape, while a high Eotvos number results in distorted bubble shapes and elevated bubble velocity. The Eotvos number is frequently employed in conjunction with the Morton number to describe the shapes of bubbles and droplets.

In multiphase flow, forces such as surface tension can notably impact flow morphology and, therefore, must be taken into account. Under the assumption that inertia and viscous forces in the gas phase are significantly smaller than those in the liquid phase, a set of three dimensionless numbers is well-suited to describe the interplay of relevant forces. Commonly encountered groups of dimensionless numbers characterizing gas-liquid flow in literature include Froude & Morton & Eotvos number.

An illustration of the utilization of the first dimensionless group is depicted in **Fig.2.1**, showcasing the correlation of experimental data regarding the ascent of Taylor bubbles conducted by White[23]. The observation of Taylor bubbles occurred in vertical tubes ascending through various stagnant fluids. In the graph, the Morton number reflects fluid properties, the Froude number indicates bubble ascent velocity, and the Eotvos number illustrates the impact of surface tension. Notably, there exists a range for  $Eo < 70$  where the Froude number, or ascent velocity, is solely a function of the Eotvos number. In contrast, at  $Eo > 200$ , an inertial region prevails where liquid viscosity and surface tension become less influential.



**Fig. 2.1** Correlation of the Rise Velocity of Cylindrical Bubbles [23]

The reciprocal viscosity ( $N_f$ ) dimensionless number, characterizes the impact of liquid viscosity ( $\nu_l$ ) and geometry on phase mixing in slug flow. [24].

$$N_f = \frac{\sqrt{gd^3}}{\nu_l} \quad (38)$$

By incorporating fluid densities into the extension of the inverse viscosity number, one obtains the buoyancy Reynolds number, denoted as  $\mathbf{R}$ , it has the following definition:

$$R = \frac{\sqrt{gd^3(\rho_l - \rho_g)\rho_l}}{\mu_l} \quad (39)$$

#### 2.4. Approaches of multiphase flow modelling:

There are several approaches that have been used to detect kicks relying on measurement of the electrical resistance, ultrasonic frequency, and hydrostatic pressure [25, 26] [27, 28]. The method of probing the electrical resistivity is one of the most popular procedures, which involves using a sensor electrode to measure the instantaneous electrical resistance in both

phases. The gas in a gas-liquid flow has high resistivity, in contrast to the water which is electrically conductive. The circuit gets closed when the sensor comes in touch with the liquid and the circuit is activated when it comes in touch with a bubble. The reduction in voltage within a sensor between  $V_{\min}$  and  $V_{\max}$  is indicative because the circuit is either open or closed based on the sensor being in touch with the liquid or the gas. Every sensor and the return electrodes are linked together in the case of a double-sensor probe approach [29]. However, these sensors are very expensive, but they are very important to determine the size of gas kick and the regime of gas flow in the annulus and bottomhole pressure (BHP). Most of kick models do not accurately calculate the pressure, temperature of the fluid and phase composition fluctuation in the annulus, especially since the phase fraction changes along the annulus with time when gas kick occur [26, 27]. **Sleiti** [30] mentions that suitable Navier-Stokes equations must be deployed to accurately represent the hydrodynamics in the annular region based on boundary conditions at the inlet and the outlet. They also state that the multiphase flow models determine the velocity, Gas-Liquid phase ratio, and the amount of flow rate through the annulus for each phase.

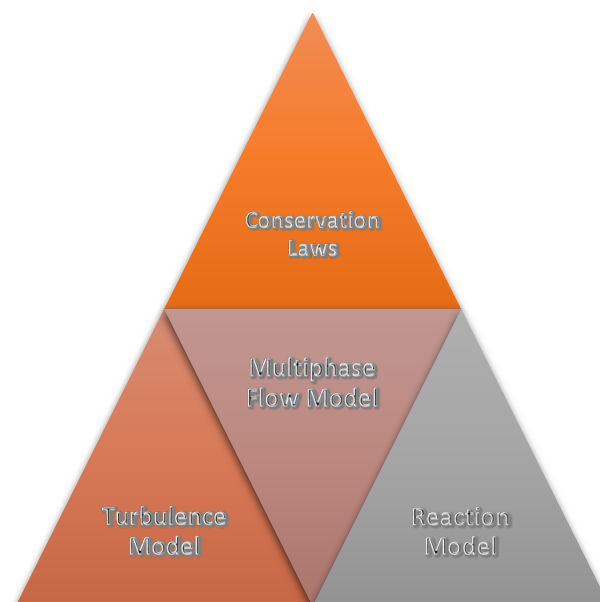
There are three categories of flow models:

- Empirical correlation
- Homogenous, and
- Mechanistic flow models.

Of these three models, the homogeneous flow model has been used extensively in vast majority of the previously reported research papers, specifically the drift flux model (DFM). This is due to the ease of calculating velocity of different phases and gas percentage, therefore, it is suitable for mixtures and combines the features of two-phase gas liquids into one-phase flow models. Consequently, various researchers have worked on simplifying the

multiphase flow models to simulate and properly predict the gas kick situation to obtain good well control and prevent shut in.

**Sutkar** [31] stated that most of the available multiphase flow mathematical models applied in the EKD models take into consideration heat transfer, and gas solubility are one-dimensional empirical correlations based on numerous of simple assumptions that are not appropriate for all conditions and situations. **Pouryoussefi** and **Guo** [14, 32] used CFD to simulate air-water interactions in annuli and vertical pipeline using Volume of Fraction (VOF) model and K- $\epsilon$  turbulence model for air fraction in an air-water system at varying superficial velocities. In two phase flow modelling it can be distinguished between different degrees of sophistication and different approaches to model the phase interaction, as shown in **Fig.2.2** the model relationship based on multiphase flow models, conservation laws, reaction models, and turbulence models. An overview of popular modelling techniques is provided below, along with a brief description of each methodology.



**Fig. 2.2** Model Relationship and Hierarchy

### 2.4.1. Turbulence models

The majority of fluid flow-related engineering processes are typified by unpredictable changes in flow volumes. These variations frequently occur at high frequencies and microscopic scales, making it extremely expensive to resolve them in terms of both time and space. To approximate the influence of the little changing structures, it is less expensive to solve for averaged or filtered values rather than the actual governing equations of turbulent flows Direct Numerical Simulation (DNS). There are several methods for simulating these structures with turbulence models.

The turbulence models can be subdivided into two categories:

- I. Reynolds-Averaged Navier-Stokes turbulence models
- II. Scale-resolving simulations

It is widely acknowledged that all turbulence models currently in use are imperfect representations of the actual phenomena of turbulence. The level of approximation in each model is contingent on the specific nature of the flow to which it is applied. Determining the conditions under which a model performs well or poorly is primarily based on experiential knowledge.

#### 2.4.1.1. The Reynolds-Averaged Navier-Stokes (RANS) Turbulence Model

The model establishes closure relations for the Reynolds-Averaged Navier-Stokes equations, which govern the transport of mean flow quantities. In deriving the Reynolds-Averaged Navier-Stokes equations, each solution variable in the instantaneous Navier-Stokes equations undergoes decomposition into its mean, or averaged, value and its fluctuating component, encompassing velocity components, pressure, energy, or species concentration. The averaging process can be conceptualized as time-averaging for steady-state situations and ensemble averaging for repeatable transient situations. Introducing the decomposed solution



variables into the Navier-Stokes equations yields equations for the mean quantities. The challenges of these models revolve around the mean flow quantities, providing closure for the governing equations. Two fundamental approaches are employed:

- I. Eddy viscosity models
- II. Reynolds stress transport models

#### *2.4.1.2. Eddy Viscosity Models*

Eddy viscosity models draw upon the analogy between the molecular gradient-diffusion process and turbulent motion. Introducing the concept of turbulent eddy viscosity allows for the modelling of the stress tensor as a function of mean flow quantities. The widely employed Boussinesq approximation represents a common model in this category. While simpler models, such as the Smagorinsky Subgrid Scale model utilized in Large Eddy Simulation (LES), hinge on the concept of mixing length to represent turbulent viscosity in terms of mean flow quantities, eddy viscosity models take a more comprehensive approach by solving additional transport equations for scalar quantities. These scalar quantities facilitate the derivation of turbulent viscosity. Various turbulence models fall under this category, including:

- Spalart-Allmaras model.
- K-Epsilon model.
- K-Omega model.
- Elliptic Blending model.
- V<sub>2</sub>F model.

The assumption that the stress tensor is linearly related to the mean strain rate overlooks the anisotropy inherent in turbulence. To address this turbulence anisotropy, certain models offer

the option to extend the linear approximation by incorporating non-linear constitutive relations.

In the case of K-Omega and K-Epsilon models, a Scale Resolving Hybrid (SRH) model is accessible. This model enables the RANS model to seamlessly transition to LES mode, providing the capability to resolve unsteady information pertaining to large-scale turbulent structures.

#### *2.4.1.3.K-Epsilon Model:*

The K-Epsilon turbulence model, a two-equation model, addresses transport equations for both turbulent kinetic energy and turbulent dissipation rate, facilitating the determination of turbulent eddy viscosity. Different versions of the K-Epsilon model have been utilized for many years, establishing itself as the predominant model in various industrial applications. Over time, numerous efforts have been made to enhance the model, with notable improvements being integrated into STAR-CCM+.

#### *2.4.1.4.High-Reynolds Number Approach*

The initial K-Epsilon turbulence model developed by Jones and Launder [33] was employed in conjunction with wall functions. Subsequently, this high-Reynolds number approach underwent modifications to account for the obstructive effects of the wall, encompassing the viscous and buffer layers, through the adoption of a low-Reynolds number approach and a two-layer approach.

#### *2.4.1.5.Low-Reynolds Number Approach*

The prevalent method involves the introduction of damping functions to one or more coefficients within the model. These functions serve to adjust the coefficients based on a turbulence Reynolds number, often taking into account the wall distance. Numerous models featuring damping functions have been suggested in literature, with the inclusion of the

Standard K-Epsilon Low-Re model. Another low-Reynolds number K-Epsilon model, known as the V2F Model, operates without utilizing wall distance or damping functions. It is asserted to remain valid across the entire flow domain while autonomously modelling the region near solid surfaces.

#### *2.4.1.6. Two-Layer Approach*

The two-layer approach, initially proposed by Rodi [34], presents an alternative to the low-Reynolds number strategy, allowing the application of the K-Epsilon model in the viscous-affected layer, encompassing the viscous sub-layer and the buffer layer.

In this methodology, the computation is segmented into two layers. In the layer adjacent to the wall, the turbulent dissipation rate and turbulent viscosity are defined as functions of the wall distance. The specified values in the near-wall layer seamlessly blend with the values calculated from solving the transport equation farther away from the wall. The equation for turbulent kinetic energy is solved throughout the entire flow domain. This explicit specification of turbulent dissipation rate and turbulent viscosity is arguably no more empirical than the damping function approach, and the outcomes are often comparable or superior.

Numerous two-layer formulations have been suggested, and three of them have been applied, with two designed for shear-driven flows and one tailored for buoyancy-driven flows:

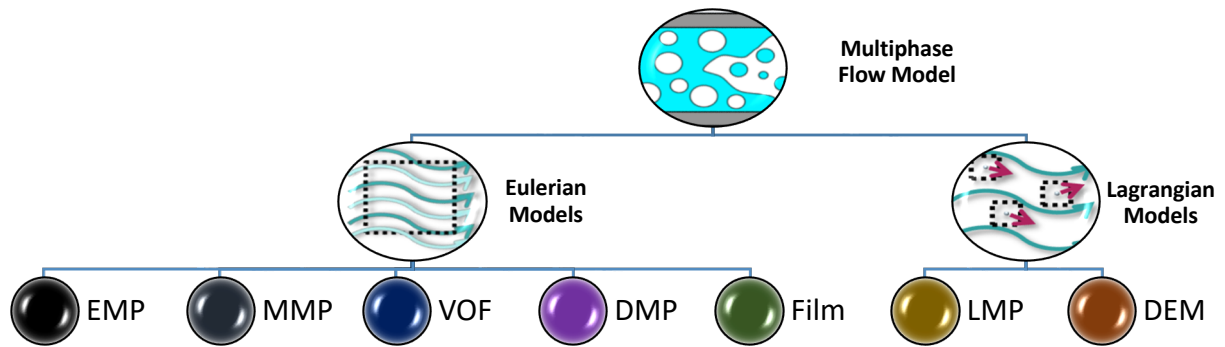
- Shear Driven (Wolfstein)
- Shear Driven (Norris-Reynolds)
- Buoyancy Driven (Xu)

#### *2.4.2. Multiphase flow models:*

Multiphase flows, involving the concurrent movement of multiple fluids within a given domain, play a crucial role in various industrial applications. Generally, these phases can be

attributed to gases, liquids, or solids, leading to simple examples of multiphase flows such as air bubbles rising in a glass of water, sand particles carried by the wind, or raindrops in the air. The definition of a phase can be broadened and applied to other fluid flow characteristics, including size, shape, density, and temperature. Numerical simulations of such flows require handling additional complexities compared to simulating single-phase flows due to the presence of interfaces, across which there is a discontinuity in fluid-fluid properties, and the exchange of mass, momentum, and heat between the phases. For modelling considerations, based on the increasing spatial scales of the interfaces between the phases, these flows may be divided into three categories: separated/stratified (film flow, annular flow, horizontal stratified flow), mixed/intermittent (slug flow, churn flow), and scattered (bubbly flow, droplet flow).

Various multiphase flow models are accessible, and the choice depends on the flow structure. The primary determinant in selecting a multiphase flow model is the scale of the interfacial structure and the desired level of resolution. Each approach to multiphase flow modelling is built on specific assumptions, resulting in distinct strengths, limitations, and applicability for modelling particular flow scenarios. The modeler is tasked with making an informed selection of the physical model and its settings tailored to the specific flow problem at hand. The modelling decision may face additional challenges due to the existence of a broad size range in interface structures and the transitions between them. An overview of multiphase flow modelling categories is illustrated in **Fig.2.3**.



**Fig. 2.3** Multiphase Flow Model Categories, STARCCM+

Broadly, two fundamental modelling strategies exist for simulating fluid flow: the Lagrangian approach and the Eulerian approach. In the Lagrangian specification of the flow field, the analysis involves tracking individual fluid parcels as they move through space and time. Essentially, the reference frame used to calculate flow variables is in motion with the flow. In the Eulerian specification of the flow field, the observer's frame of reference remains fixed. Fluid motion is observed at specific locations in space, typically represented by a computational grid, through which the fluid flows as time progresses. Depending on the computational reference frame's specifications, multiphase flow models utilize these approaches based on their advantages in computing the flow field of individual phases. The decision on which basic model to employ for computing a two-phase flow phenomenon heavily relies on the ability to resolve the gas-liquid interface within the computational mesh. Eulerian and other Lagrangian approach models can be further categorized as follows:

#### *2.4.2.1. Eulerian Models*

The observer considers the particles, bubbles, or droplets to be a continuum passing through a fixed volume

- Eulerian Multiphase (EMP)
- Mixture Multiphase (MMP)

- Volume Of Fluid (VOF)
- Dispersed Multiphase (DMP)
- Fluid Film (Film)

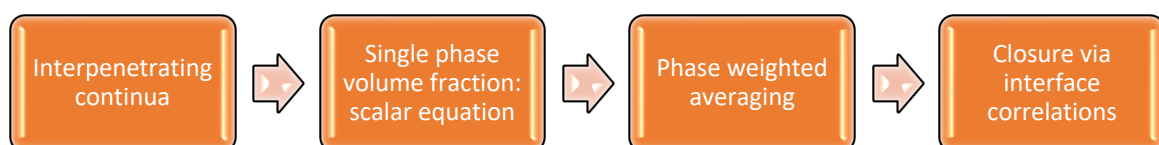
#### 2.4.2.2. Lagrangian Models

The observer tracks parcels of particles as they move through space & time

- Lagrangian Multiphase (LMP)
- Discrete Element Method (DEM)

#### 2.4.2.3. Euler-Euler Model

Within the Euler-Euler method, control volumes can be separated inside the flow region, and the flow throughout the boundaries of these control volumes is monitored. In this methodology, phases are considered as continuously piercing with differing velocities and temperatures. The introduction of the phase volume fraction concept arises from the inability of one phase to occupy the volume of another. These volume fractions are considered continuous functions of both space and time, and their combined total is always equal to one. The conservation equations for momentum and continuity are individually addressed for each phase. To complete the equations, balance equations and interface coupling relations are employed, detailing the transfer of momentum and heat across interfaces. **Fig.2.4** illustrates the primary steps in Euler-Euler modelling.



**Fig. 2.4** Euler-Euler Modelling Approach

Various Euler-Euler modelling strategies consist of the following two approaches:

I. Mixture Model:

The mixture model involves addressing three conservation equations for the mixture, a volume fraction equation dedicated to the secondary phase, and determining relative velocities through an algebraic slip relation. Users have the flexibility to define the algebraic slip relation, or they can opt for the one outlined in the previously mentioned drift flux model approach. This modelling approach is especially well-suited for the simulation of dispersed multiphase flows.

II. Eulerian Model:

The Eulerian model stands out as the most complex variation among the discussed Euler-Euler models. It independently addresses momentum and continuity equations for each phase and establishes coupling through pressure and interphase exchange coefficients. Various models support this coupling, depending on the specific phases in the system. The Eulerian model finds application in simulating dispersed multiphase flows, such as those observed in bubble columns, risers, particle suspensions, and fluidized beds. One notable limitation of phase-weighted averaging is the potential loss of detailed flow information. Since the phase interface is not resolved, a specific phase volume fraction may correspond to different flow morphologies.

#### *2.4.2.4. Volume Of Fluid (VOF) Model*

It is critical to adopt an adequate technique which can capture a moving interface between two immiscible fluids for CFD modelling under considerations. The ability of the Volume of Fluids technique (VOF) to track a fluid-fluid interaction led to its selection for this purpose [35]. This approach works by simulating two immiscible fluids moved by one fluid with

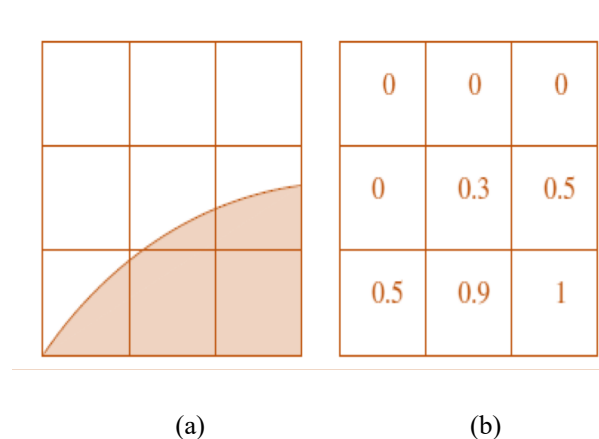
mixing characteristics. The most well-known volume-based interface tracking technique was used by Aarsnes [36]. The modelling work used mathematical equations of conservation and observing volume fraction of different phases across the region. The phases which share the same variable and features, which indicate averaged volume values identified from volume of fraction. This means any cell's characteristics and parameters are completely indicative of either a single phase or a combination of the two phases [37-39].

The definition of phase volume fraction is as follows:

$$\alpha_l = f, \alpha_g = 1 - f \quad (40)$$

where,  $\alpha_l$  represents the volume fraction of the liquid phase,  $\alpha_g$  denotes the volume fraction of the gas phase, and  $f$  serves as the phase indicator.

When a cell is totally occupied with one phase, its phase indicator ( $f$ ) is one, and when the opposing phase occupies it completely, it is zero. As shown in Fig 2.5, computational cells with a value between zero and one are those that have a phase interface because they show the immediate existence of both phases. The combined volume portions of the two phases equal one [37].



**Fig. 2.5** Volume Fractions on a Discrete Mesh (a) True Interface; (b) Volume Fractions [37]



The phases present in each computational cell specify the mixture characteristics required for the transport equations. The definition of a two-phase flow is provided by:

$$\rho_m = \alpha_l \rho_l + (1 - \alpha_l) \rho_g \quad (41)$$

$$\mu_m = \alpha_l \mu_l + (1 - \mu_l) \rho_g \quad (42)$$

where,  $\rho_m$  is mixture density,  $\mu_m$  is mixture viscosity,  $\mu_l$  is liquid phase viscosity,  $\rho_g$  is gas phase density, and  $\alpha_l$  is liquid phase volume fraction.

Simulating multiphase flows is made simpler by keeping volume fractions per cell rather than specifying interface geometry. However, when computing phase fluxes at cell faces, information about the interface geometry and orientation is required. Due to large gradients in volume fraction at the interface, applying a standard difference scheme for spatial discretization would lead to numerical smearing, causing a loss of definition in the interfaces [40].

The implementation of the Volume of Fluid (VOF) multiphase model in STAR-CCM+ is classified under interface-capturing methods, which forecast the distribution and movement of the interface between immiscible phases. This modelling approach relies on the assumption that the mesh resolution is adequate to depict the position and shape of the interface between phases. The description of phase distribution and interface position is facilitated through the fields of phase volume fraction.

This model is applicable for monitoring the movement of free surfaces in situations involving immiscible fluids with a distinct interface. It possesses the capacity to model diverse phenomena including phase change. Additionally, it allows for the inclusion of surface tension effects.

#### 2.4.2.5. Mechanistic 1D Models

Mechanistic modelling entails combining conservation equations, empirical correlations, and observations. These models are typically one-dimensional (1D) and utilize closure relations to address local flow characteristics like velocity, wall shear stress, and liquid holdup. While closure relationships are commonly derived from empirical correlations, mechanistic models offer a broader range of applications compared to purely empirical methods. The key source of uncertainty in mechanistic models lies in the closure relations, often derived from experiments conducted under low-pressure and temperature laboratory conditions, using alternative fluids and reduced pipe diameters. Extrapolating experimental results to represent actual field conditions can present challenges. Mechanistic models simplify the physical phenomenon by emphasizing the most significant processes and excluding less important effects that could complicate the problem without significantly enhancing accuracy. For example, if a flow is predominantly one-dimensional, the other two dimensions may be disregarded. The initial mechanistic model for predicting flow pattern transitions was introduced by **Taitel and Dukler** [41]. Following the introduction of flow pattern transition models, the development of comprehensive models commenced. These comprehensive models can address various flow patterns and pipe geometries by employing distinct flow models tailored to specific flow patterns. Among the frequently utilized models for solving two-phase flow challenges are the drift-flux model and the two-fluid model.

Most mechanistic models are explicitly designed for simulating two-phase flow within pipes. There are two primary categories of mechanistic models employed for this purpose. The first, simpler category involves the drift-flux model, which considers the flowing mixture with slip between individual phases. While it requires certain assumptions across the phases, it is not as precise or flexible as the two-fluid model. The two-fluid model, on the other hand, treats each flowing phase separately and incorporates interactions between them, largely neglecting

the annular conduit. Few studies have addressed the adaptation of correlations developed for vertical two-phase pipe flow to annular geometry. **Caetano** [42] introduced mechanistic models focused on predicting pressure gradients specifically for vertical two-phase flow in an annulus. These models take into account annulus parameters such casing and tube diameters and degree of eccentricity, as well as physical phenomena of two-phase flow in the context of bubble, scattered bubble, slug, and annular flow patterns. **Ozar** [43] offered a thorough summary of research conducted in experiments and models that are now in use for gas-liquid flow in annuli.

#### 2.4.2.6. High fidelity model

These models fall into a category characterized by high precision and extensive predictive capabilities across a broad range of application scenarios. Typically employed for training, analysis, and operational planning, they are not specifically tailored for a particular scenario or designed for application with specific mathematical algorithms. Thus, those are not seen as models that are appropriate for intended use.

$$\frac{\partial \mathbf{U}}{\partial t} + \mathbf{A}(\mathbf{U}, \mathbf{x}, t) \frac{\partial \mathbf{U}}{\partial \mathbf{x}} = \mathbf{D}(\mathbf{U}, \mathbf{x}, t) \frac{\partial^2 \mathbf{U}}{\partial \mathbf{x}^2} + \mathbf{Q}(\mathbf{U}, \mathbf{x}, t) \quad (43)$$

In this context,  $\mathbf{U}(\mathbf{x};t)$  denotes a vector comprising unknowns like density, momentum, and energy. By employing variable transformations, the equation can be redefined in relation to more directly observable physical quantities such as temperature or pressure [44]. The term  $\mathbf{A}$  accounts for transport effects, encompassing phenomena like convection or momentum transfer through pressure, exerting a significant influence on the velocity of high-frequency waves in the system [45].  $\mathbf{D}$  represents irreversible diffusive effects along the flow direction, including factors like viscosity, heat, or mass diffusion [46]. The term  $\mathbf{Q}$  stands for source terms, involving exchanges between the system's state and the environment. Interactions with the environment may entail factors like friction, gravity, and heat transfer. Additionally,

exchanges between state variables can involve heat, volume, mass, and momentum transfers [45].

#### *2.4.2.7. The Homogenous Model*

In this model classification, the hypothesis is that the fluid mixture flows without slippage between its phases, and the averaged bulk flow properties are integrated into a pseudo-fluid. Under this assumption, one mass conservation equation and one momentum conservation equation adequately describe the pseudo-fluid. While the homogeneous model is straightforward to implement, it exhibits inaccuracies in scenarios involving multiphase fluids with substantial density and viscosity contrasts [47].

#### *2.4.2.8. Drift Flux Model*

Drift flux models were initially formulated by **Zuber** and **Wallis** [48, 49]. The drift-flux method provides an approximate representation for two-phase flow, and its practical significance lies in its simplicity and versatility, making it applicable to a broad spectrum of two-phase flow issues, commonly employed in various wellbore simulators.

To enhance the homogenous model, an additional equation can be introduced to calculate the velocity difference between the moving phases. This modified model, incorporating slippage between the phases, is referred to as the drift flux model. In the context of two-fluid systems (e.g., liquid and gas), the drift-flux model involves two mass conservation equations and a combined momentum equation for the mixture [47, 50]. To determine the velocity of each phase, the "slip law" is applied in conjunction with the combined momentum equation [51, 52]. The drift flux approach treats multiple phases as a mixture, presenting a single momentum equation for the mixture in terms of the volume-averaged velocity of the mixture. In a general compressible formulation, the challenge in solving the multi-phase flow problem in pipes lies in the strong nonlinear coupling between pressure and velocity fields. Therefore,

a numerical solution of the full compressible three-phase problem is necessary, typically achieved through iterative schemes [53].

The drift-flux model has been widely employed in literature for simulating transient multiphase flow in drilling applications [54-58]. While these simulators share the same drift-flux model concept, variations in results may occur based on the implemented numerical schemes and slip laws.

Attempts to further simplify two-phase flow models resulted in development of the so called "no pressure wave" models or "reduced drift-flux models [59-61] Such models are more concerned with "slow" gas propagation dynamics than "fast" pressure transients [62]. However, discarding the pressure dynamics results in discrete jumps in pressure responses to changing boundary conditions. This makes such a model unsuitable for specific applications, where fast pressure dynamics are important and must be accounted for [63]. For example, pressure control during well drilling using the method managed pressure drilling (MPD).

#### 2.4.2.8.1. *The Drift Flux Model Formulation applied to well drilling multiphase flow*

The simplest approach to compute multiphase flow variables is by using empirical correlations. In the following fundamental & mechanistic transport equations as used for the homogenous-drift flux-two fluid model had been introduced. The experimental data is then used to validate the proposed drift-flux model [22].

The Drift-Flux Model and Numerical Methods is presented by:

$$\partial_t \begin{pmatrix} \alpha_l \rho_l \\ \alpha_g \rho_g \\ \alpha_l \rho_l v_l + \alpha_g \rho_g v_g \end{pmatrix} + \partial_x \begin{pmatrix} \alpha_l \rho_l v_l \\ \alpha_g \rho_g v_g \\ \alpha_l \rho_l v_l^2 + \alpha_g \rho_g v_g^2 + P \end{pmatrix} = \begin{pmatrix} 0 \\ 0 \\ -q \end{pmatrix} \quad \begin{pmatrix} \mathbf{a} \\ \mathbf{b} \\ \mathbf{c} \end{pmatrix} \quad (44)$$

where, **a** is the mass conservation for liquid phase; **b** is the mass conservation for gas phase; and **c** is the conservation of momentum for the mixture; ( $v_l$  and  $v_g$ ) are the liquid and gas

velocities; ( $\rho_l$  and  $\rho_g$ ) are the liquid and gas densities; are ( $\alpha_l$  and  $\alpha_g$ ) the liquid and gas volume fractions; and ( $p$ ) the common pressure for liquid and gas.

(Slip law) which connects the two-phase velocities

$$v_g = c_0 v_{\text{mix}} + v_d \quad (45)$$

In the given equation, ( $C_0$ ) represents the concentration profile parameter, and ( $v_d$ ) is the drift velocity. These empirical parameters can be determined using:

$$\rho_t = \rho_{l0} + \frac{p-p_{l0}}{a_l^2} \quad (46)$$

$$\rho_g = \frac{p}{a_g^2} \quad (47)$$

In this context, ( $a_l$  and  $a_g$ ) denote the sound velocity in the liquid and gas phases, respectively.

Considering that the drilling fluid, typically containing solids, is treated as the liquid phase in this study while disregarding the impact of cuttings.

$$\alpha_l + \alpha_g = 1 \quad (48)$$

Equations 44 to 48 form a set of seven equations with seven unknowns, including three nonlinear partial differential equations. No analytical solution has been put forth for this system, necessitating the use of numerical methods for resolution. The objective of this investigation was to create a resilient transient hydraulic software capable of handling both multi-phase flow and transient single-phase analysis [22].

The momentum sink/source term, denoted by ( $q$ ), is derived from the following equation:

$$q = F_w + F_g \quad (49)$$

$$F_g = g(\alpha_l \rho_l + \alpha_g \rho_g) \cos \theta \quad (50)$$

where, ( $F_w$ ) is the frictional pressure drop

Calculating the frictional pressure drop and equivalent circulating density (ECD) caused by the circulation of non-Newtonian drilling fluids in the wellbore is a significant challenge in the drilling industry. The simulation assumes constant rheological parameters for the drilling fluid throughout. The drift flux model is not only applied to the annulus but also extended to the drill string. This extension aids in predicting bottom hole pressure (BHP) and allows for the simulation of crucial parameters like standpipe and pump pressures. For directional and horizontal wells, the minimum curvature method is employed to simulate the wellbore path, and the wellbore temperature profile is obtained from an in-house thermal simulator.

The choke model for stratified flow is presented by this equation:

$$Q = \frac{c_v Z \sqrt{\max(p_{top} - p_s, 0)}}{x_l / \sqrt{\rho_{l,top}} + x_g / (Y \sqrt{\rho_{g,top}})} \quad (51)$$

where ( $Q$ ) is the total mass flow rate through the choke, ( $x_l$ ) is the liquid mass flow fraction, ( $x_g$ ) is the gas mass flow fraction, ( $P_{top}$ ) is the surface back pressure, ( $P_s$ ) is the choke downstream pressure, ( $C_v$ ) is a constant related to the choke orifice area, ( $Y$ ) is a gas expansion factor and ( $Z$ ) is the choke opening to be controlled.

For a mixed flow regime (such as bubble flow or dispersed bubble flow), the following choke model is used:

$$Q = c_v Z \sqrt{\frac{\max(p_{top} - p_s, 0)}{x_l / \rho_{l,top} + x_g / (Y^2 \rho_{g,top})}} \quad (52)$$

The choke opening,  $Z$ , is obtained from the following control law:

$$Z = K_P (P_{BH} - P_{BH,Set\ point}) + K_I (\int (P_{BH} - P_{BH,Set\ point}) dt) \quad (53)$$

Where, (Kp) is the proportional coefficient and (Ki) being the integral coefficient.

The general expression for the area-averaged drift-flux model is given by:

$$UG = \frac{UGS}{\alpha} = C_0U + U_d \quad (54)$$

In the given equation,  $\alpha$  represents the void fraction,  $U_G$  denotes the gas velocity,  $UGS$  signifies the superficial gas velocity,  $U$  represents the total superficial velocity,  $C_0$  is the phase distribution parameter, and  $U_d$  stands for the drift velocity.

Different drift flux correlations provide methodologies for calculating the empirical parameters  $C_0$  and  $U_d$ . The phase distribution parameter arises from the non-uniform radial distribution of the total volumetric flux and void fraction. The choice of correlations for computing  $C_0$  and  $U_d$  depends on the flow pattern and channel geometry.

The drift flux model is commonly used for bubble flow and plug flow but is less appropriate for annular flow. In annular flow, the liquid phase exhibits two distinct velocities—the liquid film velocity and the liquid drop velocity—an aspect that the drift flux model cannot account for. Overall, the drift flux modelling approach is not well-suited for modelling separated flows, primarily because the fluid motion strongly relies on local pressure and velocity gradients in the phases rather than an external force.

#### 2.4.2.9. Two Fluid Model (1D)

The model was initially formulated by Wallis, Drew, and Ishii [49, 64, 65]. Ishii and Hibiki [66] have provided one of the most accurate versions of the model. Two-fluid and multiple-fluid models are based on separated flows for each phase, considering slippage between the phases through interphase shear stresses. These shear stress terms primarily contribute to drag forces between the fluids, governing the slippage of one phase over the other. The two-fluid model requires one mass conservation equation and one momentum conservation equation



for each phase [67], making it computationally more challenging. Furthermore, the introduction of two momentum equations in the two-fluid model formulation introduces mathematical complexities, uncertainties in specifying interfacial interaction terms between two phases, and potential numerical instabilities [68].

The primary challenge in numerical modelling of multiphase flows stems from the dynamic movement of the phase interface, where flow properties such as density, viscosity, and pressure experience discontinuities. Constructing accurate phase interaction terms poses a fundamental challenge in modelling multiphase flows, and there is no universally applicable methodology that is independent of the flow's topology. The characteristics of gas-liquid interfaces differentiate between segregated, transitional, and dispersed two-phase flow based on their structure. **Table 2.3** illustrates the distinctions between the Two-Fluid and Drift Flux model approaches. Generally, the Drift Flux model compared to the Two-Fluid model, the Drift Flux model is easier to understand and requires less computing power.

**Table 2.3**  
Comparison between two fluid and drift flux model approaches

Two fluid Approach	Drift flux Approach
A set of momentum conservation is written for each phase	Momentum conservation equation is written for the volume averaged mixture velocity
The equations contain terms that describe the momentum exchange between phases	Momentum exchange between phases is not specified since it is considered as mixture
Closure relations are required for the momentum exchange terms	Additional closure relations are required for the phase velocities
It contains two or three momentum equations which requires more CPU time to calculate	Contains only one momentum equation which requires less CPU time to calculate

The need for early gas detection in during drilling operations, small influx sizes for early kick detection and the presence of bubble or slug flow patterns are paramount for well control.

Those aspects are better represented by the drift-flux model. Furthermore, Recent progress in the development of numerical techniques, fluid flow modelling, and drilling practices has motivated the creation of an advanced multiphase simulator designed for drilling and production operations.

#### *2.4.3. Principle of Flow Patterns for Two-Phase Flow (Gas–Liquid)*

Two-phase gas and liquid flows, as well as the physical processes associated with them are highly complex. If the characteristics of a flexible interface and the degree of compressibility for one of the phases are merged, the flow within each of the phases is going to rely on the geometric pattern. All these features highlight the complex two-way connection between the flow in each phase and the geometry of the two-phase flow [69, 70]. The flow patterns that occur in multiphase flow include:

- Bubble flow where one phase is continuous and the other becomes dispersed as bubbles inside the continuous phase
- Slug Flow where bubbles merge to form larger bubbles.
- Churn flow where the slug flow bubbles break up, resulting in an oscillatory flow regime.
- Annular or Stratified Flow, in which the phases are divided by a wall film and a core flow, and
- Wispy Flow wherein the secondary phase breaks up and generates huge ligaments in the main phase core flow [30, 66, 71-73].

A schematic presentation of the flow patterns indicating the gas-liquid flows classification is shown in **Fig. 2.6 and Table 2.4** [74]. Many researchers have been investigating the bubble flow and found that this occurs under a variety of operating conditions [71].

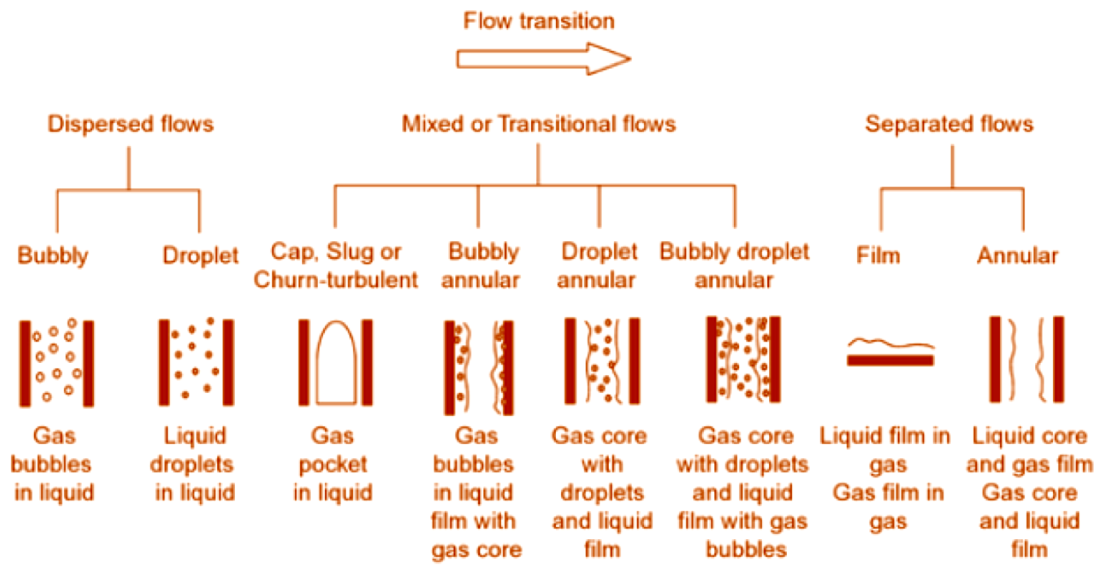

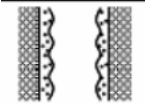
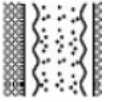
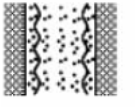
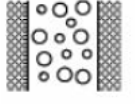
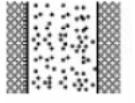
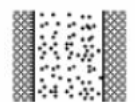


Fig. 2.6 Classification of Gas-Liquid Flows [74]

Table 2.4

Classification of Gas-Liquid Flows (STARCCM+)

Type	Flow Regime	Geometry	Characteristics	Examples
Stratified flows	Film Flow		<ul style="list-style-type: none"> <li>Liquid film in gas</li> <li>Gas film in liquid</li> </ul>	<ul style="list-style-type: none"> <li>Film condensation</li> <li>Film boiling</li> </ul>
	Annular Flow		<ul style="list-style-type: none"> <li>Liquid core and gas film</li> <li>Gas core and liquid film</li> </ul>	<ul style="list-style-type: none"> <li>Boilers</li> <li>Film boiling</li> </ul>
	Jet Flow		Gas pocket in liquid	<ul style="list-style-type: none"> <li>Atomization</li> <li>Jet Condenser</li> </ul>
	Free surface		Tank filled with liquid and gas above	<ul style="list-style-type: none"> <li>Marine towing tank and waves</li> <li>sloshing</li> </ul>

Mixed or transitional flows	Slug flow		Gas pocket in liquid	Sodium boiling in forced convection
	Bubbly annular flow		Gas bubbles in liquid film with gas core	Evaporation with wall nucleation
	Droplet annular flow		Gas core with droplets and liquid film	Steam generator
	Bubbly droplet annular flow		Gas core with droplet and liquid film with gas bubbles	Boiling nuclear reactor channel
Dispersed Flows	Bubbly flow		Gas bubbles in liquid	Chemical reactor
	Droplet flow		Liquid droplets in gas	Spray cooling
	Particulate flow		Solid particles in gas or liquid	Transportation of power

### 2.5. Early Kick Detection (EKD)

The well control system's early kick detection (EKD) component is essential. Because Deepwater drilling operations include complicated equipment and processes, it is very important to prevent or control the incidence of kicks and/or fluid loss during drilling operations. Because of non-productive time (NPT) and/or blowout incidents, well control failure events may often cost the oil and gas sector billions of dollars annually and jeopardise the safety of drilling personnel. Deepwater drilling is a complicated process, and many of these wells have tight pressure margins between the fracture gradient and pore pressure. These factors increase the possibility of unforeseen occurrences like fluid loss or kick. Oil

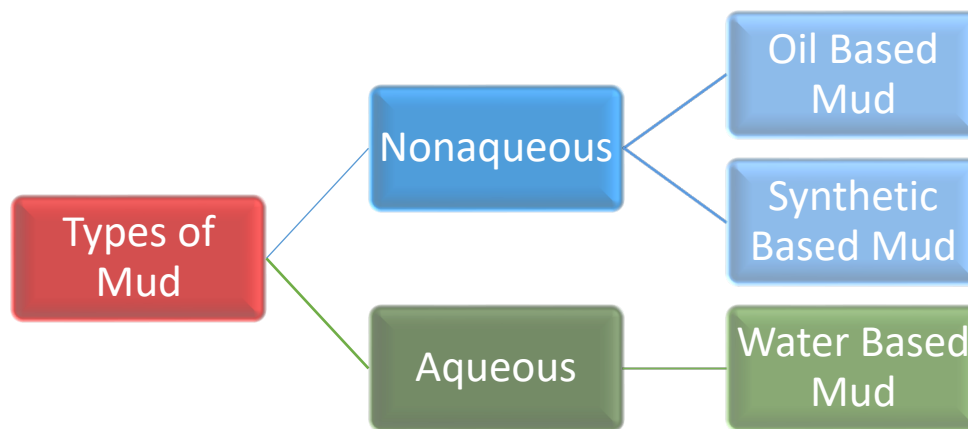
and gas operators are always working to increase drilling efficiency and comprehend downhole fluid behaviour to thrive and expand, given the scope of these difficult drilling operations. EKD improves the efficiency of the wellbore mitigation plan by incorporating a straightforward model of gas influx dynamics in the annulus of the wellbore. Modelling the transient multi-phase flow characteristics along with the dynamics of gas intrusion in the wellbore annulus is highly advantageous. [30].

### *2.5.1. Surface monitoring parameters for early gas kick detection (EKD)*

**Rommetveit** [51] mentioned that the main parameters considered to monitor early kick detection (EKD) in well drilling are: well head pressure (WHP), pit gain volume, drilling fluid flow in and out, Pressure-Volume-Temperature (PVT) of the drilling fluid and choke pressure. These parameters are critical to evaluate bottomhole pressure, pore pressure of the reservoir and kill mud properties for gas kick scenarios and advanced well control. The drilling fluid in the well annulus displaced by gas influx, which lead raise in the mud level in the storage tanks. To detect this gas kick this, rise in volume of the mud should be accurately measured. Yin [75] reported that a large fraction of entering gas can be soluble in the drilling fluid especially in oil based drilling fluids (OBM) and synthetic based drilling fluids (SBM) at the bottom of the well pressure and temperature conditions, so it is very difficult to identify the incidence of gas influx in terms of pit gain to confirm gas kick scenario, especially in high pressure high temperature drilling operations (HTHP).

Drilling fluid function is to remove the rock particles from the well during drilling and to maintain the wellbore thermal stability during drilling operations to reduce the temperature of the drill bit. At present, aqueous Water Based Mud (WBM), non-aqueous Synthetic Based Mud (SBM) and Oil Based Mud (OBM) are three drilling mixtures considered widely for wellbore drilling process as shown in **Fig.2.7**. Nonaqueous drilling fluids such as OBM and

SBM used in HPHT deep well drilling operation because they are better thermal stability under HPHT deep well drilling.



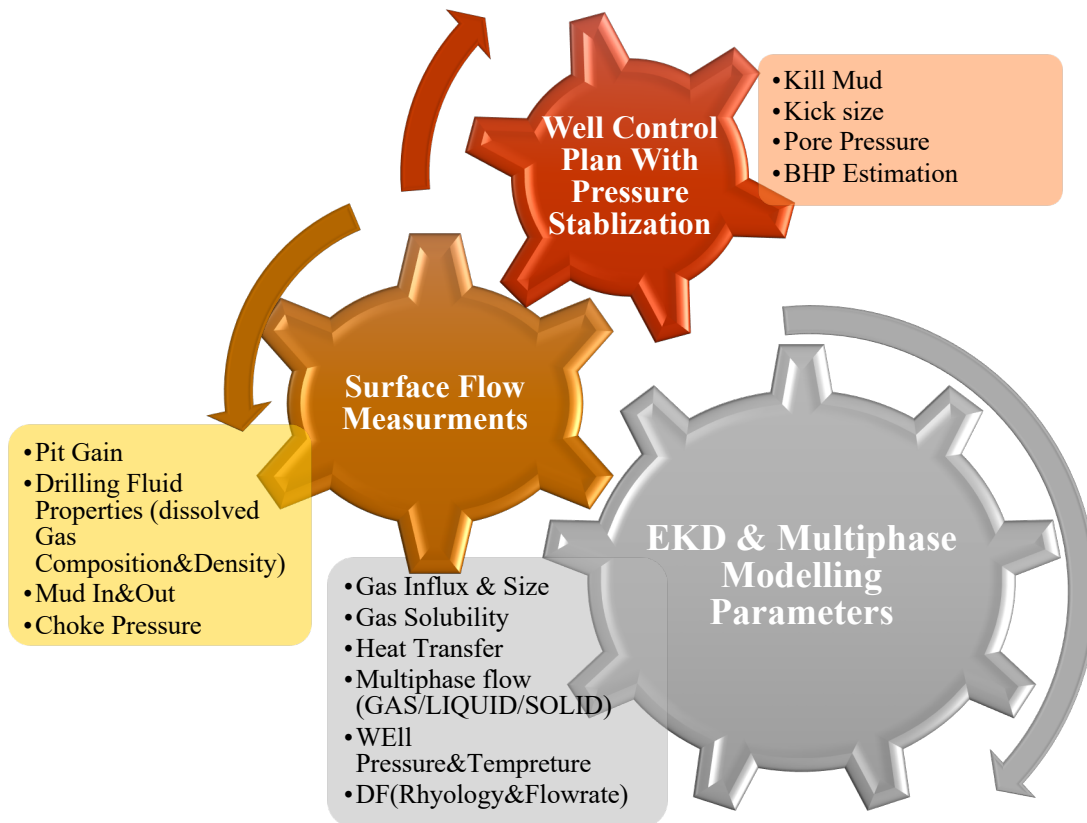
**Fig. 2.7** Types of Drilling Mud used in drilling process

**Agbakwum, Amin, and Yin** [75-77] mention that when a gas kick reaches the riser of the well at lower pressure and temperature, the gas will expand with a higher rate displacing drilling fluid rapidly in a very short period, causing blowout as the well control and any mitigation procedures will be impossible in such short period. Due to the consequences risks and hazard, researchers are effectively studying time detection of gas kick as it's extremely important to prevent any blowouts.

#### 2.5.2. *EKD influencing factors for modelling*

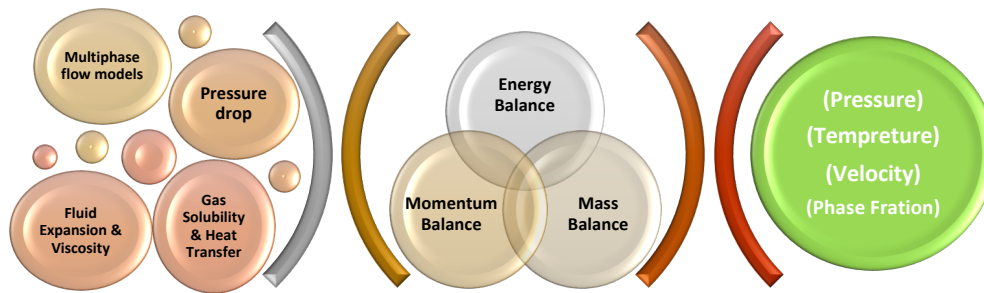
The early kick detection depends on various parameters as mentioned in **Fig.2.8**. The mud flow rate in the annulus depends on gas expansion rate and gas rise velocity, which depend on the pressure and temperature across the well depth. Hence, for modelling early kick detection, it is essential to include heat and momentum transport, gas and liquid Pressure-Volume-Temperature (PVT) relations, and the formulation of governing equations for mass, momentum, and energy. These equations generate constitutive equations, including mass and momentum balances for different well depths. These balances are expressed in terms of

variables such as wellbore fluid density, fluid velocity, cross-sectional flow area, and other pertinent factors required to solve fluid flow.



**Fig. 2.8** Early Kick Detection modelling parameters in well control process

**Avelar, Mao, Rommetveit, Sun, and Xu** [51, 57, 78-80] reported in the open literature all mathematical governing conservation equations used to solve numerically and analytically mass free gas and mud, momentum, and energy. **Fig.2.9** shows the early kick detection modelling to solve for pressure, temperature, and phase behaviour in wellbore.



**Fig. 2.9** EKD Multiphase Modelling Parameters

In the literature found that electrical resistance technology, ultrasonic, hydrostatic, video, and other several technologies have been used to detect kicks [25, 28, 81]. However, these sensors are very expensive but it's very important to identify the gas kick size, gas flow regime in the annulus and BHP.

### **Brief conclusion**

The theoretical basis of multiphase fluid flow is critically reviewed, incorporating solid knowledge from previously reported approaches in Multi-Phase Flow Modelling. In the field of drilling engineering, determining a flow-pattern image is essential for simulating two-phase or three-phase flow in pipe or annular geometries. Flow shape characterization has historically been used to assess drilling and production performance, influencing physical phenomena like mass, heat exchange, and pressure drop. Establishing an experimental model for the two-phase flow condition of a gas kick can be challenging and expensive. Due to the harmful effects of gas kicks and the high-pressure conditions required to replicate bottom-hole conditions, an accurate conceptual and computational model becomes a crucial alternative.



## CHAPTER 3

### Literature review

#### Outline of the chapter

The review discusses the multiphase flow modelling approaches at different operational conditions and the widely accepted idea of flow pattern visualisations. Their advantages and disadvantages and common two-phase flow characteristics in vertical pipes have also been highlighted where the fundamental definitions of the single-phase flow equations that regulate the flow were reconsidered. These have been followed by the review on methods for simulating two-phase flows based on their degree of complexity have been reviewed in detail. Furthermore, this research was conducted to expand the use of Computational Fluid Dynamics from one-dimension mechanistic models to multiphase flow modelling techniques.

#### 3. Multiphase flow model for different operation conditions

##### *3.1. Two phases flow*

**Spoerker** [58] use an artificial tracking method which is volume of fluid method (VOF) to simulate the unsteady of incompressible drilling fluid and compressible gas, considering turbulence and non-Newtonian rheology, focus on bottom hole region in vertical well.

Adding that FLUENT used for transient simulation of gas influx in drilling fluid during kick, using 2d axisymmetric of area near the wellbore with 3m length, constant Pressure boundary condition, rotating drill string, and considered gravity. Following the completion of the simulation work, the research revealed a consistent occupation of 85% of the available space by the gas phase. They notice that the flow regimes can change their characteristics along the wellbore. **Spoerker** [58] recommend further research needs in phase interface due to the presence of small fluid droplets, also take in consideration cuttings effect.

**Bacon** [59] proposed technique offers accurate determination of influx cessation, even when compressibility is significant. New pressure and pressure derivative-based parameters that carry the signature of influx cessation are defined. The moment of influx cessation during the proposed dynamic well control method is given by pressure-based signatures. Incorporated into these signatures is a transient, non-dimensional term defined as the 'Pressure Transfer Parameter (PTP). The PTP physically represents the response of BHP to changes in Well Head Pressure (WHP) during dynamic well control, and the influence of influx compressibility and volumetric changes within the annulus on the transfer of pressure. It is shown that the behavior of this parameter carries important information regarding the progress of dynamic well control and can be used to determine when influx has ceased. The results of this work are expected to improve the reliability of dynamic well control using ABP during Managed Pressure Drilling operations. Further, the new signature parameters are easy to monitor and interpret, and together with flow rate provide valuable additional information to assist dynamic well control; minimize influx size, reduce, or eliminate excessive backpressure during dynamic well control, and provide a more positive indication of influx cessation for the case of compressible influx fluid. Several numerical simulations using a transient, multiphase flow simulator support the key analytical conclusions of this work and validate the new pressure-based well control signatures. **Bacon** [59] recommend

further work is ongoing to refine the proposed dynamic well control approach and to extend its applicability to other well control situations and techniques, as using Pressure Transfer Parameter (PTP) to convey valuable information about MPD operation.

**Aarsnes** [44] develop simple models of gas liquid two-phase flow in drilling for control and estimation applications. A simulation study evaluates 3 different gas-liquid scenarios in drilling, the Mathematical structure, Closure Relations, and the Numerical Scheme are three components which make up a complete simulation model as shown in **Table 3.1**.

In the simulations study, a total of 6 models are used for the kick scenario and 5 for the two UBD scenarios. Use OLGA simulator as reference to illustrate the dynamics that recreate with the simpler models. At this point the paper does not evaluate quantitative performance of the models, as this is mainly determined by which closure relations are used and these are beyond the scope of this paper. The models considered in this paper follows the simplification processes. **Table 3.2** shows the ability of models used in the simulation study to qualitatively represent dynamics in different scenarios.

**Table 3.1**

The three components of a complete simulation model.

Mathematical structure	Closure Relations	Numerical scheme
<ul style="list-style-type: none"> <li>PDE or ODE</li> </ul>	<ul style="list-style-type: none"> <li>Slip law</li> </ul>	<ul style="list-style-type: none"> <li>Numerical accuracy</li> </ul>
<ul style="list-style-type: none"> <li>Hyperbolic or Parabolic PDE</li> </ul>	<ul style="list-style-type: none"> <li>Equation of state</li> </ul>	<ul style="list-style-type: none"> <li>Numerical stability / robustness</li> </ul>
<ul style="list-style-type: none"> <li>Number of equations</li> </ul>	<ul style="list-style-type: none"> <li>Frictional Pressure Loss</li> </ul>	<ul style="list-style-type: none"> <li>Implementation complexity</li> </ul>
<ul style="list-style-type: none"> <li>Stiffness</li> </ul>	<ul style="list-style-type: none"> <li>Other Source terms</li> </ul>	<ul style="list-style-type: none"> <li>Solution speed</li> </ul>

**Table 3.2**

Ability of models used in the simulation study to qualitatively represent dynamics in given scenario.

Model	Equations	Reference	Scenario Suitability		
			Scenario 1	Scenario 2	Scenario 3
<b>High fidelity models:</b>	OLGA Simulator	[49]	<i>Reference model</i>		
<b>Drift-flux Models:</b>					
<b>Full DFM</b>	$\frac{\partial}{\partial t}(\alpha_g \rho_g) + \frac{\partial}{\partial x}(\alpha_g \rho_g v_g) = \Gamma$ $\frac{\partial}{\partial t}(\alpha_\ell \rho_\ell) + \frac{\partial}{\partial x}(\alpha_\ell \rho_\ell v_\ell) = -\Gamma$ $\frac{\partial}{\partial t}(\alpha_\ell \rho_\ell v_\ell + \alpha_g \rho_g v_g) + \frac{\partial}{\partial x}(\alpha_\ell \rho_\ell v_\ell^2 + \alpha_g \rho_g v_g^2 + P) = -F - G,$	[60]	<i>Good</i>	<i>Good</i>	<i>Good</i>
<b>Red DFM</b>	$\dot{p}_a = \frac{\beta_a}{V_a}(q_{inj} - q_c + q_{res} + A \int_0^L E_G dx),$ $E_G = \frac{\alpha_g(1 - C_0 \alpha_g) \alpha_\ell}{\gamma} \frac{1}{P} \left( \frac{\partial P}{\partial t} + v_g \frac{\partial P}{\partial x} \right),$ $\frac{\partial \alpha_g}{\partial t} + v_g \frac{\partial \alpha_g}{\partial x} = E_G,$	[61]	<i>Good</i>	<i>Good</i>	<i>Good</i>
<b>ODE models:</b>					
<b>LOL mod</b>	$\dot{n}_d = W_{g,inj} - W_{g,bit}$ $\dot{m}_d = W_{\ell,inj} - W_{\ell,bit}$	[62]	<i>Poor</i>	<i>Fair</i>	<i>Fair</i>
<b>1-ph mod</b>	$\dot{p}_a = \frac{\beta_a}{V_a}(q_p + q_{res} - q_c).$	[63]	<i>Poor</i>	<i>Poor</i>	<i>Poor</i>
<b>Lagrangian</b>	$\dot{L}_1 = - \frac{2(q_c - q_{bit})}{A_p \alpha_{dist}} + v_g$ $\dot{V}_G = q_c - q_{bit}.$	[64]	<i>Good</i>	<i>N/A</i>	<i>N/A</i>

Aarsnes [44] mention that one of the key challenges for future work involves addressing the need to tailor closure relations for simplified models and exploring effective ways to integrate them with estimation techniques. Additionally, tackling the robust design of controllers and

estimators directly based on partial differential equations (PDEs) remains a challenge, given the intricate nature of many proposed solutions in this domain.

**Rommetveit** [65] indicate the necessity for advanced numerical simulators capable of integrating various technologies. Develop a grid that encompasses three distinct phase regions: a) Gas, b) Liquid, and c) Gas and Liquid. Determine critical pressure values for each discrete temperature to accurately calculate parameters near phase boundaries. Through interpolation, determine gas fraction, gas density, fluid density, and other thermodynamic properties of the mixture when the fluid is at a specific pressure and temperature. The model calculates, at each time step, the total gas and liquid in each numerical box. As the fluid transitions to the next box in the subsequent timestep, any difference in the amount of gas required for saturation becomes free gas.

**Rommetveit** [65] found the development of measurement and well control tools highlights the importance of having sophisticated simulator software as an essential component. This software enhances the utilization of technology by optimizing the information extracted from measurements and providing suggestions or direct control over tools. By doing so, it contributes to making future well operations safer, more cost-effective, and facilitating drilling operations that might otherwise be challenging. Understanding the dynamic physics and chemistry occurring in the well during operations is crucial. The presented dynamic model has demonstrated the necessary flexibility and accuracy to become an integral element of advanced well construction control systems.

**Patrício** [66] introduce a two-phase flow model (DFM) designed for automated control, validated through kick experiments conducted across the entire range of operating conditions. The model makes specific assumptions such as isothermal flow, no mass transfer between phases, pressure-dependent flow, utilization of an empirical slip equation establishing a

relationship between phase velocities, and consideration of the relative volume change of the fluid. **Patrício** [66] found that the design of the experimental unit was formulated through dimensional analysis, assessing geometries, optimal operational conditions, and achieving similarity. The obtained similarity between the experimental unit (model) and an actual well configuration (prototype) underscores the significance of the experimental results in relation to field conditions.

### *3.2. Three phases flow*

**Xie** [53] developed a gas-liquid-solid flow model that incorporates the impact of cuttings on the pressure drop in annular flow within deep wells, a numerical code is created to compute thermal and flow parameters, including temperature and pressure distributions. The model's validity is confirmed through field data, and its efficacy is compared with various commercial software. The study investigates the influence of key parameters, such as well depth, gas kick, cuttings, and drilling fluid properties, on temperature and pressure distributions. The formulation involves several assumptions to create a steady-state thermal model for describing the heat transfer process. **Xie** [53] found that temperature and pressure experience significant variations influenced by factors such as well depth, drilling mud density, and the presence of a gas kick. Additionally, drilling mud viscosity has a minor impact on overall pressure. Moreover, as the gas kick volume increases, multiple flow patterns emerge along the wellbore, and the transition from bubble flow to slug flow occurs at greater depths. The magnitude of pressure is notably affected by the gas kick, with larger gas kick volumes resulting in reduced pressure. This reduction is attributed to the lower density of the drilling fluid, leading to a diminished gravitational force at the bottomhole. **Xie** [53] observed that cuttings do indeed impact pressure, but the magnitude of their influence is relatively modest. The effect of cuttings on the overall pressure drop is determined to be minimal. Well depth,

drilling mud density, and the presence of a gas kick significantly affect both temperature and pressure. Although drilling mud viscosity has a limited impact on total pressure, it can notably influence temperature distributions within the annulus.

**Ghobadpouri** [67] in this investigation, a numerical simulation is conducted to model gas-liquid-solid three-phase flow within the wellbore annulus, employing the actual dimensions of the well. A one-dimensional steady-state three-fluid model in the Eulerian frame of reference is utilized for simulating the three-phase flow. The accuracy of the results is validated against both actual field data and the outcomes of a gas-liquid two-phase flow model. Comparative analysis reveals that the three-phase numerical simulation provides superior accuracy in predicting bottomhole pressure (BHP) compared to the two-phase numerical simulation and various other models employing a mechanistic approach. The impact of incorporating a solid phase on BHP prediction is heightened with increased drilling velocity, larger cutting size, and reduced liquid and gas flow rates.

**Dabiri** [68] state that to explore the pressure profile while accounting for wellbore influx, an analytical solution for aerated mud was utilized. Additionally, a numerical simulation, employing the transient Eulerian model flow with the turbulence  $k$ - $\epsilon$  model, was conducted to simulate three-phase flow within the annulus. The investigation also took into account the influence of solid particle size and the rotation of the inner pipe on the pressure drop. **Dabiri** [68] observed that the pressure drop exhibited a significant increase with larger solid particle sizes, while it remained relatively constant with an increase in the rotation of the inner pipe. The findings indicated that Computational Fluid Dynamics (CFD) demonstrated excellent potential for simulating three-phase flow systems. The velocity was observed to sharply decrease with radius in a region near the inner pipe and gradually approach zero at the outer casing wall. The axial velocity of water and solids at the narrow gap side neared zero, even with a high pipe rotary speed. However, in a low eccentricity annulus where the narrower

side widens, pipe rotation can introduce more fluid particles through the narrow gap over a specific period. A comparison of analytical and numerical results with published experimental data showed good agreement.

**Liao** [69] investigate a dynamic gas-liquid-solid multiphase flow model for gas kick, taking into account the influence of dynamic wellhead back-pressure, temperature field, and the velocity relationship among different phases. **Liao** [69] revealed that in the initial stages, the expanding gas during a gas kick is limited due to the high pressure at the bottom-hole. Consequently, there is an almost linear relationship between the pit gain and outlet flow rate increase, and the decrease in bottom-hole pressure. As the invading gas continues to migrate and expand upwards, the pit gain and outlet flow rate further rise, and the speed continues to increase until the gas reaches the wellhead, reaching its peak outlet flow rate. During the upward migration, the expanding gas in the wellbore leads to a non-linear correlation between wellbore back-pressure and bottom-hole pressure. The maximum wellhead back-pressure tends to increase with greater well depth, albeit the increase is minimal and nearly negligible.

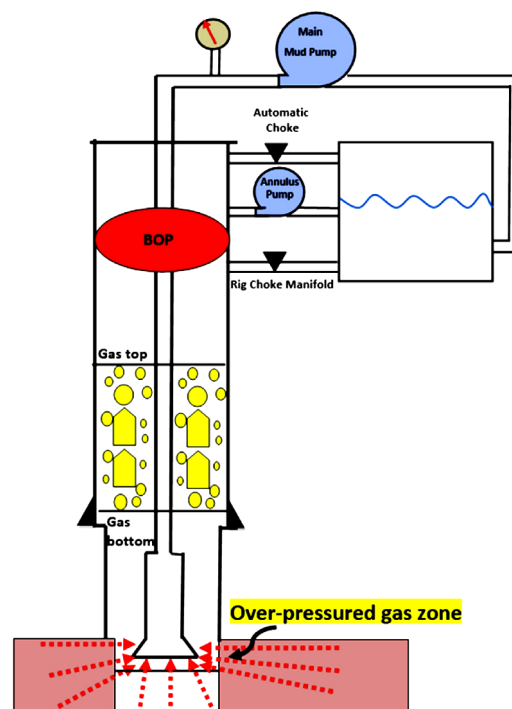
### *3.3. Managed Pressure Drilling (MPD)*

Managed Pressure Drilling (MPD) constitutes a set of techniques designed to regulate the annular pressure profile by manipulating wellhead pressure, drilling fluid density, and flow rate simultaneously. By offering the capability to adjust back-pressure, MPD allows for the control of influx without the conventional method of shutting in the well. This approach involves closely managing wellbore pressures within the pore pressure/fracture pressure window, thereby enhancing the chances of successful well control and minimizing non-productive time. The practice of well control without the conventional shut-in is termed dynamic well control.



In the MPD context, when an influx is detected, a crucial decision is determining whether to employ dynamic well control instead of conventional well control. Dynamic well control is effective within certain limits of influx size and rate, ensuring safe and efficient control and circulation of the influx out of the system. An essential aspect in deciding the application of dynamic well control is the quantification of peak surface flow rates and identifying the point at which conventional shut-in would no longer be safe. When applied judiciously, dynamic well control facilitates faster management of an influx, leading to a significant reduction in non-productive time.

**Ambrus** [61] stated that constant bottom-hole pressure (CBHP) method uses a choke valve at the surface to apply backpressure by manipulating the choke orifice size and either trapping pressure passively against the mud pumps or adding pressure actively through a dedicated back-pressure pump. The CBHP MPD technique enables circulating small and medium size influxes out of the well without requiring a shut-in operation as shown in **Fig. 3.1**.



**Fig. 3.1** Schematic View of CBHP MPD set up during influx removal [61].

**Ambrus** [61] claim that reduced Drift-Flux approach used in this paper in modelling multi-phase well control situations preserves the transient multi-phase behaviour of liquids and gas in the well and suited for real-time decision making and automated well control applications, and particularly for MPD purposes. The model is designed to predict and regulate surface pressures in response to a well control event, considering the specific size and intensity of a kick. Its accuracy is verified by comparing the model's predictions with experimental data obtained from Louisiana State University, which conducted tests involving a simulated gas kick event in a test well. Additionally, the model's performance is assessed by comparing it to a well control scenario simulated using a widely utilized commercial multi-phase flow simulator within the industry. The results demonstrate favourable agreement between the proposed model, experimental data, and the outcomes of the commercial simulator.

**Ma** [45] mention that the experimental data set from a test well used to validate the proposed drift-flux model. Natural gas was injected through diameter tubing and water-based mud was pumped down the annulus formed by the presence of drill pipe and the gas injection tubing. The return flow was taken through the annulus. During the experiment, gas was injected into the well during mud circulation. Then, after the influx was detected, a manual choke was used to keep the BHP constant while removing the influx. A mud gas separator was used to divert the gas to a flare. Standpipe pressure, casing and gas injection pressures, mud flow rate in (computed from pump strokes), mud flow rate out, gas injection rate and total mud volume were recorded during the test and compared with the simulation results.

**Ma** [45] had found that after early influx detection, automatic choke control can be used for dynamic well control, for instance by increasing surface back-pressure to arrest the influx followed by a controlled circulation out of the hole. The advanced modelling approach and new software package described here are capable of simulating complex multi-phase flow phenomena that can occur during MPD and regular drilling operations.

**Liao** [69] the study suggests a dynamic gas-liquid-solid multiphase flow model for gas kicks during Managed Pressure Drilling (MPD). The model takes into account the impact of dynamic wellhead back-pressure, temperature distribution, and the velocity relationships among various phases. The research employs numerical simulations to investigate the behaviour of the multiphase flow. Liao [69] underscores the crucial importance of having a well-designed and accurate wellbore multiphase flow model for understanding real-time wellhead back-pressure control and the response patterns of outlet flow rates.

**Chen** [71] summarize focuses on the application of Nonlinear Model Predictive Controllers (NMPC) algorithms in the automatic control technology of Managed Pressure Drilling (MPD). The use of NMPC algorithms is highlighted for real-time intelligent optimization and decision-making in MPD operations. **Chen** [71] the model is designed to detect gas kick signals and, when combined with Managed Pressure Drilling (MPD) technology, rapidly identify and control wellhead conditions intelligently. The system achieves intelligent detection of automatic overflow conditions, as illustrated in **Fig. 3.2**. It utilizes optimization algorithms to minimize the error functional, obtaining the distribution of physical parameters for improved control.



**Fig.3.2** Integrated schematic of automatic intelligent gas kick condition detection and identification.[71]

### *3.4. Underbalance Drilling (UBD)*

Under-balanced drilling (UBD) is a drilling technique where the pressure at the bottom-hole is intentionally maintained lower than the formation pressure. This is typically achieved by using a two-phase fluid or aerated liquid during drilling. In UBD operations, a gas, such as nitrogen, is injected into the well along with the drilling liquid to ensure that the mud pressure remains below the formation pressure. This approach is employed in situations where it is necessary to keep the Bottom Hole Pressure (BHP) lower than the formation pressure [72].

The successful execution of UBD relies on effectively controlling the flow pressure at the bottom-hole. If the BHP exceeds the formation pressure, the operation shifts from under-balanced drilling to over-balanced drilling (OBD). On the other hand, if the BHP becomes too low compared to the formation pressure, it may result in a well kick or lead to the collapse of the wellbore walls. Therefore, maintaining the bottom-hole pressure within a specific pressure range, known as the pressure window, is crucial for the safe and successful implementation of UBD [72].

**Khezrian** [72] construct a one-dimensional steady-state two-fluid model in the Eulerian frame of reference employed to simulate the two-phase flow in Under-Balanced Drilling (UBD) operations. The simulation involves the calculation of parameters such as pressure, volume fraction, and velocities of the two phases in various flow regimes, including bubbly, slug, and churn turbulent flow. The numerical investigation explores the impact of gas and liquid injection flow rates, as well as choke pressure, on wellbore pressures, with a particular focus on Bottom Hole Pressure (BHP).

To validate the results obtained from the two-fluid model, comparisons are made with actual field data, and the outcomes are contrasted with those from the WELLFLO software utilizing

different mechanistic models. The comparisons demonstrate that the two-fluid model is capable of accurately predicting BHP and other parameters related to two-phase flow, showcasing good agreement with the field data. The study concludes that the flow of aerated mud in UBD operations can be effectively simulated using the two-fluid model for two-phase flow. Finally, **Khezrian** [72] discovered that the choke pressure must not exceed a certain level in order to maintain the well's UBD status.

**Ghobadpouri** [67] simulate gas-liquid-solid three-phase flow in the annulus of a well with actual dimensions, specific considerations are made for under-balanced drilling (UBD) operations. The findings suggest that enhancing gas flow rates, while adhering to Bottom Hole Pressure (BHP) limitations, serves as an effective approach to improve hole cleaning in UBD operations. Additionally, it is identified that a favourable method for enhancing well hole-cleaning in UBD operations, without raising concerns about BHP increases, involves reducing the size of the cuttings.

**Dabiri** [68] generate the pressure profile in Under-Balanced Drilling (UBD) operations using an analytical solution for aerated mud, a numerical simulation was conducted. The simulation employed a transient Eulerian model with the turbulence  $k-\varepsilon$  model to represent three-phase flow in the annulus during UBD. The observations indicated a notable increase in pressure drop with larger solid particle sizes, while it remained nearly constant with increased rotation of the inner pipe. The results highlighted the potential of Computational Fluid Dynamics (CFD) for effectively simulating three-phase flow systems. Comparative analysis with published experimental results demonstrated good agreement between analytical, numerical, and experimental findings.

### *3.5. Gas kick solubility*

**Ma** [73] present hydraulic model to simulate a gas kick in non-aqueous drilling fluids. Using

transient drift-flux based on conservation of mass and momentum also PVT models used to investigate and predict the effect of gas solubility in drilling fluid. A numerical scheme is developed to solve the mathematical equations efficiently and accurately. **Ma** [73] develop model using graphical user interface (GUI) to simulate (CBHP-MPD-driller method-wait and weight method – underbalance drilling – pressurized mud cap drilling – loss of circulation – multiple influxes – handling gas solubility – automated choke control – non-Newtonian drilling fluid – 3d wellbore path (directional – horizontal wells). **Ma** [73] found that gas influx was entirely dissolved in SBM under downhole conditions delaying the kick detection, which demonstrate that the gas solubility in drilling fluid is very important in both planning and operation.

**An** [74] simulate behaviour of kicks in HPHT conditions in offshore wells with OBM, obtaining reliable surface choke pressure with modified two-phase well-control and considering OBM properties. Comparing three cases to analyse effects of gas solubility and mud compressibility during well-control with HPHT, then simulate well-control in two offshore wells.

**An** [74] found realistic modelling with OBM for HPHT wells by considering mud compressibility and solubility of a gas kick in OBM. Gas kick in OBM becomes smaller and reaches the surface later than in WBM. Pit volume in OBM does not always increase as the kick rises to surface because of combined effects of gas solubility, pressure, and temperature on kick volume. Considering mud compressibility, higher surface choke pressure is needed with OBM because of smaller hydrostatic pressure caused by reduced mud density. The difference in surface choke pressure with and without considering OBM density variation in the wellbore can be out of safety margin in HPHT conditions, resulting in well-control problems

**Linga** [75] conduct experiments to investigate gas kick characteristics in High Pressure High Temperature (HPHT) drilling using two classes of Oil Base Drilling Fluid (OBDF), specifically Normal Mineral base oil and linear paraffin base oil, at conditions of 200°C temperature and 1000 bar pressure. The experimental studies aim to determine the behaviour and response of methane in Oil Base Drilling Fluid under these extreme HPHT conditions.

**Linga** [75] Following the experimental studies, it was observed that the maximum methane gas loading capabilities for both classes of Oil Base Drilling Fluid (Normal Mineral base oil and linear paraffin base oil) are similar, exhibiting a linear relationship between maximum gas mass loading and pressure below 400 bars. Additionally, it was found that above the bubble point pressure and temperature, methane is completely dissolved in the diesel, resulting in a single-phase liquid flow. Below the bubble point pressure and temperature, the dissolved methane begins to separate from the diesel, leading to gas-liquid two-phase flow. The model presented satisfactory results when compared with the O'Bryan [81] experimental data.

**Linga** [75] suggested to pursue further research and investigation into a new method for early detection of gas kicks in Oil-Based Mud (OBM) drilling, specifically before the degassing of dissolved gases. Detecting a kick in OBM before the degassing process can be advantageous, as it may allow for easier control compared to Water-Based Mud (WBM), where bottom hole pressure changes more rapidly. This proposed method could enhance the safety and efficiency of drilling operations using OBM.

**Ma** [73] states well control problems caused by gas solubility and predict that the amount of gas that can be dissolved in an oil-based drilling fluid would be 10 to 100 times greater than the water-based fluids. This paper present hydraulic model to simulate a gas kick in non-aqueous drilling fluids, using transient drift-flux based on conservation of mass and

momentum, also PVT models used to investigate and predict the effect of gas solubility in drilling fluid. The maximum amount of dissolved gas in terms of density (solution gas threshold) at a certain pressure and temperature determined by the following equation:

$$\rho_{g,\max} = \frac{R_{sm}(p,t)}{B_m(p,t)} \rho_{g,sc} \quad (55)$$

Where, the gas solubility ( $R_{sm}$ ), mud formation volume factor ( $B_m$ ), the density of gas at standard condition ( $\rho_{g,sc}$ ).

**Ma** [73] found that the new modelling approach ideal for single/multi-phase hydraulic planning/ monitoring. furthermore, the gas influx was entirely dissolved in SBM under downhole conditions. If gas kick remains undetected in non-aqueous drilling fluids, the crew will only have a short period to react before gas reaches the surface. The gas solubility in drilling fluid is important in both planning and operation.

**Jahanpeyma** [76] proposed a mathematical algorithm aimed at simulating gas kicks in oil-based mud. The algorithm seeks to enhance the precision of control parameters by considering the impact of kick fluid dissolution in drilling mud. This is achieved through the application of flash calculations at different depths and time intervals. The study emphasizes that gas bubbles rising towards the surface and expanding can increase surface pressure, affecting equipment life and proper operation. To mitigate this, the crew is advised to promptly prepare new mud, reducing wait times. The dissolution of kick fluid in drilling mud alters the mud density from the bottom hole to the surface, necessitating increased surface choke pressure to maintain bottom-hole pressure.

**Sun** [19] develop an unsteady-state multiphase flow model which consider the dissolving and separating out of gas. The model covers both saturated and unsaturated conditions of oil-based drilling mud. The proposal includes the use of the mass concentration of dissolved gas



in oil-based drilling mud to characterize gas dissolving and separating out in the wellbore. A numerical solution method is implemented, and a new gas solubility correlation is established through the nonlinear least square method. The average predicted error is reduced from 24.1% to 9.3%. Validation is conducted through gas solubility experiments, resulting in discrepancies between predicted and experimental values of 5.22%, 8.06%, and 4.33% for three types of oil-based drilling muds.

**Sun** [19] discovered that in the water-based mud (WBM), the bottom hole pressure rapidly decreases during a gas kick since gas does not dissolve into the WBM. The pit gain of WBM exponentially increases with a growing rate that intensifies over time. Conversely, the pit gain of oil-based mud (OBM) increases linearly, with a constant growth rate. Only when the OBM becomes saturated and some gas begins to separate out, the growth rate of pit gain slightly increases. Utilizing OBM in drilling operations delays the detection time of a gas kick, postponing it by 507 seconds in the case study used. Gas dissolving in OBM only results in a 6.2% increase in the drilling mud outflow rate, concealing the occurrence of a gas kick during drilling. Conventional gas-kick detection methods may not efficiently monitor gas kicks when OBM is used.

**Xu** [77] this investigation introduces a dynamic gas-liquid two-phase flow model that incorporates gas solubility and heat transfer effects to simulate multiphase flow behaviours following a gas kick in oil-based drilling fluids. The governing equations are solved using the finite difference method. The model's predictions of wellbore temperature and pressure distributions align well with field data, affirming the accuracy of the proposed model.

The study reveals that neglecting the gas solubility effect may result in an underestimation of bottomhole pressure by 4.2%, while the bottomhole temperature is overestimated by 3.2%. Additionally, excluding the heat transfer effect could lead to an overestimation of bottomhole

pressure by 11.4% under steady flow conditions. The research indicates that increasing reservoir pressure causes a decrease in bottomhole pressure and an increase in bottomhole temperature. Moreover, a higher reservoir pressure results in a larger gas fraction in the wellbore. However, the impact of reservoir pressure on steady wellbore temperature is marginal. With increasing choke pressure, less gas is present in the annulus in the form of free gas, and choke pressure has a minor effect on wellbore temperature.

**Omrani** [78] develop in this paper a model-based approach enabling the estimation of pressure and flowrate conditions from the borehole to the return line related to a drilling process. Gas kick event is modelled, representing the source of the gas phase, while pumping drilling mud, which represents the liquid phase. A two-phase flow numerical model is developed to solve the phase continuity and momentum equations.

**He** [79] proposes a model for predicting the solubility of  $\text{CO}_2$ ,  $\text{CH}_4$ , and  $\text{C}_2\text{H}_6$  in pure water within the temperature range of 273–448 K and pressures of 0–100 MPa, aiming for an error of less than 5.5%. It is highlighted that the impact of moisture in the gas phase during gas-liquid equilibrium cannot be disregarded. Comparative analysis with existing mixed gas solubility experimental data reveals that the new model successfully predicts the solubility of  $\text{CO}_2$ ,  $\text{CH}_4$ , and  $\text{C}_2\text{H}_6$  in water with an error below 5%. However, the prediction deviation for  $\text{H}_2\text{S}$  exceeds 10%, emphasizing the significance of water in the equilibrium gas phase. The model exhibits accurate predictions for each non-polar gas component. Yet, when polar and non-polar gases are mixed, accurate predictions of gas solubility for each component in water are challenging. The accuracy improves for polar gases when their content is high, while successful predictions are achieved for the water solubility of non-polar gases when their content is low.

**He** [79] recommended to develop a more accurate calculation model and conduct further studies on the solubility of mixed gases. This approach is suggested to ensure the availability of sufficient experimental data, emphasizing the need for continued research to enhance the precision and reliability of solubility predictions, especially in scenarios involving mixed gases.

**Sun** [80] proposes experimental analysis which investigates the phase change of an acid-gas mixture in a wellbore. The findings reveal that, under specific conditions of wellbore temperature and pressure, the acid-gas mixture enters the supercritical phase, exhibiting abrupt changes in its physical properties near the critical point. Taking into account both the phase change and dissolution of the acid-gas mixture in drilling fluids, the multiphase flow experiences transitions between single-phase flow, supercritical-liquid two-phase flow, liquid-liquid two-phase flow, and gas-liquid two-phase flow (including bubbly flow, slug flow, churn flow, and annular flow). As the mixed fluids ascend from the bottom hole to the wellhead, the transformation of flow types, particularly from supercritical-liquid (or liquid-liquid) to gas-liquid flow, can result in significant volume expansion, heightening the risk of a blowout. These results offer guidance for designing hydrostatic parameters during the drilling of acid reservoirs.

### *3.6. Early kick detection (EKD) simulation*

**Rommetveit** [32] stated the primary parameters essential for monitoring early kick detection (EKD) in deep well drilling include wellhead pressure (WHP), pit gain, drilling fluid flow in and out, Pressure-Volume-Temperature (PVT) of the drilling fluid, and choke pressure. These parameters play a crucial role in assessing bottomhole pressure, reservoir pore pressure, and the properties of kill mud during gas kick scenarios and advanced well control. In the context of gas influx displacing the drilling fluid in the well annulus, the rise in mud level in the

storage tanks is indicative of a gas kick. Accurate measurement of this increase in mud volume is necessary for detecting the gas kick effectively.

**Yin** [82] Moreover, a significant portion of the entering gas tends to dissolve in the drilling fluid, particularly in Oil-Based Mud (OBM) and Synthetic-Based Mud (SBM), at the well's bottom. This makes it challenging to confirm the occurrence of a gas influx based on pit gain alone, especially in the context of deep-water High-Temperature High-Pressure (HTHP) drilling.

Prior studies [85, 86] employed a variety of theoretical techniques to analyse the flow behaviour. These models, however, have limitations in terms of flow regime forecasting, and their outputs may not match experimental values [87]. Additionally, few transition models for flow regimes have been developed for annular geometry. However, comparing these models to real experimental data may reveal mistakes and inconsistencies. As a result, improved models and methods must be created to comprehend the flow behaviour inside invisible pipelines and annulus safely and affordably.

**White and Walton** [88] demonstrate computer codes designed for simulating early gas kicks incorporate factors such as wellbore hydrodynamics, temperature models, mud rheology, gas dispersion, gas dissolution, and multiphase flow. However, these models may not accurately capture multiphase characteristics. The authors noted that relying solely on indicators like the rise in pit gain and annuli flow rate may not be sufficient to detect small kicks in Oil-Based Mud (OBM) due to gas saturation.

Furthermore, many available mathematical models for multiphase flow in Early Kick Detection (EKD) simulations utilize one-dimension empirical correlations for factors like heat transfer and gas solubility, often with simplified assumptions. It is acknowledged that these models may not be universally applicable across different ranges and scenarios.

**Podryabinkin** and **Loyseau** [89, 90] recommended the use of appropriate turbulence models, such as the K- $\epsilon$  model, to overcome the limitations present in current one-dimensional models. This is deemed essential for the rapid and accurate identification of gas kicks during drilling operations.

**Lote** [91] conducted a Computational Fluid Dynamics (CFD) analysis focused on the formation of bubbles in a vertically flowing air-water mixture within a pipe. Their model took into account interfacial factors including drag, lift, wall lubrication, and turbulent dispersion.

**Sun** [19] employed Computational Fluid Dynamics (CFD) modelling to simulate gas bubble formation during a gas kick and its impact on temperature and pressure changes. They considered factors such as gas flow rate, density, viscosity, and bubble movement. The study focused on understanding the effects of bubble formation and migration under various pressure and temperature conditions. The conclusion drawn from their findings was that, following a gas kick in the wellbore, there is an accumulation of gas bubbles at the bottom of the well.

**Sutkar** [92] emphasized that solving multiphase systems with three-dimensional equations requires advanced numerical techniques, specifically employing Computational Fluid Dynamics (CFD).

**Lote** [91] conducted a Computational Fluid Dynamics (CFD) analysis to study the formation of bubbles in an upward-flowing air-water mixture within a pipe. Their model accounted for interfacial forces, including drag, lift, wall lubrication, and turbulent dispersion.

**Sun** [20] utilized Computational Fluid Dynamics (CFD) simulation to investigate the formation of gas bubbles during a gas kick and its impact on temperature and pressure variations. The study considered factors such as gas flow rate, density, viscosity, and bubble

movement. The findings suggested that after a gas kick occurs in the well, there is an accumulation of gas bubbles at the bottom of the well. The analysis involved studying the effects of bubble formation and migration under different pressure and temperature variations.

**Guo** [93] employed Computational Fluid Dynamics (CFD) to simulate air-water flow in both wide and narrow annuli using the Volume of Fraction model and K- $\epsilon$  turbulence model. The study involved varying superficial velocities for the air fraction of the air-water system, and the results were successfully validated.

**Sultan** [94-96] utilized Computational Fluid Dynamics (CFD) simulations to investigate multiphase gas-liquid-solid flow in both horizontal and vertical annuli pipes. Their study demonstrated good agreement with experimental data, particularly in predicting pressure loss for various cross-sectional areas (CSA) of the pipe.

**Sleiti** [54] identified a gap in existing studies related to the initial dynamics of gas influx interacting with drilling fluid at the wellbore bottom. Then emphasized the need for the development of more sophisticated two-phase transient models, considering actual mechanistic flow in two-dimensions and three-dimensions well annuli flow. These models would be instrumental in determining drilling liquid velocities (axial, radial), pressure, and temperature patterns as gas bubbles rise against gravity. The recommendation for future research includes advanced two-dimensions and three-dimensions of transient multiphase (gas-liquid) flow models using computational fluid dynamics (CFD) tools. These simulations should consider critical multiphase flow parameters, fluid properties, annular pipe geometry, and employ appropriate turbulence models, such as K- $\epsilon$ . Utilizing advanced turbulence models in two-dimensions and three-dimensions flow simulations has the potential to

improve accuracy in calculating phase velocities, temperature, and pressure patterns within wellbore annuli, thereby advancing early gas-kick detection capabilities.

### 3.7. Summary of the chapter

**Table 3.3**  
Literature Review Summary

Computational Approach	Authors	Limitations	Considerations
<b>Two-phase fluid flow</b>	Spoerker, et al (2012)	Neglecting cutting effect, gas solubility	Non-Newtonian rheology & Turbulence & Compressible gas & incompressible D.F & unsteady
	Bacon, et al (2012)	Neglecting effect of cuttings and neglecting solubility of gas in mud	Considering the effect of compressibility on dynamic well control
	U.J.F., et al (2016)	Neglecting effect of cuttings and neglecting solubility of gas in mud	
	Rommetveit, et al (2008)	All variables depend on only one spatial dimension	Considering effect of cuttings and considering solubility of gas in mud
	Patrício, et al (2019)	Neglecting effect of cuttings and Neglecting solubility of gas in mud	Evaluate ideal operational conditions. Good similarity between the experimental unit (model) and a real well configuration showing the experimental results relative to field conditions.
<b>Three-phase fluid flow</b>	Xie, et al (2013)	Neglecting solubility	Considering cuttings effect
	(Ghobadpouri, et al (2017)	Neglecting solubility of gas in mud	Considering cuttings effect cuttings size & drilling velocity & choke pressure & gas flow rate are assumed constant & follow the geothermal gradient & Assume liquid incompressible

			& 1D flow model.
	Dabiri, et al (2018)	Neglecting solubility of gas in mud	Considering cuttings effect and consider rotation of inner pipe & 2D flow model.
	Liao, et al (2020)	Neglecting solubility of gas in mud	Considering cuttings effect and Drilling fluids and cuttings are incompressible & 1D flow & Gas and liquid phases have the same pressure and temperature & Only gas enters the wellbore, excluding oil and water, and gas influx occurs at the bottom of the well
<b>Managed Pressure Drilling</b>	Aarsnes, et al (2015)	Neglecting effect of cuttings and Neglecting solubility of gas in mud	Considering a reduced Drift-Flux approach to model multi-phase well control situations
	Ma, et al (2016)	Neglecting effect of cuttings and Neglecting solubility of gas in mud	
	Ma, et al (2018)	Neglecting cuttings effect	Considering solubility of gas in mud and use drift-flux model for non-aqueous drilling fluid & considering drilling fluid non-Newtonian
	Liao, et al (2020)	Neglecting solubility of gas in mud	Considering cuttings effect & Drilling fluids and cuttings are incompressible & 1D flow & Gas and liquid phases have the same pressure and temperature & Only gas enters the wellbore, excluding oil and water, and gas influx occurs at the bottom of the well
	Chen, et al (2023)	Review paper that describes the technical characteristics of MPD operations, draws conclusions about several variants of MPD and their applications weather conventional gas kick detection and unconventional gas kick detection, and compares different states of equivalent circulating density (ECD) and bottomhole pressure in conventional drilling and MPD	
<b>Underbalance Drilling</b>	Khezrian, et al (2015)	Neglecting cuttings effect and Neglecting solubility of gas in mud	Assume gas compressible and liquid incompressible Drilling fluids & 1D flow & steady state model
	Ghobadpouri, et	Neglecting solubility of	Considering cuttings effect



	al (2017)	gas in mud	
	Dabiri, et al (2018)	Neglecting solubility of gas in mud	Considering cuttings effect & cuttings size & drilling velocity & choke pressure & gas flow rate are assumed constant & follow the geothermal gradient & Assume liquid incompressible & 1D flow model.
<b>Gas solubility in OBM</b>	An, et al (2015)	Neglecting effect of cuttings	Considering mud compressibility and considering solubility of gas in mud
	Linga, et al (2016)	Neglecting effect of cuttings	Considering solubility of gas in mud
	Ma, et al (2018)	Neglecting effect of cuttings	Considering solubility of gas in mud & assuming non-Newtonian drilling fluid
	Chen, et al (2018)	Neglecting effect of cuttings	Considering solubility of gas in mud
	Jahanpeyma, et al (2018)	Neglecting effect of cuttings	Concurrent well control method considering & considering solubility of gas in mud
	Sun, et al (2019)	Neglecting effect of cuttings	Liquid and the gas phase have same temperature & considering solubility of gas in OBM as a mass transfer
	Xu, et al (2019)	Neglecting effect of cuttings	Considering solubility of gas in OBM as a mass and heat transfer & 1D flow is assumed along the wellbore
	Omrani, et al (2019)	Neglecting effect of cuttings	Considering solubility of gas in OBM
	He, et al (2020)	Neglecting effect of cuttings	Considering solubility of gas in WBM
	Sun, et al (2018)	Neglecting effect of cuttings	Considering solubility of acid gas Co <sub>2</sub> & H <sub>2</sub> S)
<b>EKD simulation models</b>	Bacon, et al (2012)	Neglecting cuttings effect and Neglecting solubility of gas in mud	Considering the effect of compressibility on dynamic well control
	Rommetveit, et al (2008)	All variables depend on only one spatial dimension	Considering effect of cuttings and considering solubility of gas in mud

	Yin, et al (2017)	Neglecting effect of cuttings	Considering solubility of gas in mud
	Podryabinkin, et al (2013)	Neglecting effect of cuttings and Neglecting solubility of gas in mud	Considering rotation and eccentricity of the drill string
	Sleiti, et al (2020)	<p>Highlights a common limitation in existing kick models, these models typically lack the capability to account for the dynamic changes in fluid phase fraction over time, especially as a kick is occurring.</p> <p>Suggests a need for more comprehensive models that can capture the evolving nature of fluid phase fractions during a kick event.</p> <p>Collect Literature studies on the Transient-ID-two phase EKD simulation models.</p>	
	Meng, et al. (2015)	Neglecting solubility of gas in mud	1-D Transient two-phase flow, Drift Flux Model (General and modified), Lab experiments validation
	Ambrus, et al. (2015)	1-D Transient two-phase flow, Reduced Drift Flux Model approach, Experimental mid commercial simulator Validated, Assumed constant T and geothermal gradient	
	Wang, et al. (2016)	Assumed Constant drilling fluid viscosity	1-D- Transient G-L for WBM, Flow patten independent DFM, Experimental data
	Yin, et al. (2017)		1-D Transient two-phase flow, OBM, published data
	Xu, et al. (2018)	1-D Transient two-phase flow, DFM with Shi Correlation, Experimental and field data Validated: transient T and BHP, Inlet phase mass assumed zero	
	Xu, et al. (2019)	Transient, 1-D, Two-phase flow (G-L) OBM, Drift Flux Model with Shi Correlation, Both, Field and Experimental data Parameters: Pit gain, BHP with time	
	Yang, et al. (2019a, b)	Transient, 1-D, two phase flow (G-L) OBM, Drift Flux Model with Shi Correlation, Both Field and Experimental data Parameters: Pit gain, BHP with time	
	Mao, et al. (2019)	Transient, 1-D, two phase flow (G-L) OBM and for gas (CH <sub>4</sub> + H <sub>2</sub> S), DFM with different C <sub>o</sub> and V <sub>d</sub> . correlation for bubble, slug, chum, Experimental data of BHP, pit gain, H <sub>2</sub> S solubility via PR – EOS, Used empirical correlation	

	Manikonda, et al. (2019)	No Validation, Heat Transfer not studied assumed linear variation of T, Mud friction loss is reduced to zero, Used constant gas influx.	Transient 1-D, two Phase flow WBM, OBM, DFM, Taylor bubble flow through annuli, Semi Analytical Models, Gas solubility correl., Four correlation model of $B_0$ (for mud)
	Chandrasekaran, et al (2019)	Transient 1-D, two Phase flow, OBM, DFM with Shi correl. with $C_0 = 1-1.2$ and $V_d = 0.55$ m/s, Experimental data, Wall and gravity friction correlation, Averaged Mixture calculated Empirical correlation of $\rho_L$ and $\rho_g$ , Mixture calculated using phase fraction	
	Sun, et al. (2019a)	Steady state Temperature model by Kabir, Ideal gas law, $\rho_s$	1-D Transient, two-Phase flow, OBM and WBM, Drift Flux Model, Developed new gas solubility correlation, Experimental data for gas solubility

### Brief conclusion

The review examines various approaches to modelling multiphase flow in diverse operational conditions, focusing on flow pattern visualizations and discussing their pros and cons. It highlights typical characteristics of two-phase flow in vertical pipes, reassessing fundamental definitions of single-phase flow equations. The review also scrutinizes methods for simulating two-phase flows based on their complexity levels.

## CHAPTER 4

# Modelling and validating water-air multiphase flow in different geometries

### Outline of the chapter

This chapter aims to investigate two-phase flow drilling fluid and gas in an annulus of a drilling well using CFD simulation. This would advance our extant understanding about the gas-kick dynamics. The study involved a sensitivity analysis of different drilling conditions to understand the parameters that can influence the occurrence of kick the most. Due to the complex nature of two-phase flows, it is necessary to validate the CFD model with experimental data before applying the analysis to more complex systems. Validation of the model based on experimental result and key findings are illustrated with experimental results.

The validation procedures involved comparison of the simulation data with the experimental/laboratory data set available as below:

- I. A single phase (water) through a pipeline.
- II. A single phase (water) through annuli.
- III. A two-phase flow (water-air) through a pipeline.

## 4. Modelling Simulation Methodology and Validation

### 4.1. Research methodology

In the context of petroleum engineering, modelling two-phase flows in pipe or annular geometries, either experimentally or numerically, is a common task. Flow-pattern maps are often employed in this field to identify different flow patterns, serving as a tool to assess transportation of multiphase in petroleum engineering. The way the flow pattern is shaped plays a crucial role in phenomena. When dealing with the multiphase flow scenario, setting up an experimental model is challenging and expensive. The potentially dangerous characteristics of gas kicks and the conditions of extremely high pressure required to replicate drilling well conditions necessitate research on a massive scale experiment scarce in the literature. Instead, researchers often resort to conducting water-air experiments in small-scale test apparatuses to gather information for characterizing the two-phase flow process. Due to the extreme dimensions and pressure conditions involved in gas kicks, there is a greater reliance on reliable theoretical or computational models.

Two-phase flow described mathematically and physically can be approached at different levels of sophistication based on the required information and available resources. In this context, one could conceptualize the flow as consist of one phase region separated by shifting boundaries. The challenges in modelling two-phase flow stem from the dynamic nature of these boundaries and their impact on the overall flow field. Additionally, processes such as heat and mass transfer at the phase interface introduce additional formulas that must be resolved. Attempting to model the detailed distribution of interfaces in both time and space for every flow scenario is impractical. Rather, simplifications are necessary, customised to the degree of data required for certain uses.

The objective of this study is to thoroughly investigate and analyse gas-liquid flow. To accomplish this goal, computational modelling emerges as the most suitable approach.

#### *4.2. Modelling Approach*

Computational fluid dynamics, or CFD, has become a very useful tool for scientists and engineers in recent years. The technological advancements in numerical models, coupled with sophisticated computational systems, have led to remarkable progress in modelling multiphase flows. When it comes to modelling the transient behaviour of a gas kick, Computational Fluid Dynamics poses several challenges. The extreme geometric configuration, with a well depth exceeding 3000 ft and a narrow annular clearance, the uncertainties surrounding the inflowing gas in terms of composition, pressure, and location, and the demand for high spatial resolution all contribute to the complexity of modelling multiphase flows, making it a computational challenge.

Computational Fluid Dynamics (CFD) is the most detailed and accurate approach for modelling multiphase flow compared to the previously mentioned methods, but it may also be the most computationally expensive. It is the tool that allows for the most precise modelling of transient flow phenomena. However, multiphase flow modelling using CFD is still not as mature as other simulation branches. Various physical modelling approaches are employed in CFD for the numerical computation of multiphase flows. In general, a CFD modelling approach involves applying several models based on the specific flow problem and the level of detail required. The basic fluid flow is modelled using the conservation laws for mass, momentum, and energy with time-averaged quantities. Turbulence models account for random, brief, and small-scale variations in flow amounts. Various multiphase flow models are approachable based on the flow morphology, and reaction kinetics can be simulated with

an appropriate reaction model. All these models are interconnected through the exchange of flow quantities.

Given these considerations, a comprehensive comprehension of the flow issue is essential for physically significant simplifications. Assumptions about the nature of the gas and the input scenario identifying the dominant forces is essential to determine which physical models are required and which effects can be disregarded. Without these considerations, a complete simulation is not theoretically possible to map the flow problem.

The objective of this study is to enhance the comprehension of gas-kick behaviour through Computational Fluid Dynamics (CFD) simulations and to assess potential simulation strategies.

#### *4.3. Simulation Tool*

The present study utilized the commercially available CFD solver STAR-CCM+ as the primary simulation tool. STAR-CCM+ is an integrated engineering solution for solving multidisciplinary problems, developed by CD-Adapco and initially released in 2004. Employing the finite volume method to discretize transport equations, STAR-CCM+ incorporates various features for multiphase flow analysis. These include volume of fluid methods, Lagrangian particle tracking methods, Eulerian multiphase mixture models such as the Homogeneous Equilibrium Model (HEM) and the Drift Flux Model (DFM), as well as Eulerian-Eulerian dispersed phase models. STAR-CCM+ offers a wide array of mathematical models for transport phenomena and allows enhanced model capabilities through user-defined functions (UDF). In this research, the latter method was employed to calculate gas solubility and mass transfer coefficients.

#### 4.4. Modelling multiphase flows

The co-flow of water and oil, where the two fluids maintain their distinct layers due to differences in density, exemplifies stratified flow. Typically observed in the oil industry during reservoir production, the denser water tends to settle beneath the lighter oil, resulting in stratification with the oil flowing above the water layer.

#### Modelling of Multiphase Flows

- More than one phase present (gas, liquid, solid).
- Diabatic and Adiabatic flows-related to heat transfer (or not).
- Direction of flow: Vertical, horizontal, inclined.
- Different momentum, mass, and energy equations for each phase.
- Closure Models for: Drag force; lift force, etc

For the computational modelling aspect, need:

- The partial differential equations:  $\frac{\partial y}{\partial x}$ ,  $\frac{\partial y}{\partial t}$ , etc. for the momentum, mass, and heat thermal conservation laws.
- Equations of state defining the physical properties
- Semi-empirical relations e.g., for friction factors, or drag coefficients etc....
- Numerical schemes to translate the continuous equations on a mesh.

Four approaches in general are used to model multiphase flows

- Empirical approach: Ignores individual flow regimes and derives empirical equations between variables based on data measurements, usually. e.g., correlating frictional pressure with mass flux.



- Phenomenological approach: Considers calculations for each flow regime. Use Measurements and observations and build physical models of theoretical or semi-theoretical type to describe the phenomena observations; these are sometimes called *mechanistic models*.
- Multifluid approach: Considers the phases as interpenetrating media, with a given volume fraction at any point in time and space. The phases interact via *Interfacial interactions*. Hence looking at momentum, mass, and heat transfers at /the interfaces.
- Computational Fluid Dynamics (CFD): The partial differential equations:  $\frac{\partial y}{\partial x}$ ,  $\frac{\partial y}{\partial t}$ , etc. for the momentum, mass, and heat thermal conservation laws. Equations of state defining the physical properties; Semi-empirical relations e.g., for friction factors, or drag coefficients etc; Numerical schemes to translate the continuous equations on a mesh.

#### 4.4.1. Modelling Geometry

There are two primary methods for defining geometry in STAR-CCM+. Users can either utilize the software's built-in 3D-CAD functionality or import geometry from an external Computer-Aided Design (CAD) package. The 3D-CAD feature allows users to sketch a shape and convert it into a 3D object using tools like extrude, revolve, or sweep, depending on the desired object. Once the 3D-CAD model is finished, it needs to be converted into a new geometry part before application. Alternatively, a part can be created by specifying the object's coordinates based on its dimensions, such as a block, cone, cylinder, or sphere. The part is then divided into various components to establish boundaries. For instance, in simulating pipe flow, components like the pipe's inlet, wall, and pressure outlet must be defined by splitting the part surfaces accordingly. STAR-CCM+ also offers the flexibility of

designing geometry in an external CAD package like Solidworks and importing the finalized model for simulation purposes.

#### *4.4.2. Defining the Simulation Topology*

The architecture of the simulation refers to the arrangement or interrelation of constituent parts inside the simulation boundaries. This process involves transforming faces, edges, and vertices into regions, boundaries, and interfaces that constitute the region utilised for mesh generation and solving the physics of the model. Once the boundaries are established, they can be configured to suit their intended purposes. For instance, in a pipe simulation, the fluid entrance at the top can be designated as a velocity inlet, the pipe itself can be defined as a wall, and the exit can be specified as a pressure outlet.

#### *4.4.3. Meshing*

Meshing is the process of representing a geometric object through a set of finite elements, essentially discretizing the geometry into a representation of the domain. The selection of the mesh for a simulation is dependent on the type of geometry or application in use. The size and type of mesh play a crucial role in determining the accuracy of the solution process and the computational time required for the simulation, making meshing an integral part of the pre-processing step. There are two primary types of meshes: structured and unstructured. Structured meshes have grid points located at the intersections of coordinate system lines, with a fixed number of neighbouring points for interior nodes. They are computationally efficient but challenging to create for intricate geometries. Unstructured meshes have irregularly placed grid points, and the number of neighbouring points can vary from node to node. These meshes are easier to create for complex geometries but come with lower computational efficiency. The base size of the mesh is a crucial factor influencing the size of

the finite elements generated, and it directly impacts the accuracy of the simulation results. A high-quality mesh is essential for the successful execution of a simulation.

#### 4.4.4. Solver

The physics models in the simulation encompass the settings that dictate how the software will solve equations related to the represented flow. The key aspects of the physics models utilized for simulating multiphase flows include spatial dimensions, temporal characteristics, material properties, multiphase model, and viscous regime. Spatial dimensions can be either two-dimensional or three-dimensional. The temporal model can be steady or unsteady, with unsteady further classified as implicit or explicit. Material properties involve categorization into solid, liquid, gas, or, in this project's context, Eulerian multiphase. The chosen Eulerian multiphase model for this investigation is the Volume of Fluid model. The viscous regime can be specified as laminar, turbulent, or inviscid, depending on the model selection. Additionally, an optional model allows for the inclusion of gravity effects in the simulation.

#### 4.4.5. CFD Tools

The "tools" section within the solver encompasses various objects employed to facilitate the Computational Fluid Dynamics (CFD) process. Notable components in this investigation include coordinate systems, field functions, and engineering units. Coordinate systems are available in Cartesian ( $x, y, z$ ), cylindrical ( $r, \Theta, z$ ), and spherical ( $r, \Theta, \Phi$ ) forms. Field functions play a crucial role in retrieving or modifying data related to variable fields defined on sections, particularly significant in multiphase flows for delineating the distribution of materials or phases within the model. Engineering units define the units applied when solving the modelled flow.

#### 4.4.6. Analysis

STAR-CCM+ offers a range of features to users, including derived parts, scenes for visualizing solutions, reports, monitors, and plots. Derived parts are additional components that can be added to the model to assist in analysis without impacting the simulation. These can include points, lines, or planes that aid in studying different sections of the model. For example, a plane section can be added to view the middle section of a three-dimensional representation. Scenes are used to visualize specific aspects of the simulation. Different types of scenes include geometry scenes for displaying surface geometry, mesh scenes for visualizing mesh grid lines and surfaces, scalar scenes for viewing scalar fields like volume fraction in multiphase flows, and vector scenes for displaying vector fields such as velocity or flow direction. Scenes are highly flexible, allowing users to customize angles, transparency, and other elements to meet their requirements. Users can also save snapshots of scene updates for future reference.

#### 4.4.7. Volume of Fluid (VOF) Method

The Volume of Fluid (VOF) method is a free-surface modelling technique employed for solving the Navier-Stokes equations (NSE) in multiphase flows, representing an individual cell that contains a specific fluid (e.g., water). In this approach, the CFD package solves the NSE for the given cell using the properties of the fluid, including pressure and density. In multiphase flows, a cell may contain more than one fluid, such as water and air. To solve the NSE in such cases, the solver determines the fraction of each fluid in the cell, assigning values like one for water and zero for air. The solver then calculates average values for each required property to solve the NSE. This process is repeated for every cell in the domain at each time-step during the simulation.

There are two primary approaches in CFD packages for multiphase flow: Eulerian and Lagrangian. The Volume of Fluid method employs the Eulerian approach to solve the flow equations, and it was initially introduced by Noh & Woodward in 1976 [122].

#### *4.5. Modelling and validation cases*

The application of CFD for complex flow geometries used in oilfield operations are getting more widespread, but there is scarcity of experimental data in the field especially for two-phase drilling fluid and gas kick (methane gas). This study aims to investigate two-phase flow drilling fluid and gas in an annulus of a drilling well using CFD simulation. This would advance our extant understanding about the gas-kick dynamics. The study involved a sensitivity analysis of different drilling conditions to understand the parameters that can influence the occurrence of kick the most.

##### *4.5.1. Validation procedure and experimental data acquisition*

The validation procedures involved comparison of the simulation data with the experimental/laboratory data set available as below:

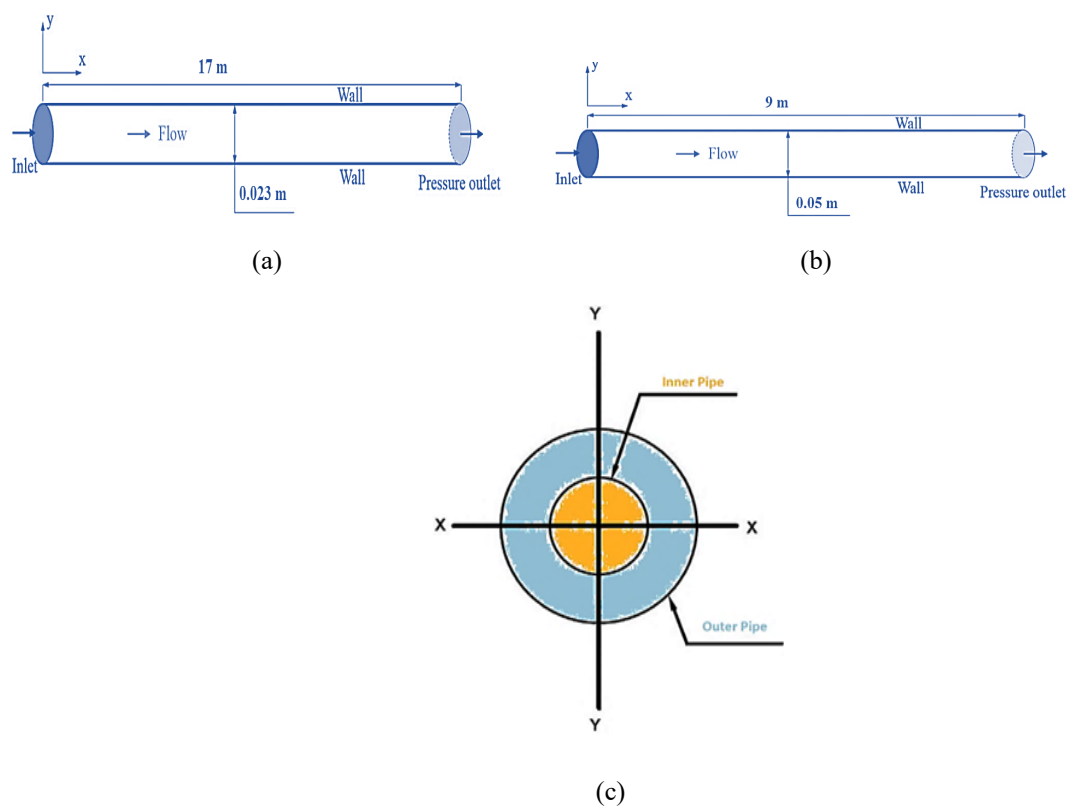
- a) A single phase (water) through a pipeline.
- b) A single phase (water) through annuli.
- c) A two-phase flow (water-air) through a pipeline.

##### *4.5.1.1. Single phase data sets (water)*

In this study, 16 experimental single-phase datasets were extracted from the works of Skudarnov et al. [123] and Kelessidis [124]. In their work, Skudarnov et al. [123] used a pipeline of length 17 m; with diameter of 0.023 m, water density of 998.2 kg/m<sup>3</sup>, with a viscosity of 0.001003 kg/m·s, and roughness of the stainless steel wall material of about 0.032 mm (see **Fig. 4.1a**). Kelessidis et al. [124] used a pipeline length of 5 m, an annulus with an inner diameter (ID) of 40 mm, outer diameter (OD) of 70 mm (see **Fig. 4.1b** and c).

Besides, the wall materials were plexiglas and aluminium and the flowing fluid used was water in both setups.

To mimic these scenarios, a CFD model was constructed using horizontal pipe, and a grid mesh distribution was established using STARCCM+ to generate the material and demonstrate its suitability. At liquid inlet, uniform velocity was used as one boundary condition. Atmospheric pressure outlet condition was tested to avoid any concerns with backflow at the tube exit and wall type for the whole pipe except the inlet and outlet of the pipe boundary conditions. The gravitational effect on the flow was considered. Inlet and outlet pressure were assumed to be identical. It was found that a tetrahedral grid mesh was most optimal, allowing quick convergence. Also, the fluid domain was asymmetrical due to the annular conduit geometry. The grid independence analysis was determined by the velocity of the water and pressure gradient at the exit.

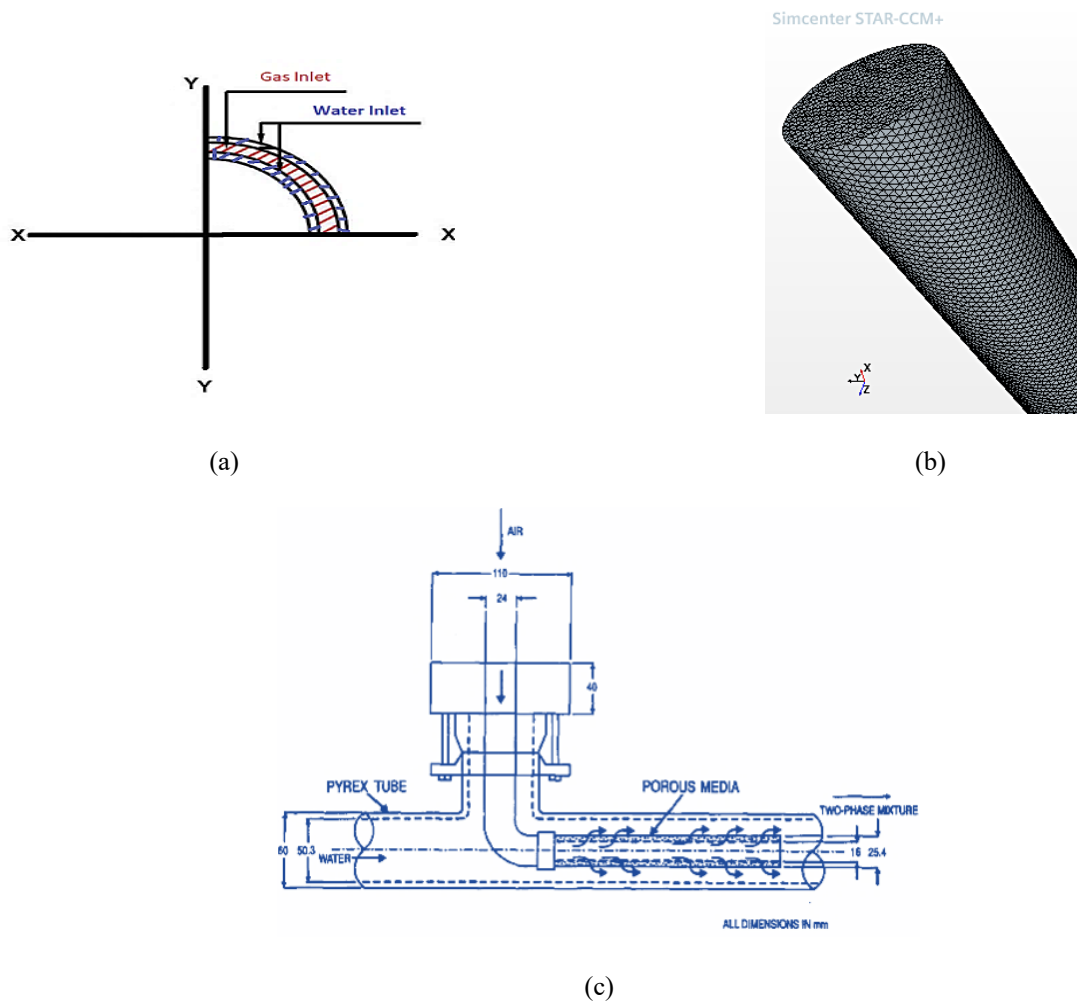


**Fig. 4.1.** Demonstration of computational domain (a) schematic draw for the pipeline with dimensions implemented using CFD with number of cells 4,500,000; (b) annular pipe with dimensions implemented using CFD with number of cells 1,500,000; (c) schematic draw for the annuli on x-y plane.

#### 4.5.1.2. Two-phase (air-water)

In addition, a total of 21 experimental two-phase datasets were obtained from the studies conducted by Kocamustafaogullari and Wang [29], Kocamustafaogullari and Huang [125], and Iskandrani and Kojasoy [126]. These datasets encompassed measurements related to the horizontal positions within the pipe, axial velocity, and gas void fraction. The input parameters employed for the two-phase flow are described here: The 2-D geometry had a length of 9 m, and the pipe diameter measured 50.4 mm. **Fig. 4.2a** presents a modelled configuration simultaneous injection of water and air through the pipeline at certain velocity designed to simulate the same configuration as utilized in the experimental setup, enabling the injection of a two-phase flow consisting of water and air, **Fig. 4.2b** illustrates the tetrahedral mesh used for the CFD-constructed model representation, **Fig. 4.2c** provides a schematic representation the experimental setup showing the air entering the mixing chamber from a 90 ° vertical leg and is injected into the water flow through a porous cylindrical media of 100µm porosity to achieve a uniform mixing and the quick development of a bubbly two-phase flow pattern. The model allows for monitoring the distribution of air within the water and the axial velocity throughout the domain. VOF was employed to simulate the behaviour of water and air within the system.

To understand the effect of water and air inlet position on the numerical simulations, were carried out to investigate the sensitivity for water and air inlet position. The result showed change in void fraction and gas volume fraction distribution across the length. The gas volume fraction profile showed good agreement with the experimental data. The following section show a comparison of the gas volume fraction and the axial liquid velocity prediction for the best sensitivity case. It can be observed that there is no significant change in the predictions of axial liquid velocity prediction but vice versa in the gas volume fraction, will affect the lateral phase distribution for horizontal flow.



**Fig. 4.2** The geometry of two-phase (gas–liquid) flow through pipeline (a) schematic draw for the pipeline on x-y plane showing water and air inlet configuration; (b) Constructed mesh for CFD model; (c) Schematic of the air-water mixing chamber used in the experiment.

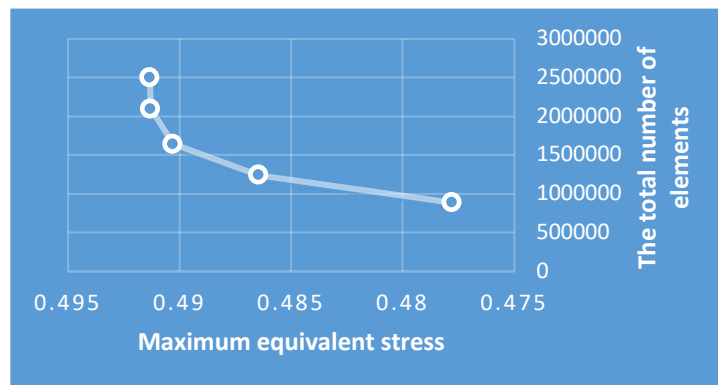
The uniform velocity inlet was employed as the boundary condition at the gas and liquid inlets. In addition, the atmospheric pressure outlet condition throughout the outlet was determined to avoid any issues related to backflow at the pipe outlet and wall type for the whole pipe except the inlet and outlet of the pipe boundary conditions. The gravitational effect on the flow was considered. The inlet and exit pressures were the same. It was found that a tetrahedral grid mesh with number of cells 2,500,000 was most optimal enabling faster process convergence after convergence studies conducted. The grid independence investigation was conducted as shown in **Table 4.1** using maximum equivalent stress. The



simulation done on three times with different superficial gas velocity inlet of 0.25 m/s; 0.5 m/s; and VG = 0.8 m/s with constant superficial liquid velocity of 5 m/s.

**Table 5**  
Grid independence verification

The total number of elements	9E+05	1E+06	2E+06	2E+06	2500000
Maximum equivalent stress	0.478	0.486	0.49	0.491	0.49133858



**Fig. 4.3** Convergence studies based on maximum equivalent stress plot from **Table 4.1**

#### 4.6. Development of CFD model to mimic the experimental datasets

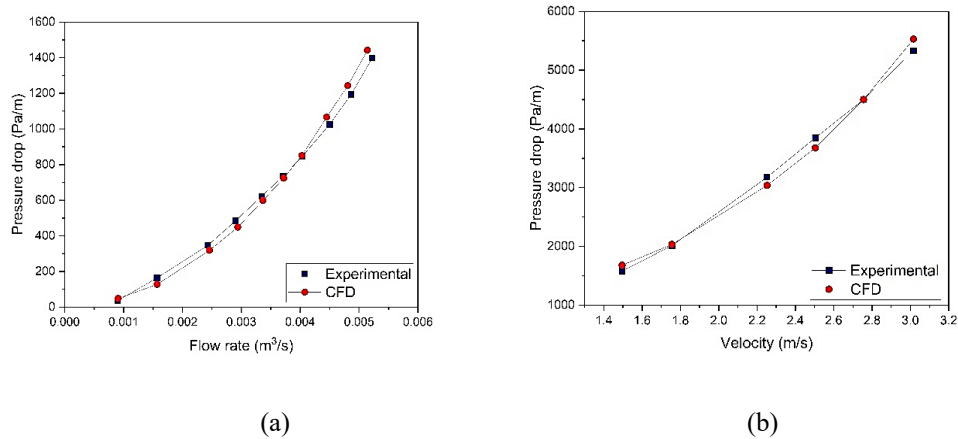
The simulations were run as a two-dimensional transient flow pattern in a horizontal and vertical pipe of varying dimensions ranging from 3000-17000mm length and 23-70 mm diameter as shown in **Table 4.2**. The outcomes of the simulation were obtained near the pipe's outlet and along a horizontal line running through the centre of the pipe axis, where  $y/D$  are the normalised horizontal positions throughout the pipe.

**Table 6**  
Range of parameters considered for the baseline model development.

Parameters	Ranges
Diameter, (mm)	23 - 70
Length, (m)	3 - 17
Input Water velocity, (m/s)	0.05 - 5
Input Air velocity, (m/s)	0.2 - 1

#### 4.6.1. CFD model of Single phase in a pipe and annulus

The CFD results, specifically the pressure gradients versus velocity, were compared with the corresponding experimental datasets. The findings are shown in **Fig. 4.4a** and **b**, and it indicated a satisfactory agreement between the CFD results and the experimental values reported by Skudarnov et al. [123] and Kelessidis et al. [124] respectively. The average disparity between the CFD findings and the data obtained was within 5%.

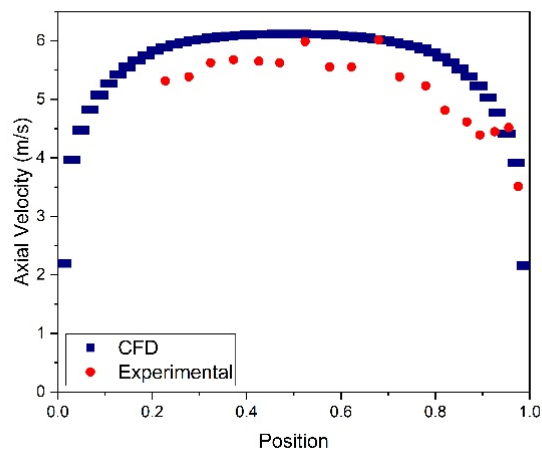


**Fig. 4.4** Comparison of simulated pressure gradient with experimental data (a) through pipeline; (b) through annuli.

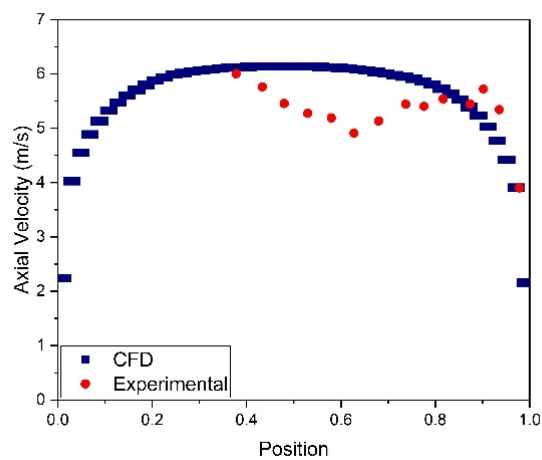
#### 4.6.2. CFD model of two-phase (gas–liquid) flow through pipeline

A CFD model of the two-phase (gas-liquid) flowing through a pipeline to further benchmark the developed model. The results of the study in **Fig. 4.5** revealed insignificant asymmetry in the experimental velocity profile with velocity in the top section of the pipeline being lower than that in the bottom section. The liquid percentage in the top section of the pipeline reduces due to the presence of particles of gas and the gravitational impact on gas. Moreover, the mean bubble velocity drops approach the upper wall. The velocity profiles showed a uniform distribution over a large portion of the flow area, except for the wall region. **Fig. 4.5** compares the axial liquid velocity profiles of experimental and predicted CFD data for various superficial gas and liquid velocities. It illustrated the effect of various interface forces

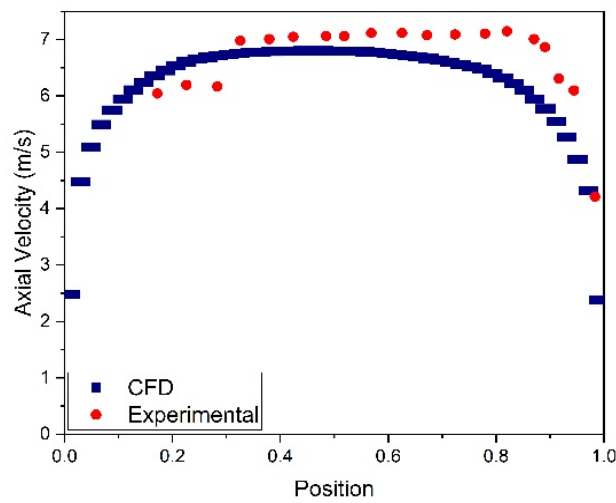
on the gas volume fraction, comparing the experimental results with the corresponding CFD results. The liquid velocity in the top section of the pipe was seen identical to the liquid velocity in the bottom region, demonstrating a perfect asymmetry when single liquid phase moves through the pipe. However, these findings demonstrate that the presence of gas flow causes incipient asymmetry in the axial liquid velocity profile. Increase in liquid flow or decreases in gas flow causes a reduction in the degree of asymmetry for steadily increasing gas velocities.



(a)



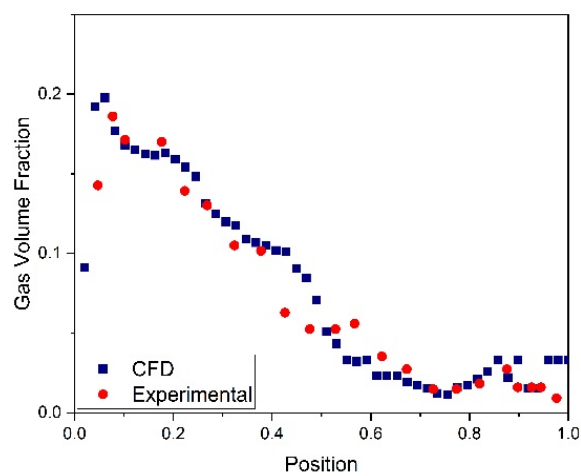
(b)



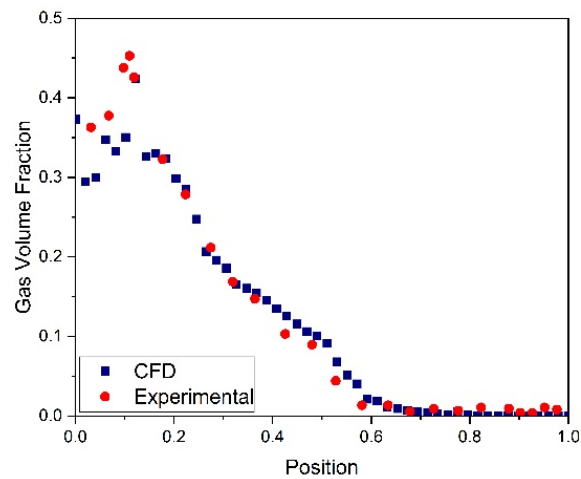
(c)

**Fig. 4.5** Effect of superficial liquid velocity on axial liquid velocity for constant  $V_L = 5$  m/s and variable  $V_g$  (a)  $V_g = 0.25$  m/s; (b)  $V_g = 0.5$  m/s; (c)  $V_g = 0.8$  m/s.

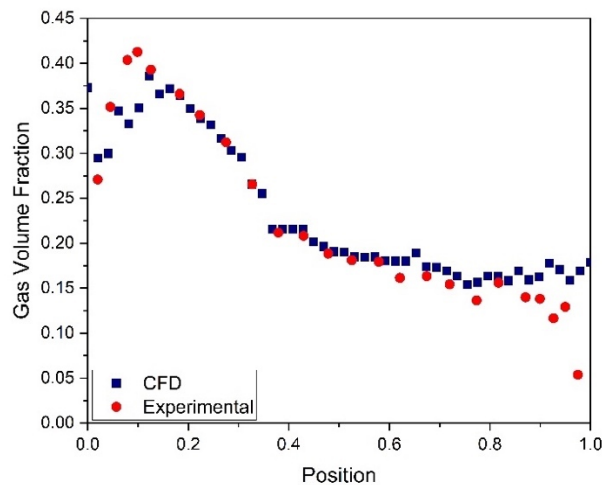
**Fig. 4.6** show the void fraction of gas phase exhibited the profiles showing flattening as the gas void fraction became larger, with a regional peak at the pipe's upper section. as shown in (c) with inlet gas velocity of 0.8m/s. The findings revealed that increasing the gas flow while maintaining a fixed liquid flow, led to an increase in the local void fraction. The bubble velocity increases when the liquid and or gas flow rate increases.



(a)



(b)



(c)

**Fig. 4.6** Effect of different interface forces on gas volume fraction for constant  $V_L = 5$  m/s and variable  $V_g$  (a)  $V_g = 0.25$  m/s; (b)  $V_g = 0.5$  m/s; (c)  $V_g = 0.8$  m/s.

### Brief conclusion

This chapter aims to advance the existing knowledge of two-phase flow behaviour by using CFD modelling. The study includes different conditions to identify the most impactful parameters influencing the multiphase flow models. Given the complexity of two-phase flows, it is crucial to validate the CFD model with experimental data before applying the analysis to more intricate systems. The model's validation is based on experimental results.

## CHAPTER 5

# Modelling a gas kick-drilling fluid model for calibration purposes.

### 5. Modelling a gas kick-drilling fluid model for calibration purposes

#### *5.1. Problem definition*

The interaction between the gas (methane) from reservoirs into a well's annulus and the drilling fluid (mud) is the issue that needs to be resolved in actual gas kick scenarios, which can lead to kicks and blowouts while moving to the surface. In the present study, a CFD model of this interaction of methane with drilling fluid through an annulus is developed and subsequently validated against experimental data of one, and two-phase flows. In most of the previous CFD studies, the numerical model was validated using a very limited number of data sets; the number of data sets was typically as low as one or two (e.g., Dewangan and Sinha [127]; Chen [128]; Gopaliya and Kaushal [129]). The objective of the study is to verify was to fully calibrate CFD baseline model and simulate the multiphase flows under a wide range of process conditions.

#### *5.2. Development of the baseline CFD model*

##### *5.2.1. Predictive modelling and simulation of drilling fluids with gas kick*

After the model validation, the liquid (water) and gas (air) phase fluids were changed to drilling fluid and methane gas respectively resulting in variations in the velocity and void fraction. A new model was constructed, and physical conditions for drilling fluid and gas inlet were adjusted to explore the effects of gas kicks during drilling conditions.

### 5.2.2. Baseline CFD model of two-phase (gas–liquid) flow through pipeline

The CFD modelling process involves three main steps: pre-processing, processing, and post-processing. In the pre-processing step, various aspects such as geometry, mesh, physics, boundary conditions, and initial values are defined. To illustrate, a straight pipe with a 50 mm inner diameter and 9 m in length was generated using STAR-CCM+.

The model consisted of both structural and fluid domains. In the annulus fluid domain, the inlet boundary was set as a velocity inlet, the outlet boundary as a pressure outlet, and the coupling surfaces were defined on the outer surface of the drill string and the inner surface of the fluid domain. A single drill string was chosen as the structural model, and the fluid in the pipe comprised drilling fluid and methane gas. The main parameters for both structure and fluid are provided in **Table 5.1**, while additional fluid parameters and specific boundary condition details were determined based on specific working conditions.

**Table 5.1**  
Structural and fluid model including drilling fluid and methane gas.

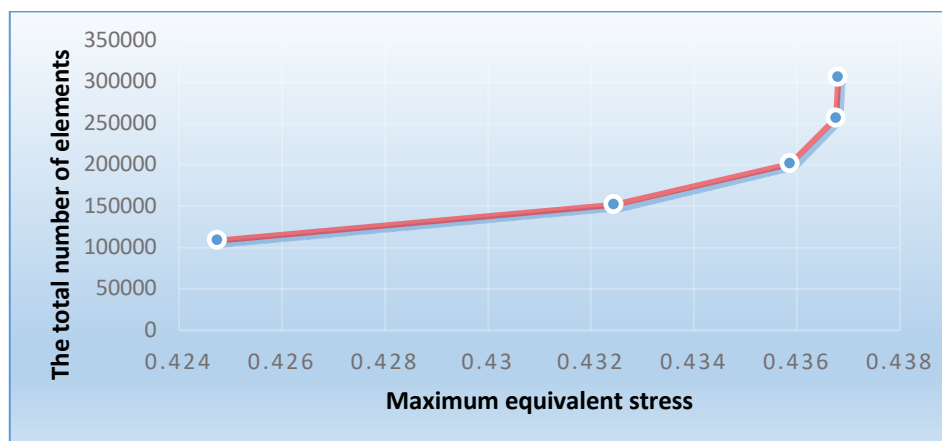
	Parameters	Value
<b>Structure parameter</b>	Density (kg/m <sup>3</sup> )	7850
	Length (m)	9
	Diameter (mm)	50.3
	Wall thickness (mm)	8
	Elastic modulus (GPa)	210
	Poisson's ratio	0.3
	<b>Fluid parameter</b>	Drilling fluid density (kg/m <sup>3</sup> )
Drilling fluid viscosity (Pa·s)		0.015
Gas Molecular weight (g/mol)		16.043
Natural gas viscosity (Pa·s)		$1.11906 \times 10^{-5}$

The simulation utilized quadrilateral and tetrahedral mesh types, ensuring a constant cell density throughout the domain with direct control over cell size. This type of mesh facilitated refinement near the wall for accurate boundary layer resolution. To model the mixture behaviour, an unsteady study was conducted using the Volume of Fluid model (VOF),

allowing tracking of the interface between phases through an additional transport equation for volume fraction. The interaction between phases was driven by surface tension forces, with the liquid considered incompressible and the gas modelled as an ideal gas due to low pressure and velocities relative to sound speed. Gravity was included to account for density differences causing phase segregation. The inlet of the phases was set as a velocity inlet where phases are segregated, with the inlet velocities adjusted to match the volumetric flows of each experimental point. The outlet boundary was modelled as a pressure outlet, simulating the degasification tank in the experimental loop. The time step for each simulation was determined based on a Courant number (CFL) of 0.25, considering the higher inlet velocity of the phase and the axial length of one cell. The time steps varied for each simulation, and **Table 5.2** and **Fig.5.1** presents the grid independence verification, showing the total number of elements versus the maximum equivalent stress. The results indicate convergence, and a time step of 0.005 sec was selected based on a comprehensive consideration of computing resources and accuracy.

**Table 5.2**  
Grid independence verification

The total number of elements	108454	151754	201142	256753	305895
Maximum equivalent stress	0.42475	0.43245	0.43587	0.43676	0.43680



**Fig. 5.1** Convergence studies plot from **Table 5.2**



### 5.2.3. *Investigating two-phase flow (Mud / Gas) and understanding gas-kick dynamics*

A gas kick typically results in a multiphase flow scenario within both the wellbore and annulus. Specifically, a gas kick leads to a two-phase flow in the annulus. To understand the nature of a gas kick, it is essential to first comprehend the phenomenon of gas bubble ascent in the wellbore.

In the modelling of gas kicks, a crucial assumption is often made, assuming that gas enters the wellbore from the formation as a solitary bubble and maintains a consistent profile along the wellbore. However, this modelling approach may oversimplify the situation, especially with regard to the solubility of the gas or bubble in synthetic-based mud (SBM) and oil-based mud (OBM). The gas rise velocity calculation often neglects the solubility of the gas in SBM and OBM for the sake of simplification. As a result, the calculated pressure for a single bubble is consistently higher than anticipated.

In drilling muds like SBM or OBM, where the mud is non-aqueous, the solubility of gas is not uniform. Consequently, the variability in gas solubility becomes a significant concern that cannot be disregarded. Therefore, the accuracy of kick detection time and pit volume calculations may vary depending on mud characteristics. A more comprehensive approach that considers the non-uniform gas solubility in non-aqueous drilling muds is recommended for a more precise representation of the gas kick scenario.

The fluid flow in the annulus can exist in two states: the flow of drilling fluid alone and the co-flow of drilling fluid and natural gas. In the latter state, the gas-phase natural gas entering the annulus displaces a portion of the liquid-phase drilling fluid. Given that the density of natural gas is significantly lower than that of the drilling fluid, the pressure exerted on the outer wall surface of the drill string and the additional mass imparted to the drill string by

natural gas are comparatively lower than those caused by the drilling fluid. Consequently, the overall coupling effect on the drill string is reduced after the mixing of gas and liquid. Changes in the physical parameters, such as density, viscosity, and velocity, of the drilling fluid or natural gas result in corresponding alterations in the pressure on the outer wall of the drill string and the additional mass of the drill string.

#### 5.2.4. Sensitivity analysis

The majority of two-phase flow models are grounded in small-scale experimental results for scenarios like vertical wells, inclined tubing, and annuli. However, these simplistic models do not accurately represent the complex wellbore geometry encountered in real-time drilling operations. Various mechanistic models have been proposed to characterize the annular behaviour of two-phase flow, and different researchers have contributed to these efforts.

The annular geometry is identified as a critical factor influencing the propagation of bubbles along a wellbore. Liquid velocity and gas expansion rates exert significant influence, while the impact of mud viscosity and wellbore orientation is minimal. **Table 5.3** outlines the factors affecting the flow of gas bubbles through tubing or annuli and their dependencies on other parameters.

**Table 5.3**

Factors affecting gas bubble flow and dependency on other parameters.

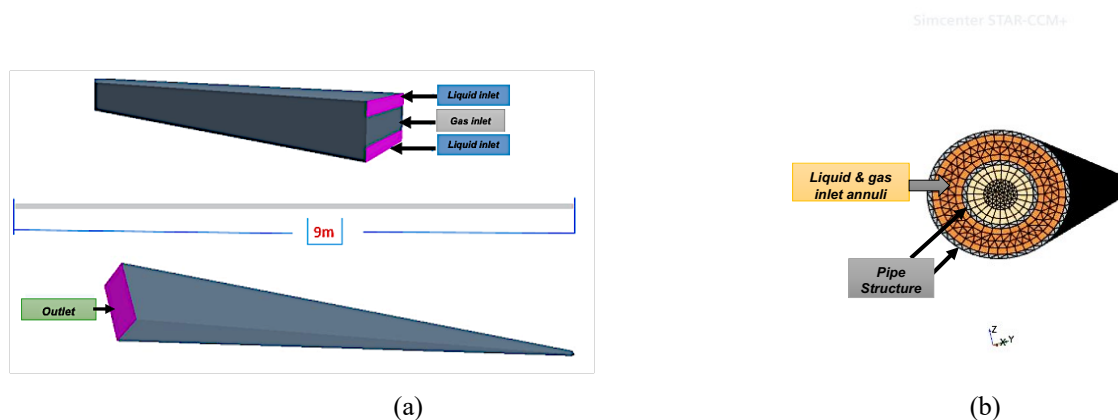
Factors	Dependency on other parameters	Impact on bubble rise velocity
Fluid density	<i>Independent</i>	<i>Negligible</i>
Gas void fraction	<i>Independent</i>	<i>Negligible</i>
Mud rheology	<i>Independent</i>	<i>Negligible</i>
Mud viscosity	<i>Decreases with increasing annulus size</i>	<i>Small</i>
Surface tension	<i>Independent</i>	<i>Negligible</i>
Pipe inclination	<i>Maximum rise velocity as 45°</i>	<i>Small</i>
Gas expansion rate	<i>Depends on annulus backpressure</i>	<i>Significant</i>
Annular geometry	<i>Increase with increasing annular diameter</i>	<i>High</i>
Liquid velocity	<i>Increasing with flow velocity</i>	<i>Significant</i>

### 5.2.5. Model Geometry

The 2-D geometry used to simulate the drilling fluid with methane gas is the same as used when simulating the experiments by Kocamustafaogullari and Wang (1991), Kocamustafaogullari and Huang (1994), and Iskandrani and Kojasoy (2001). The model pressure domain was kept constant at a temperature of 25°C. The model represents two-phase flow, instead of liquid water Newtonian it will be mud non-Newtonian and methane gas instead of air (mud–methane) flow through a horizontal pipeline with the above conditions. This experiment produces velocity and void fraction profiles for a certain range.

**Fig. 5.2a.** and **Fig. 5.2b.** shows the 2-D geometry model and 3-D mesh distributions for annular geometry in STARCCM+ used for the simulation domain. Monitoring the distribution of methane in the mud through the model and the axial velocity in the model, using volume of fraction method (VOF) to simulate mud and methane. i.e., the geometry remains constant throughout the simulation.

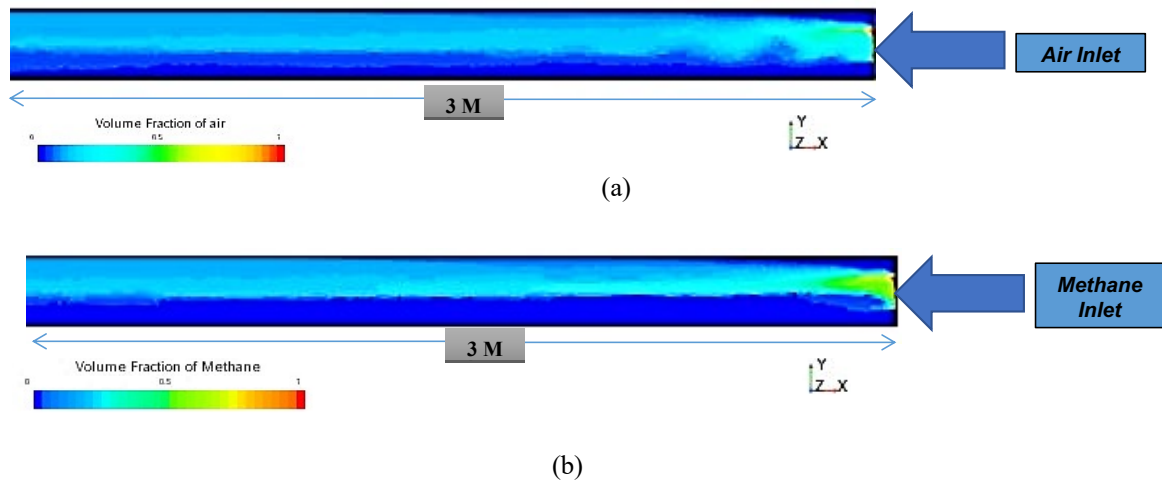
The constructed model simulated the same trend while simulating water- air flow. To understand the effect of drilling fluid – methane inlet position on the simulations, sensitivity analysis was performed for drilling fluid and methane inlet position as used for air-water flow.



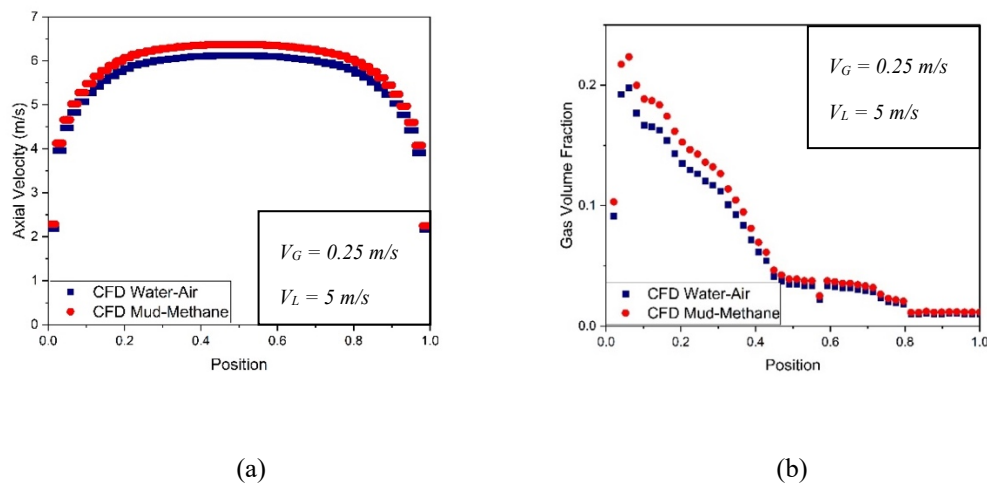
**Fig. 5.2** Model 2-D geometry (a) 2-D pipe geometry of the modelled domain; (b) Orthogonal mesh for annular geometry for a 3-D geometry domain section used in CFD.

### *5.3. Modelling of phase change from water-air to mud-gas*

With the aim of predicting the change in phase behaviour dealing with drilling fluid mud with methane gas intrusion during drilling, water was replaced by the drilling fluid and air was replaced with the methane gas. It was observed that the superficial gas velocity affecting axial liquid velocity changed by changing the liquid phase and gas phase from water air to drilling fluid and gas (methane) respectively as shown in **Fig. 5.4a**. The void fraction is frequently employed as a predictor of the transition from bubbly flow to slug flow as shown in **Fig. 5.4b**. The axial velocity for the mud-methane system tends to have the same distribution over the whole pipe including the wall region. In contrast to **Fig. 5.3** and **Fig. 5.4b**, the difference in void fraction was maximum in the upper pipe and it tends to decrease towards the other pipe wall. It is also worth mentioning that the difference between the axial velocity for mud-methane system and water-air system is not significant across the upper and lower pipe. It has also been observed that the axial liquid velocity for mud-Gas system increases by 5% compared to the Water-Air system. It is also worth noting that the gas void fraction value and position in the pipe gets changed due to the change of liquid phase and gas phase from water air to drilling fluid - gas (methane) as indicated in **Fig. 5.4b**. The gas void fraction for Mud-Gas system increased by 10%-15% compared to the Water-Air system as shown in **Fig. 5.3**. The methane gas acts differently compared to air in water, as it's concentrated more with less tendency to spread through the pipe. Furthermore, the void fraction of the methane gas was higher than that of the air in water.



**Fig. 5.3** Different gas volume fraction for a two-phase flow at the beginning of the pipe used to inject both fluids (a) Water-Air; (b) Mud-Methane.



**Fig. 5.4.** (a) The effect of superficial gas velocity on axial liquid velocity, and (b) The effect of different interface forces on Gas Void Fraction.

#### 5.4. Computational efficiency using parallel processing architecture

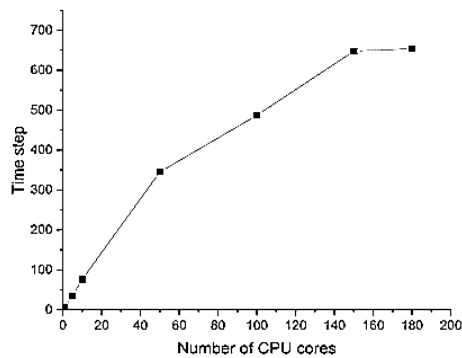
The scaling performance of the CFD code was accessed on a high-performance computing (HPC) system having 192 number of CPU cores [130]. The simulation was ran using different number of cores and a speed up factor showing the scaling efficiency was plotted. Thus, **Table 5.4** and **Fig. 5.5** establishes the correlation between the number of cores and scalability of STARCCM+ while using the Message Passing Interface (MPI) library. **Fig. 5.5a** showed the numbers of timesteps solved by code with increasing number of cores and **Fig. 5.5b** shows normalised timestep with minutes of run to establish the speedup gain with

the use of increasing number of cores. It appeared the code scaled linearly until 50 cores beyond which the scaling performance becomes saturated.

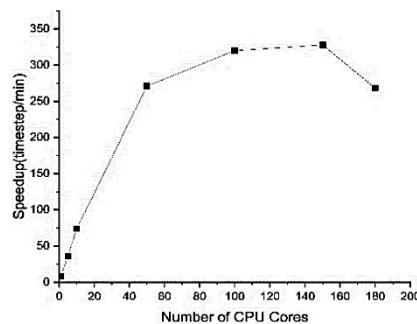
**Table 5.4**

The effect of number of cores on time step and on speedup simulation.

Cores	Time	Iteration	Time Step	Time (min)	Iteration	Time Step	Speedup (time step/min)
1	5 min	37	7	31	250	50	8
5		178	35	6.9			36
10		380	76	3.36			74
50		1728	345	0.92			271
100		2435	487	0.78			320
150		3241	648	0.76			328
180		3270	654	0.93			268



(a)

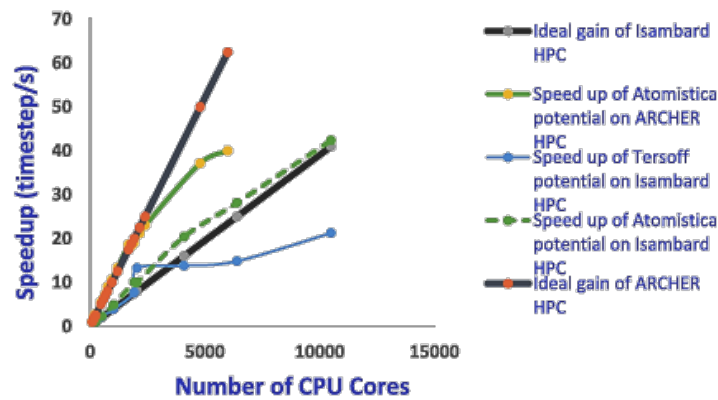


(b)

**Fig. 5.5** The effect of number of cores on: (a) time step for 5 minutes simulation; (b) speedup simulation for 50 timestep.

The sensitivity study was designed to evaluate scaling up the performance of bond order potentials on HPC (high-performance computing) to configure the number of cores needed to run the simulation with the fastest performance. The results show that the HPC used is speeding up the simulation time till certain number of cores but then, the number of cores is not improving the running time consumed on that constructed model, and the running time consumed is not directly proportionally with increasing the number of cores. After comparing

the results with the Fig 5.6 having different types of models, it had been concluded that, the model follows Tersoff potential on Isambard HPC Model.



**Fig. 5.6** Scaling performance of bond order potentials on two HPCs (high-performance computing) (<http://www.archer.ac.uk/>)

Concluding the linear scaling happens only until 50 cores and the speedup was not linear beyond this number of cores. All, the simulations were run with 140 cores maximum. This research work resulted in an integrated simulation technique that incorporated a detailed multiphase flow simulation with a two-dimensional or three-dimensional model. It is not computationally viable for constructing a full-scale wellbore model with similar modelling detail. The models investigated in the present study are limited by the dimensions (length scale) because of the limited cores for a commercial code STARCCM+.

## Brief conclusion

Using a Computational Fluid Dynamics (CFD) model validated against experimental data, to fully calibrate the CFD baseline model and predict changes in phase behaviour during drilling with methane gas intrusion into drilling fluid mud. Key findings include:

1. Substituting water with drilling fluid and air with methane gas resulted in changes in superficial gas velocity, influencing axial liquid velocity.
2. Void fraction, a predictor for the transition from bubbly flow to slug flow, exhibited significant differences in the mud-methane system, particularly in the upper pipe, decreasing towards the other pipe wall.
3. Axial liquid velocity for the mud-methane system increased by 5% compared to the water-air system.
4. Gas void fraction and its position in the pipe changed with the shift from water-air to drilling fluid-gas (methane), with a 10%-15% increase in gas void fraction for the mud-gas system compared to the water-air system.
5. Methane gas behaved differently than air in water, concentrating more and showing less tendency to spread through the pipe, resulting in higher void fraction than air in water.

Overall, these findings contribute to understanding the complex dynamics of drilling with methane gas intrusion into drilling fluid mud, offering insights into phase behaviour changes and fluid interactions.

The study found linear scaling up to 50 cores, with non-linear speedup beyond this number, limiting simulations to a maximum of 140 cores. The findings emphasize the complexity of modelling full-scale wellbores with current computational limitations.



## CHAPTER 6

# Predictive Modelling of Realistic gas kick in a vertical well

### Outline of the chapter

After the model validation, the liquid (water) and gas (air) phase fluids were changed to drilling fluid and methane gas, respectively. The real modelling methodology and model configuration for gas-kick scenario simulation are explained, simplified assumptions were made to facilitate the analysis.

### 6. Predictive Modelling of Realistic gas kick in a vertical well

#### *6.1. Problem definition*

The multiphase flow pattern throughout a gas-kick can be determined using Navier-Stokes solution using non-Newtonian properties for a liquid fluid flow. In an ideal situation, it seems necessary to fully reflect the wellbore in three dimensions. This flow problem lacks an analytical solution, and a full-size numerical simulation would be computationally too expensive. For that reason, simplified assumptions were made to facilitate the analysis of this situation.

#### *6.2. CFD assumptions for complex flow geometries*

The present study involves computational investigation by using CFD simulating a gas kick in a downhole wellbore. It is not computationally viable for constructing a full-scale wellbore model with similar modelling detail after checking computational efficiency of the CFD code

when running in parallel architecture as presented in chapter 4. Therefore, the models investigated in the present study are limited by the dimensions (length scale) scaled down version concentrating at the wellbore bottomhole circumstances, on the transient start of the gas-kick initiation, which is when a kick is most likely to begin and progress.

The following actions and procedures are simulated in the gas-kick modelling methodology:

- I. Circulation of drilling fluid with non-Newtonian properties;
- II. Water is considered as the base for drilling fluid (WBM) with some modification to suits the drilling fluid real properties;
- III. To simulate and study the gas kick behaviour, pure methane without any accompanying gases is considered as the kick gas;
- IV. The entry of gas into the annular space of the wellbore.;
- V. The blending between the drilling fluid (mud) and the gas (methane);
- VI. To analyse the compressibility effect, methane is considered as an ideal gas;
- VII. In simulations, leaking of fluid is not considered, as it is a minor issue;
- VIII. Gas dissolution in the drilling fluid;
- IX. Evaluation and measurement of key flow variables.

The assumptions made in this model are listed below:

- a. Flow with both gas and liquid phases only, without the influence of cuttings(solid).
- b. Mud properties (non-Newtonian mud).
- c. VOF multiphase model employed to track a fluid-fluid interaction.
- d. Constant mud pump rate and formation pore pressure.
- e. Constant annular geometry and concentric annulus.
- f. Drill pipe rotation.
- g. The effect of drilling cuttings is not considered.

The kick depends on the pressure and temperature, and especially on the pressure difference, annular clearance is based on the geometry of the annulus, drilling fluid properties such as mud type, density, and rheology, operational conditions for the well during drilling (circulation) or, shut off, and the gas kick location and configuration. Assuming there is no communication between the annulus and adjacent layer, except for focused position for modelling the gas-kick entry. Knowing that the drilling operation is not considered in the simulation, therefore the well model geometry dimensions kept fixed during the entire simulation.

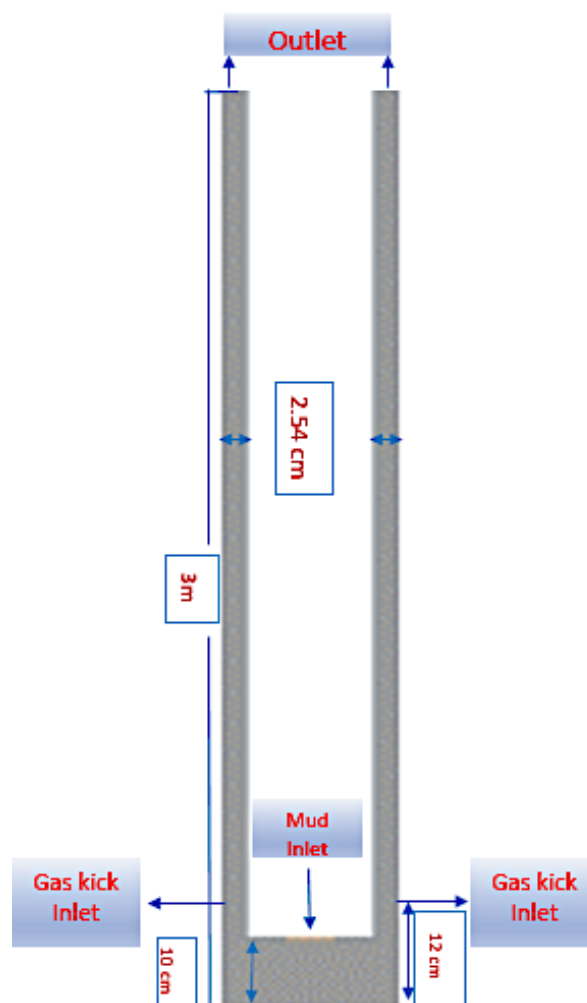
### *6.3. Model setup simulation of gas-kick scenarios*

To characterize the multiphase flow pattern that created after a gas kick occur, taking into account gas dissolution, it is necessary to solve the Navier-Stokes formulas for a transient multiphase flow with turbulent non-Newtonian mud flow. Therefore, a comprehensive 3-D model of the wellbore would be needed. However, given the complexity of the flow problem, there is no analytical solution available, and a numerical simulation at full scale is computationally prohibitive.

#### *6.3.1. Model Geometry Setup & Representation of the Drill Bit*

The geometry length was set to 3 meters to guarantee adequate grid accuracy and reasonable CPU power. This length equivalent to a clearance space that is 100 times the size of the annular gap of 1 inch, providing sufficient coverage of the kick entry zone and allowing for the whole development of the flow. It is presumed that the open-hole segment is free of any washouts, ensuring complete concentricity between the drill pipe and the formation. The open-hole portion is characterized by a diameter measuring 8.5 inches, and a deliberate selection designates the outer diameter of the drill pipe at 6.5 inches.

The modelled domain includes the bottomhole area, the location of the drill bit is positioned, and the annulus within the space separating the formation and the drill pipe. The transfer of flow between the annulus and the neighbouring formation is disregarded, apart from designated locations created to simulate the entry of gas kicks. The external boundary of the wellbore is considered hydrodynamically uniform and is represented as a no-slip boundary. At the boundary of the drill pipe, a condition of no-slip is enforced, causing the fluid to adhere to the wall and move at the same velocity as the pipe rotates. The simulation does not encompass the actual drilling process; thus, the geometry within the wellbore remains unchanged throughout the entire simulation period. **Fig. 6.1** provides a schematic illustration of the computational domain in the cross-section considered for modelling purposes.



**Fig. 6.1** CFD model geometry with dimensions used to simulate the kick during drilling process.

In the project's initial phases, considerable attention was given to modelling the drilling bit and its impact on the flow pattern. Directly incorporating the intricate geometry of the drilling bit into the constructed model would demand extensive efforts to capture the design intricacies and nozzle configuration accurately. Alternatively, a more pragmatic approach was adopted, utilizing a simplified depiction of the flow characteristics in the vicinity of the drilling bit. This representation involves a single central drilling mud inlet positioned at the model's centreline. The mud's mass flow remains constant, directed towards the bottom directly closer to the formation. The space usually taken up by the drilling bit having a 10 cm length and restricted by the outer model radius is consistently rotate counterclockwise at a rate of 100 rotations per minute. Upon entering the annular gap, the mud stream is diverted from the bottom-hole vortex and requires a certain amount of movement to align with the vertical plane.

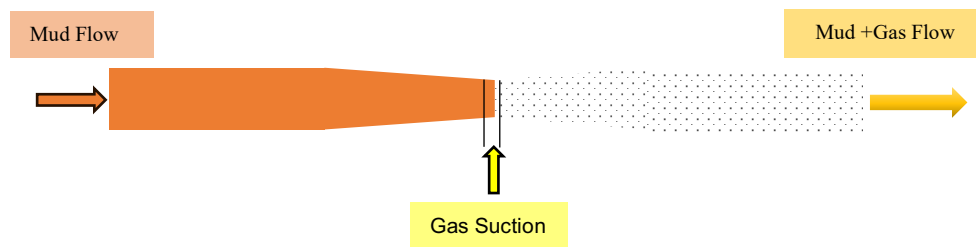
### *6.3.2. Boundary Condition & Kick-Gas Inlet Condition & position*

When evaluating potential gas-kick scenarios, it is common for a kick of gas to happen when the pressure in the formation exceeds what was expected and forecasted, or when the pressure at the bottom hole is inadequate for overcoming the unexpected pressure in the formation during the drilling operation. Since wellbore pressure is not the same across the well, the kick occurs next to the most vulnerable location close to the well and formation boundary.

This phenomenon is particularly pronounced in narrow flow passages or areas with significant deflections in the flow path. When the passage narrows, the velocity of the mud passing through increases, leading to a drop in static fluid pressure—similar to the principle behind a Venturi pipe, as depicted in **Fig.6.2**. This reduction in static pressure is commonly utilized to introduce air into flows, resembling a form of "desired gas-kick" scenario.

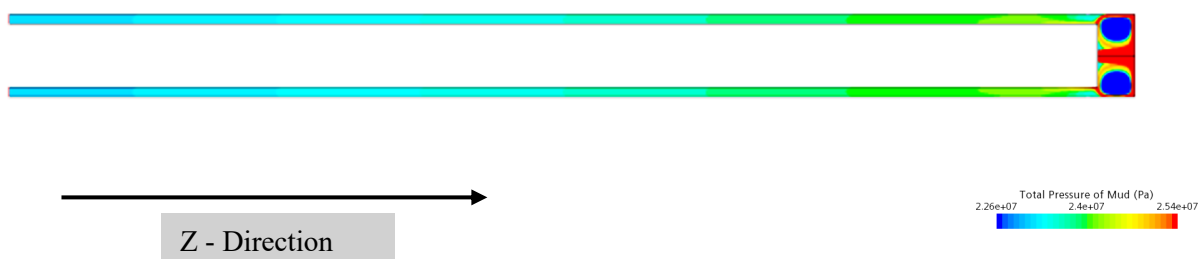
Similarly, if the static wellbore pressure significantly decreases compared to the formation

pore pressure, fluid can be drawn into the wellbore. These regions of low static pressure may result in a continuous inflow of small amounts of gas. While this inflow may not pose a severe threat to overall well control, it can have a significant impact on the drilling string, particularly in terms of corrosion.



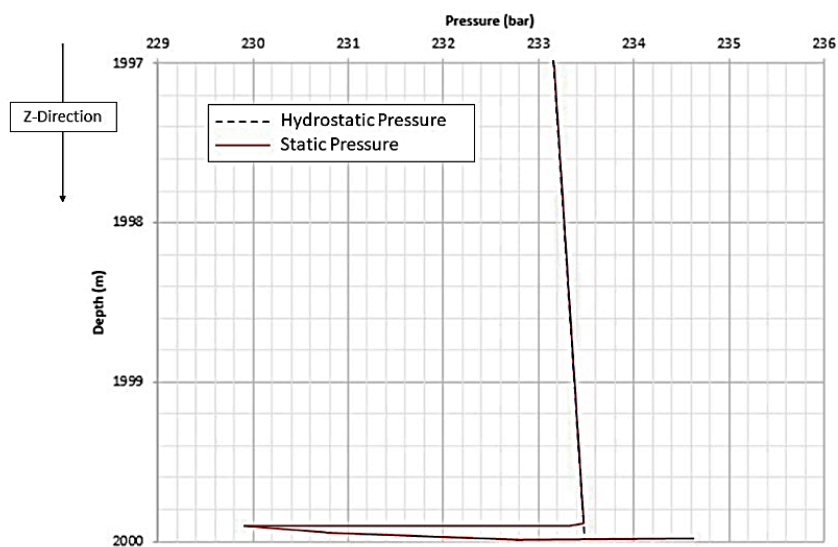
**Fig. 6.2** Venturi pipe showing working principle of a draw gas into the mud stream.

In simple terms, the gas may pass through the open hole part laterally by cracks, or pores. Since gas kick's composition is not known clearly, instead of using many gas components, a single gas composition of methane that most likely reflects the behaviour as well as the physical appearance in reality was chosen. **Table 6.1** shows the properties of methane gas used to simulate the kick and its results are described in this section. **Fig.6.3** shows the total pressure distribution in the constructed model while the flow of mud, revealing increased hydrostatic pressure and elevated dynamic pressure around the drill bit area. The model accurately depicts the intense bottom-hole pressure conditions encountered in real operational scenarios.



**Fig. 6.3** Pressure (Pa) during Mud circulation.

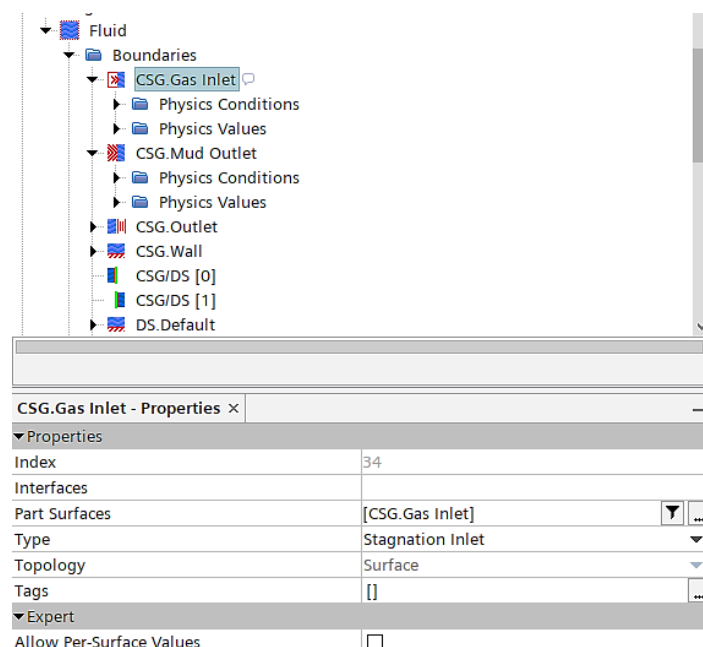
**Fig.6.4** shows the Pressure situation profile during mud circulation. The wellbore bottom or drill bit area is the volume below the annular channel. The rapid ejection of drilling fluid from the nozzles on the drilling bit, combined with the confined gap across the drilling bit and the formation, leads to a dynamically varying pressure distribution across the boundary. This phenomenon is especially prominent in the segment positioned at the initiation of the annulus, directly on the top of drilling bit. Strong entry effects are noticeable when the drilling mud enters the annulus of the wellbore, primarily attributed to the abrupt change in geometry at this specific point. The static pressure along the wellbore boundary demonstrates a steady profile. The pressure distribution aligns with common expectations in wellbore analysis. The observed flow field results from the model configuration, and irrespective of the design of the drill bit, pronounced entry effects will endure until the drilling fluid attains a velocity distribution in line with the flow in annular space.



**Fig. 6.4** Pressure profile during mud circulation.

Various geometric possibilities for the entry of the gas kick were explored, and it was determined that the gas kick at the entrance might be a pressure boundary condition with a pressure value greater than the pressure boundary throughout the wellbore as shown in

**Fig.6.5.** This boundary condition is reasonable given that the gas migration into the wellbore won't impact the reservoir's pressure over the short term. The sudden beginning of the gas influx is not properly represented by the mass flow boundary condition, which also fails to capture an uncontrolled kick situation. Essentially, the gas may ingress through fractures or openings within the uncased part, occurring either sideways or at the lower part of the well. Different situations of gas ingress are investigated and thoroughly outlined in the chapter 6 in the thesis. The maximum drop in pressure across boundaries in the current model setup is 1E6 Pa (145 psi).



**Fig. 6.5** Boundary condition for gas inlet in STARCCM+ constructed model.

The mud mass flow rate was maintained fixed at 40 kg/s and heading downward precisely in the direction of the formation to simulate drilling bit nozzle. The drill bit typically filled a space of 0.1 m in length and was constrained by the outside design radius. Spoerker et al. [131] examined Early Kick Detection within an annulus CFD simulation, modelling the mud as non-Newtonian in order to simulate its behaviour assuming a rheological model Herschel Bulkley with parameters according to **Table 6.1**. Mud enters the model region through a



single 0.03 m diameter nozzle located in the model's centre with constant pressure boundary condition of 2.33E7 Pa (3380 Psi).

Phase mixture and distribution of gases into the mud have been found to be significantly influenced by the position as well as the dimensions of the entrance point via which the gas flows towards the well, this gas entrance is tiny representing a little crack or huge to indicate a void. The occurrence of side kick situation with only one little crack was chosen for first CFD simulations.

**Table 6.1**

Drilling Mud and gas kick Properties.

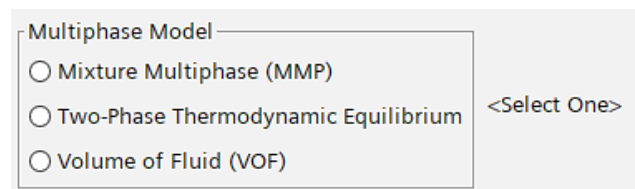
Drilling Fluid Properties							Gas Kick Properties			
Density	Consistency Index (k)	Power Law Index (n)	Yield Stress Threshold	Plastic Viscosity	Min Viscosity Limit	Max Viscosity Limit	Specific heat (Cp)	Thermal conductivity	Viscosity	Molecular weight
kg/m <sup>3</sup>	Pa.s <sup>n</sup>		Pa	Pa.s	Pa.s	Pa.s	J/kg.K	W/mK	Pa.s	g/mol
1190	0.5438	0.5403	0.9576	0.015	0	10000	2240.07	0.0348195	1.11906E-5	16.043

### 6.3.3. Multiphase fluid flow physics model

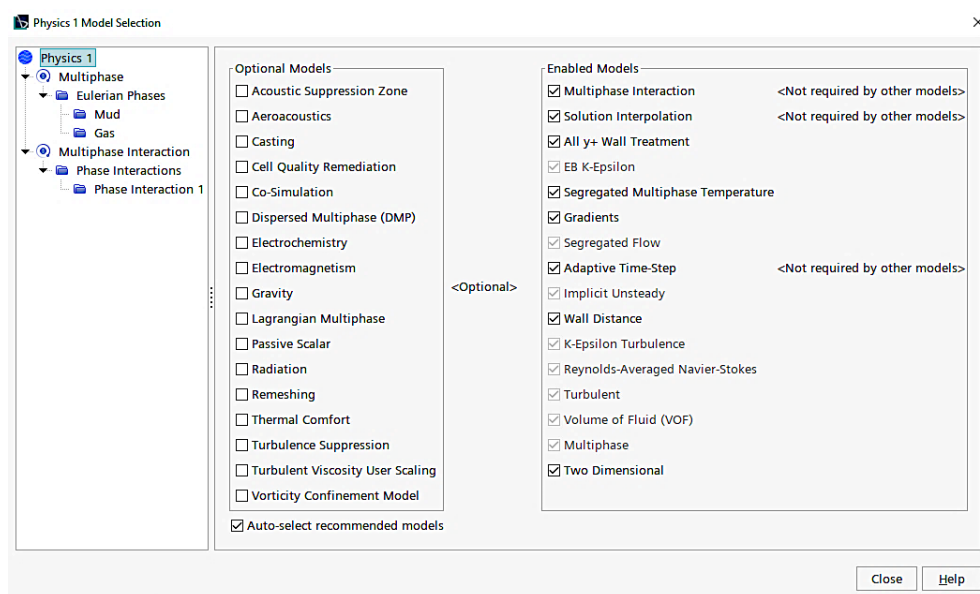
As it was previously mentioned, while using STARCCM+ to simulate a two-phase flow, the right multiphase model must be chosen in accordance with the anticipated flow pattern.

Depending on the extent of the volume fraction of each phase and if the flow is segregated or dispersed, several two-phase flow models are available. For example, an initial understanding of the droplet size distribution or bubble is required for a dispersed flow simulation. Such data is not available for the gas-kick investigation conducted. It is unclear as to what kind of flow patterns are emerging, as was previously noted. Consequently, the Euler DNS based on the volume of fluid technique (VOF) is the two-phase flow modelling methodology used for this work. The volume of fluid technique does not require any previously established basis, in

contrast to many other modelling approaches that require assumptions that restrict the nature of the solution. If the mesh size is considerably smaller than the dispersed interfacial structures, the volume of fluid approach, along with a suitable mesh resolution, can simulate not only segregated flow but also dispersed flow at any phase volume fraction. Effects related to surface tension at the interface are considered through the application of the continuum surface force (CSF) model. **Fig. 6.6a** showing available multiphase models used in STARCCM+ CFD to select one of these options, and **Fig. 6.6b** illustrate the selected multiphase models and the available optional models which can be selected in future to run some sensitivity figuring out how it can affect the simulation.



(a)



(b)

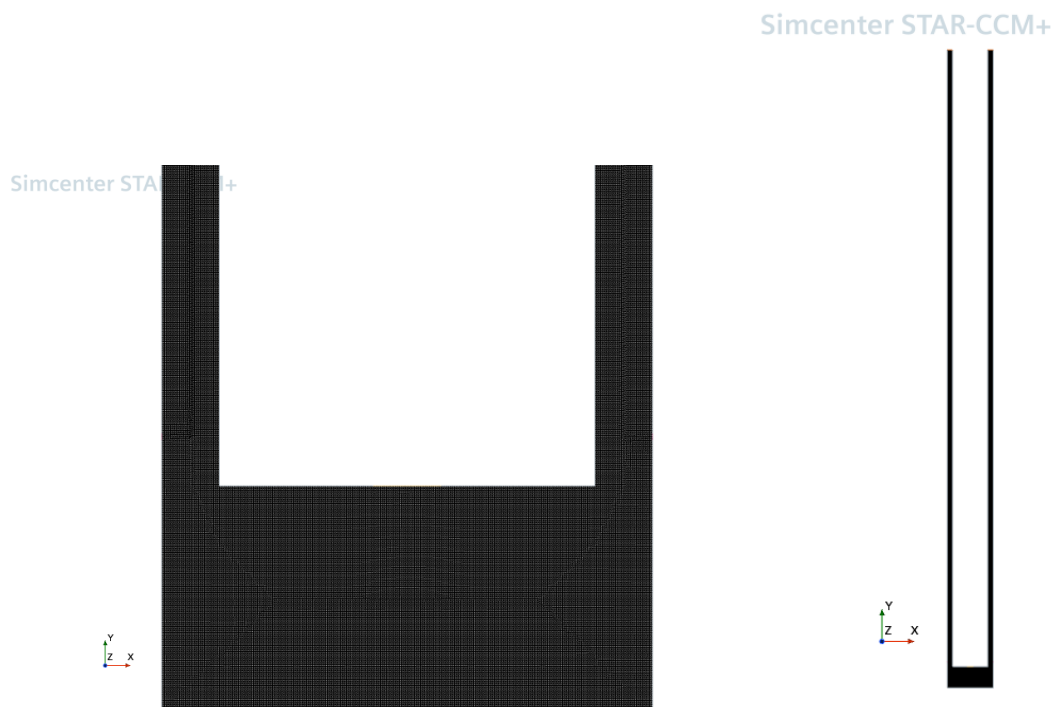
**Fig. 2(a)** STARCCM+ available multiphase models, and **(b)** selected multiphase models and the available optional models.

#### 6.3.4. *Turbulence Modelling & Grid Considerations*

The choice of mesh has a major effect on the necessary computational time, convergence rate, and validity of the result. A suitable boundary layer mesh, low cell deviation, small size ratio of nearby cells, sufficient grid resolution, and local mesh refinement when necessary are the factors that contribute to a mesh quality that ensures acceptable numerical precision and minimizes numerical diffusion.

There has been grid resolution research carried out in the initial modelling stage. When adding more cells to the solution has no effect on the outcome, grid independence has been reached. In all computations, the adaptive time step feature is chosen to maintain a Courant number (CFL) less than 0.3.

The grid independency study was attained when an increase in cell number made no impact on the spread of inflow gas kick in the mud in the annulus and the output drop in pressure became nearly constant. This target was eventually achieved through the use of rectangular shape cells with a size of  $5 \times 10^{-5}$  m consisting of 1,000,000 cells after improvement of the mesh as shown in **Fig.6.7**.



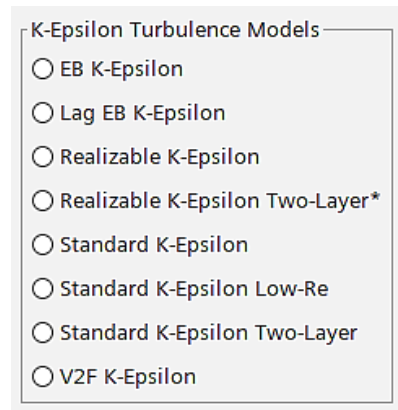
**Fig. 6.7** Mesh of constructed CFD model used after grid independency study using 2-D at STARCCM+.

This section compares the output from various turbulence models and selects the optimal model to carry out the simulation. To achieve this goal, several turbulence models were used to study slug and annular flow patterns, and the turbulence modelling findings for the void fraction. A good simulation of the slug flow has been achieved for the  $k-\epsilon$  Standard model. However, gas has been seen to adhere to the wall in the annular flow, indicating that the chosen solution was incorrect. When comparing the  $k-\epsilon$  realisable model to the  $k-\epsilon$  Standard for the slug flow pattern, it even produced more favourable outcomes.

Comparing this model to the  $k-\epsilon$  Standard, the former does not accurately predict annular flow. This model's longer simulation duration is caused by the increased Courant number and turbulence viscosity, in addition to the annular flow's inaccurate solution. The  $k-\epsilon$  RNG for turbulence modelling is shown to be highly predictive of both annular and slug flow patterns.

Based on a comparison of all the models discussed, it can be concluded that, in terms of accuracy and computing time, the realisable  $k-\epsilon$  is superior for turbulence modelling to

simulate the two-phase flow of liquid gas in a vertical pipe. A no-slip condition is applied at the tube wall for every simulation. The impact of gravitational force on the flow has been considered. Following the sensitivity test to available turbulence models in STARCCM+ as shown in **Fig.6.8**, the realisable k- $\epsilon$  model was used as it proved to be appropriate for this CFD simulation.



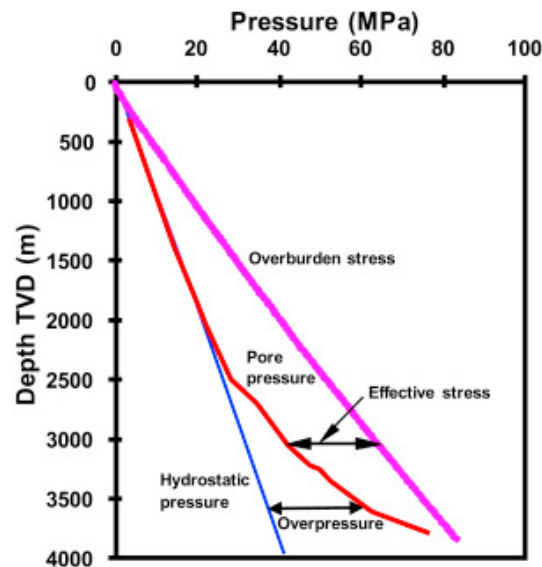
**Fig. 6.8** STARCCM+ available Turbulence models

#### 6.3.5. Pressure condition for a realistic gas kick scenario

The combination of the mud's hydrostatic pressure, the dynamic pressure produced through mud pumping, and casing pressure is the mud pressure during circulation. Consequently, if one of these elements falls without being compensated by another, there is a decrease in wellbore pressure. When a well is operated improperly, the hydrostatic head in the wellbore may decline. For example, constant mud pumping is required during tripping to replenish the volume left by the extracted pipe with mud as the drill string is withdrawn from the hole. If the process is done too rapidly swabbing is present particularly with high viscosity muds and little annular clearance, the effect results in reductions in wellbore pressure. A decrease in the hydrostatic head might also result from low drilling mud density or lost circulation. The settling of weighting material or the inflow of formation fluids can both lower the density of

the drilling fluid. The main barrier to the well is the drilling mud; if this is lost to the formation or the pressure drops too much, formation fluids will begin to leak in. The mud pressure level in the wellbore drops to the hydrostatic head of the mud column when the pumps are switched off during the connecting process. The moment a connection is made, circulation is restored, and the bore hole's mud pressure quickly increases once again. Before stabilising, there may be a very sharp decrease and rise in pressure that overshoots the equilibrium. If the negative pressure surge is less than the formation pore pressure, flow from the formation may be induced and a gas kick can occur.

The major reason of a kick is the reduced hydrostatic pressure exerted by mud column compared to the pore pressure in the formation. **Fig. 6.9** highlights the pressure gradient distribution in a wellbore during drilling and it show the hydrostatic pressure in the formation after completion of the hydraulic communication (blue line). Due to lack of hydraulic communication, some formation zones are over pressured and tend to cause kicks if not controlled. The fracture pressure is showed in purple, while the formation pressure with overpressure zone is shown in red. The amount of pressure drop in the annulus is greater than the pressure drops in the drill string because of greater frictional pressure losses in the open-hole and casing shoes restricting the flow. The pressures in drill string equivalent to the dynamic pressure applied by the pumps, minus frictional pressure losses in the drill string from hydrostatic head exerted by mud column. The hydrostatic pressure in the well must be maintained within the tight pressure range between the red (pore pressure) and purple lines (fracture pressure) during traditional overbalanced drilling operations. The desired circulation mud pressure or equivalent circulation density (ECD) is defined as the sum of the mud hydrostatic head, friction pressure, and surface annular back pressure [132].



**Fig. 6.9** Hydrostatic pressure, pore pressure, overburden stress, and effective stress in a borehole at the true vertical depth [132]

#### 6.3.6. Mud Circulation and influence of rotation

The relationship between shear rate and shear stress must be precisely described by a rheological model to appropriately simulate the non-Newtonian behaviour of the drilling mud. Based on **Table 6.1** specifications, the Herschel Bulkley model was chosen as it provides a good description of most drilling fluids. The annulus during drilling has single-phase mud flow, which is accelerated by the incoming gas's displacement and occurs above the two-phase mixture of the developing kick. The heavier drilling fluid in the wellbore is moved out of the way by the formation fluid during a kick, which lowers the well's hydrostatic pressure. As a result, the kick will rise and accelerate as the pressure difference between the wellbore and the formation grows. To take this impact into consideration, the upper end of the model pressure outlet boundary is equipped with a user-defined function that allows it to automatically adapt based on the gas flowrate at the outlet. The local gas density is analysed to calculate the hydrostatic pressure decrease caused by mud displacement.

The simulation of the drill pipe's rotation involved employing a moving boundary condition at the inner cylinder and establishing a rotating fluid zone at the drill bit location. This configuration resulted in an annular flow domain characterized by a rotating inner cylinder

and a stationary outer cylinder. To evaluate the likelihood of flow instability in this configuration, the calculation of the Taylor number was employed. The Taylor number assesses the significance of centrifugal forces induced by rotation in comparison to viscous forces and is defined as follows:

$$T_a = \frac{R_1 \Omega_1^2 d^3}{\nu^2} \quad (56)$$

In the provided equation, the symbols represent the following parameters:

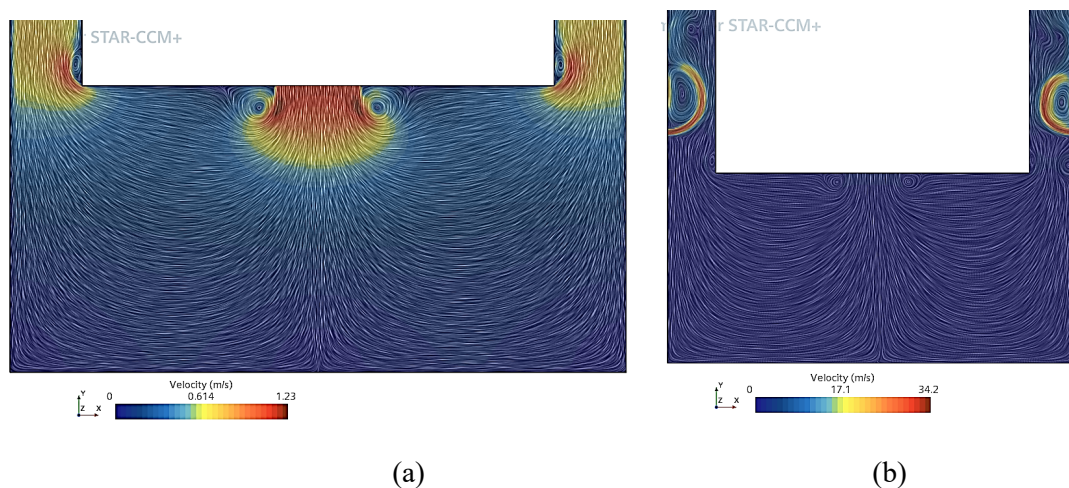
( $R_1$ ): Radius of the inner cylinder

( $\Omega_1$ ): Angular velocity of the inner cylinder

( $d$ ): Annular gap between cylinders

( $\nu$ ): Viscosity

**Fig. 6.10** provided information indicates that in the current configuration, with a drill-pipe rotation of 100 rotation per minute, with an annular space of 1 inch. The characteristics of the setup, including the high injecting flow rate, tiny annular area, low rotation rate, and high mud viscosity, act against the development of radial flow. If radial flow is desired, adjustments to these parameters would be necessary. However, It is observed that in the downhole area beneath the drill pipe, the critical Taylor number is surpassed.



**Fig. 6.10** Velocity vector with drill bit rotation 100 rpm (a) only mud, and (b) during gas kick.



#### *6.4. Modelling of Gas Dissolution*

The gas dissolution refers to the highest amount of gas that can dissolve in a fluid given particular temperature and pressure circumstances, while the bubble pressure indicates the pressure at which the gas would separate from the solution. The formation volume factor describes the volume fluctuation of saturated fluid due to dissolved gas. These properties play a crucial role in controlling the entry of formation gas into oil-based drilling muds. Research indicates that oil-based muds can dissolve higher concentrations of gas compared to water-based muds. This becomes significant considering the volumetric expansion of rising gas bubbles at greater depths. The high solubility of natural gas in oil-based drilling fluids poses challenges for gas-kick detection, especially when the gas emerges from solution and expands rapidly during ascent due to reduced pressure, a behaviour less pronounced in water-based muds with lower gas solubility.

The process of gas dissolution involves the movement of gas particles from the gas phase into the liquid solvent. This process can be conceptualized as occurring sequentially, where the gas and liquid phases initiate the procedure with their respective particles initially being spatially separated.

The initiation of the dissolving process occurs when a single gas particle (solute) separates from the gas phase without leaving a void behind. The gas particle is then transported to the phase interface, where it transitions from the gas phase to the liquid phase (solvent). Finally, it is conveyed and introduced into a void within the liquid phase.

The mass transfer rate serves as a quantitative measure for the kinetic process of dissolution and is defined as the amount of solute entering the solution per unit of time under specific parameters like temperature, pressure, phase interface, solvent composition, and flow regime.

Accurate prediction of the mass transfer rate is essential for estimating corrosion rates. Selecting the appropriate mass transfer coefficient is crucial for capturing the dynamic flow conditions during a kick event, enabling the application of mass transfer rate theory to the gas inflow scenario in a wellbore. In the vicinity of the drill bit, the unforeseen influx of formation fluid during a kick significantly influences the flow state, leading to rapid mixing of drilling mud and kick gas, thereby enhancing gas-liquid mass transfer. The computational model represents the dissolution and release of gas through an interaction of mass transfer between the liquid and gas phases. When utilizing the CFD solver STARCCM+, incorporating a mass transfer rate per unit volume involves choosing from three options: creating a user-defined function (UDF) for mass transfer rate computation, selecting a pre-built mass transfer model, or specifying a constant value.

In this model, the chosen approach involves specifying a constant value for the mass transfer rate, and this strategy has been implemented. The volumetric mass transfer rate for each computational cell is calculated and updated at every time step using a user-defined function. STARCCM+ subsequently incorporates contributions to the mass, species, and energy equations, aligning with the calculated mass transfer rate. The mass transfer rate can be expressed as:

$$\frac{dm}{dt} = kMA(C_s - C_o) \quad (57)$$

In the given equation,

**(m)** is the mass transfer rate (Kg), **(M)** molecular weight of gas (Kg/mole); **(k)** is the mass transfer coefficient (m/s), **(A)** is the interface area (m<sup>2</sup>), **(C<sub>s</sub>)** is the gas solubility (mole/m<sup>3</sup>), and **(C<sub>o</sub>)** is the concentration of dissolved gas (mole/m<sup>3</sup>).

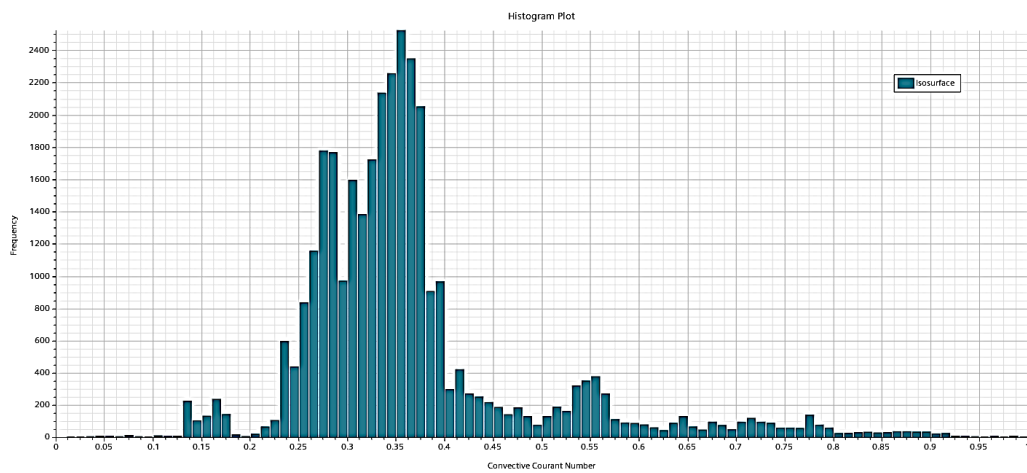
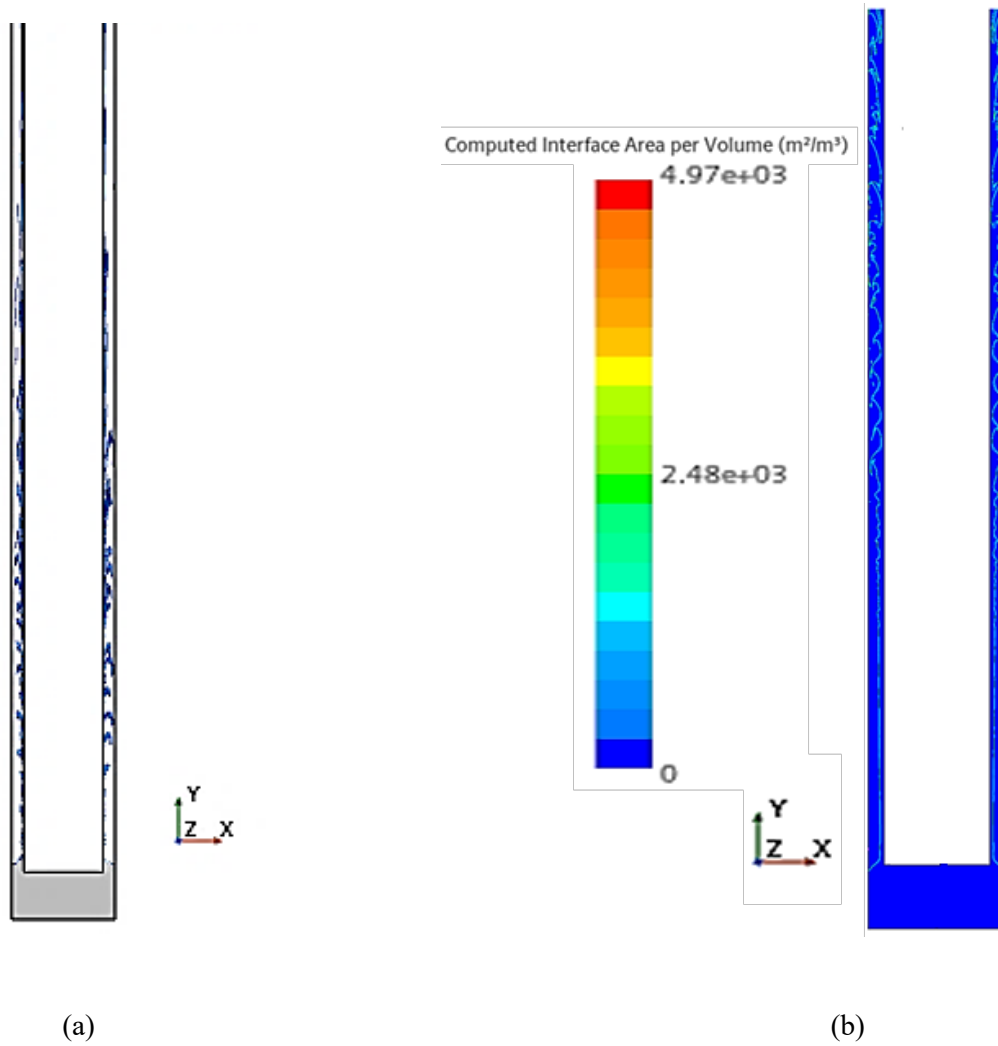
Determining the mass transfer rate necessitates accurate knowledge of the gas-liquid contact area. In dispersed flow, the dimensions of the interface area are likely to exert a more significant influence on the computed mass transfer rate compared to the selection of the mass transfer coefficient.

The challenge with the contact area lies in its inability to be precisely determined in a CFD simulation, and experimental assessment is also prone to inaccuracy. The mass transfer rate  $m$  for simulation purposes can be obtained by dividing the previously mentioned definition by the cell volume.

$$m_{gl} = kM \frac{A}{V} (C_s - C_o) \quad (58)$$

$m_{gl}$ , represents the mass transfer rate from the gas to the liquid phase ( $\text{kg}/\text{m}^3 \cdot \text{s}$ )

This equation signifies the phase interface area required per unit volume. The determined interface area was stored in a user-defined memory for this purpose, and a user-defined function was established. **Fig.6.11a** presents a typical contour plot of phase distribution in the lower third of the wellbore model, where the mud is represented in blue and the gas in white. The calculated interface area per volume is illustrated in **Fig.6.11b**, depicting the contour plot of the volume fraction gradient term, which is subsequently utilized to compute the mass transfer rate. The interface is observed to be accurately captured, and there is a notable correlation with the specific interface area plot. **Fig.6.11c** presents the Convective Courant Number (CFL) based on the isosurface between two phases, considering gas dissolution. It becomes higher at 0.45 compared to the simulation that does not take gas dissolution into account, where it is at 0.25.



(c)

**Fig. 6.11** CFD model with gas solubility (a) Phase distribution, (b) Computed interface between gas and liquid represented as Area per volume, and (c) Convective Courant Number based on isosurface between two-phases.

Updating the calculated interface area for each cell with each time step proved to be challenging, somehow. Unfortunately, the peculiarities of the simulation programme meant that there was no simple way to update this value continually. By substituting a term holding the phase indicator function gradient for the particular interface region  $A V$ , a different strategy was discovered. In essence, the interface area density is represented by the term.

$$\frac{A}{V} \alpha VOF_{grad} = \sqrt{\left[\frac{df}{dx}\right]^2 + \left[\frac{df}{dy}\right]^2} \quad (59)$$

$VOF_{grad}$       volume fraction gradient

$f$                 phase indicator function

A user-defined function makes it simple to compute and update this term on a regular basis.

In general, the computed gradient of the volume fraction is less than the estimated interface area displayed in **Fig. 6.11**. There is a factor of about 2.5 between the values, which is likely due to cell shape. Using the proportionality constant enables fitting the volume fraction gradient term to the interface region, with the highest values observed near the entrance of the gas jet, along the phase interface, and around the drill bit.

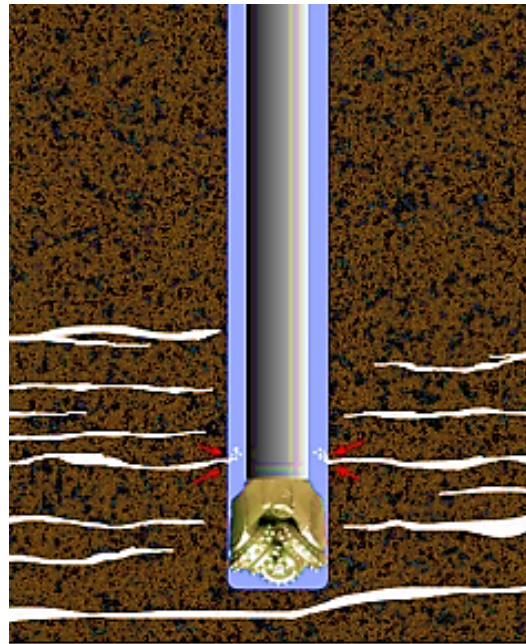
In the current simulation scenarios, the quantity of dissolved gas is negligible, resulting in minimal changes in mud characteristics. The distinction between gas solubility and dissolved gas provides the final component needed for calculating the mass transfer rate.

### *6.5. Location of Kick Entrance Sensitivity analysis*

The size and location of the entry point, where gas enters the wellbore, were found to significantly impact phase mixing and distribution. Consequently, this section will explore the outcomes of four different kick scenarios, where the opening size and position vary. Gas input ranges from small, representing a single crack, to large, simulating a cavern.

### 6.5.1. Lateral kick

As depicted in **Fig. 6.12**, the Single Fracture kick scenario involves a solitary inlet with an opening size of 0.003 meter positioned 1 inch above the drill bit (the drill bit has a height of 0.1 meter). Various simulations are conducted, with a consistent rotational speed of 100 rotation per minute for both the drill bit segment and the inner pipe in all configurations.

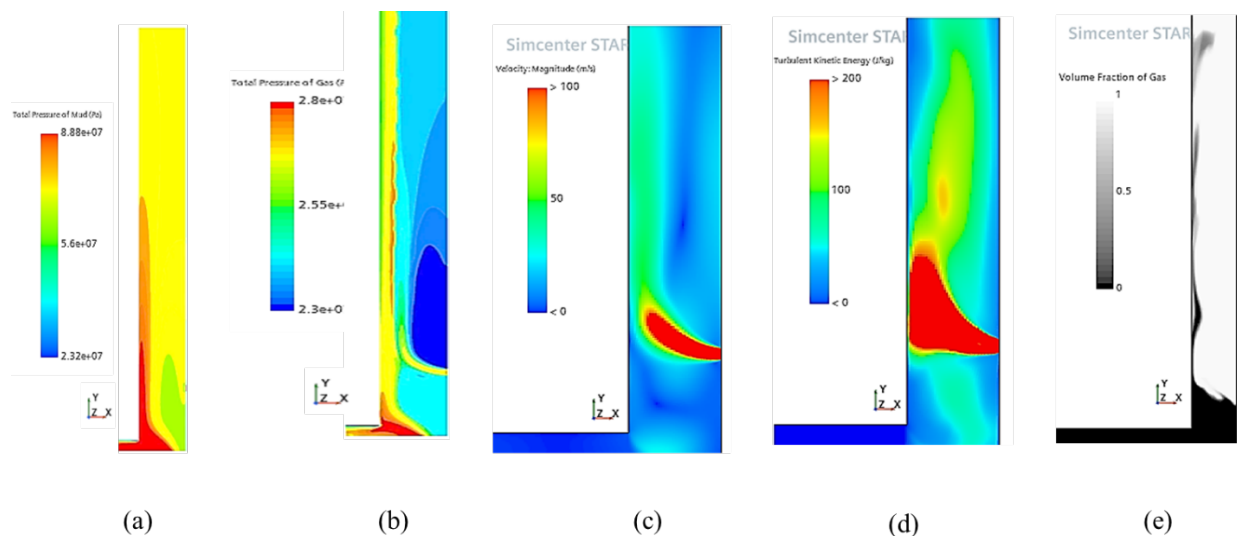


**Fig. 5.12** Single fracture model sketch.

The gas influx resembles a jet impinging perpendicularly on the continuous mud flow in the annulus in all simulated scenarios. The available cross-sectional area for the mud channel is significantly reduced, leading to an increase in mud velocity. Consequently, the mud jet points upward and is laterally impacted by the gas jet. The dominant jet formation is determined by the ratio of the driving pressure differential per fluid. For gas, the driving pressure difference is influenced by the formation pressure and wellbore pressure at the entrance spot, while the pressure gradient in the wellbore created by the pump is defined for liquid.

In certain Computational Fluid Dynamics (CFD) models, the inflow of drilling mud is specified as a constant mass flow rate, and the formation pressure is represented by a constant inflow pressure boundary for the gas. The pressure in the wellbore will naturally fluctuate based on the input of gas, continuously adjusting the flow condition until both fluids reach a balance. **Fig. 6.13a, b** illustrates the total pressure during mud circulation and the total pressure during the gas kick, respectively.

The entering gas is causing the mud to travel at a faster rate as a thin layer along the inner cylinder. A zone of lower pressure is formed just above and below the gas jet, where gas is recirculating. The gas jet's high entrance velocity is rapidly decreasing, allowing the mud jet to overtake it as the faster jet. The gas and mud velocities equalise at a given distance, smoothing out the phase boundary. **Fig. 6.13c, d** shows the contours of velocity magnitude and turbulent kinetic energy. The gas then accelerates because of buoyancy, taking over as the dominant jet. **Fig. 6.13e** showing the phase distribution through contours of gas volume fraction.



**Fig. 3** CFD model (a) Total pressure mud circulation, (b) Total pressure gas kick, (c) Contours of velocity magnitude (d) Contour of turbulent kinetic energy, and (e) Contours of gas volume fraction.

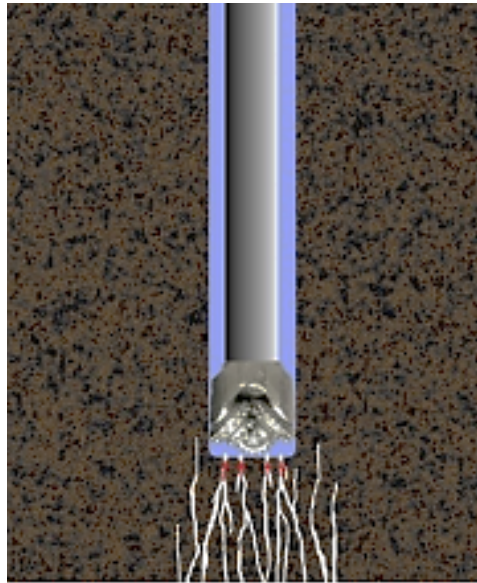
The evolution of the phase contact between the gas and mud can be analysed similarly to the breakup of a jet, though with spatial constraints imposed by the channel shape. Analogous processes occur, but the channel's form restricts their development. Parameters such as Reynolds number, which characterizes distinct breakdown possibilities of a free liquid jet, play a role in this study. In the current simulation, gas with specific momentum and buoyancy emerges from a narrow fracture and intrudes into a mud stream with different properties.

The size of the fracture entrance, density ratio of the fluids, surface tension force ratio, and viscous shear between the phases all influence the breakup of the gas jet. Disturbances rise, and waves become higher until they overturn the slower fluid. The orientation of the vortex formation indicates which of the jets dominates the flow. In simulations, it was observed how the rotational orientation of the vortices changed. For instance, the mud jet was noticeable at the tight entrance where the gas jet is introduced, followed by a segment with a relatively flat phase interface, suggesting equal phase velocities until the gas jet eventually became dominant, introducing a vortex structure at the phase interface.

#### *6.5.2. Bottom-Hole Kick Scenario – Multiple Fractures*

To simulate the scenario of multiple cracks at the wellbore bottom, two circumferential gaps with a 0.003-meter opening size are used for this kick scenario, as illustrated in **Fig.6.14**. The total inflow area is the same as in the simulated situations with a single lateral fracture. In all three simulation cases, the drill pipe and the bit section of the model are rotated at a rate of 100 rotation per minute.





**Fig. 6.14** Sketch of bottom-hole scenario with multiple fractures at the inlet model

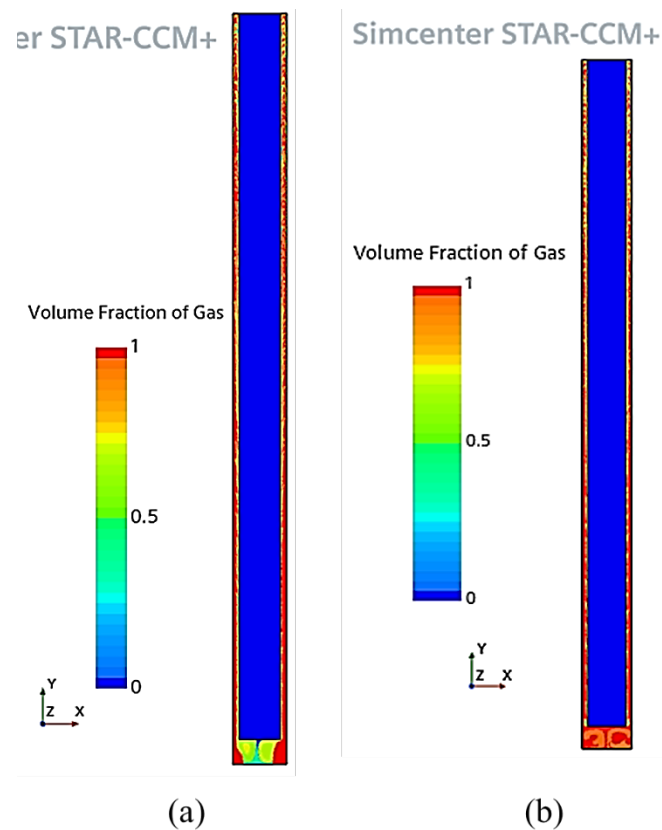
The pressure integrated along the voids in the fractures at the bottom hole prior to the kick initiation is less than the pressure at the initiation of lateral kick scenarios. As a result, the pressure differential at kick initiation is greatest in the scenario of a kick at the bottom of the wellbore. However, the gas inflow in this scenario is the least due to alterations in pressure conditions at the inflow barriers during the kick.

The mud changes its flow direction in the lateral kick situations, which causes the stagnation pressure at the gas inlet to decrease. This increases the gas influx, but the associated differences in the ultimate gas inflow rate led to various kick form. Lower flow rates occur when the gas is supplied along the wellbore bottom pores as opposed to the lateral kick scenarios. This is because there is a lot of pressure beneath the drill bit.

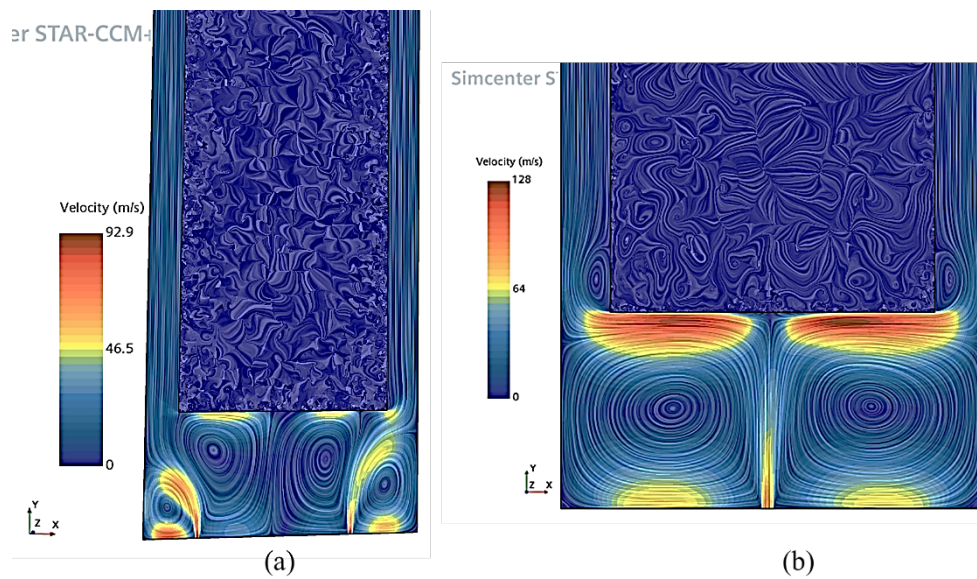
The fluid that represents the drill bit rotates, shearing off gas that enters the wellbore through the cracks. This procedure causes the phases to mix strongly and distributes the kick gas into bubbles. The injected drilling fluid is creating two big vortices that reflect the drill bit, and these bubbles are moving upward through the drill-bit zone.

Some of the gas bubbles are captured by the whirling fluid as they travel through the vortices, causing them to collide, combine, and produce bigger bubbles that are trapped in the core of the vortex. **Fig. 6.15** depicts the instantaneous phase distribution along the annulus after the flow has stabilized.

Rotating flow structures may be discovered in the bottom model area due to the intake design, as shown in **Fig. 6.16**. The centre part reveals axially sheared fluid ligaments, which indicate axial gas and mud velocity differences. The form of the gas bubbles becomes more defined in the top region of the model because of low differential fluid velocity in the channel core and higher shear near the walls.



**Fig. 6.15** Phase distribution along the annulus after the flow has stabilized (a) Injecting gas from bottom two side inlets, (b) Injecting gas from bottom one middle inlet.



**Fig. 4** Velocity distributions from scenarios with (a) Gas from bottom two inlets, (b) Gas injection from bottom one inlet.

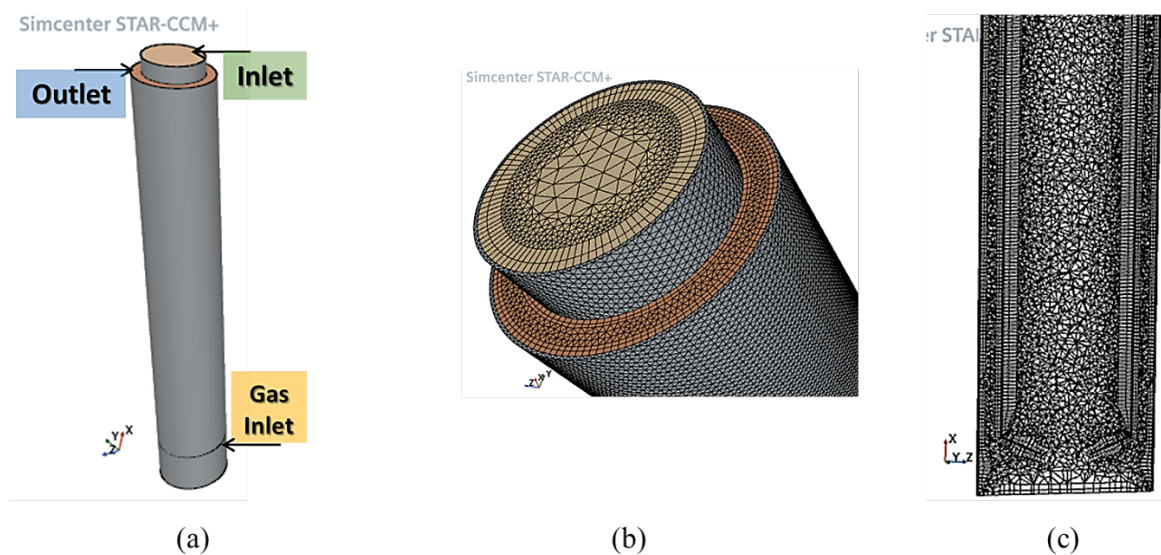
The effect of gas on the inner pipe is most at the beginning of the channel and progressively diminishes as one travels up the annulus. The gas is driven to the inner pipe by the annulus vortices before finally gathering in the channel core.

Monitoring the cross-sectional distribution of the gas after the flow has stabilized, it was discovered that the gas mud ratio along the channel walls remains rather stable, but the channel centre exhibits the greatest variations in volume fraction. Because of the annular conduit shape, the cross-sectional profiles are asymmetric; in a pipe, the profiles would be symmetric. Because the gas does not flow as a continuous stream of a bulk fluid, changes in the gas volume fraction are expected.

### 6.6. Three-dimension modelling

The three-dimensional simulation (3D-Computational-Fluid-Dynamics simulation) is the most advanced technique for extensive numerical research on any thermo-fluid dynamical topic. The given 3D-CFD models are intended to be generalizable in any fluid domain. As previously stated, these models are primarily based on empirical formulations. Aside from the

mesh impact, the general correctness of the applied 3D-CFD-models is mostly determined by the assumptions and simplifications used to represent each relevant single physical occurrence. **Fig. 6.17** show a 3-D CFD model constructed in STARCCM+, **Fig. 6.17a** show the geometry of constructed 3-D model with the Mud inlet and the position of gas kick, and the flow exit (end of the model), **Fig. 6.17b, c.** show the mesh of constructed 3-D model, and CSA mesh 3-D model used after grid independency study respectively.



**Fig. 6.17** CFD model used after grid independency study using 3-D at STARCCM+ (a) Geometry of constructed 3-D model, (b) Mesh of constructed 3-D model, and (c) CSA mesh 3-D model.

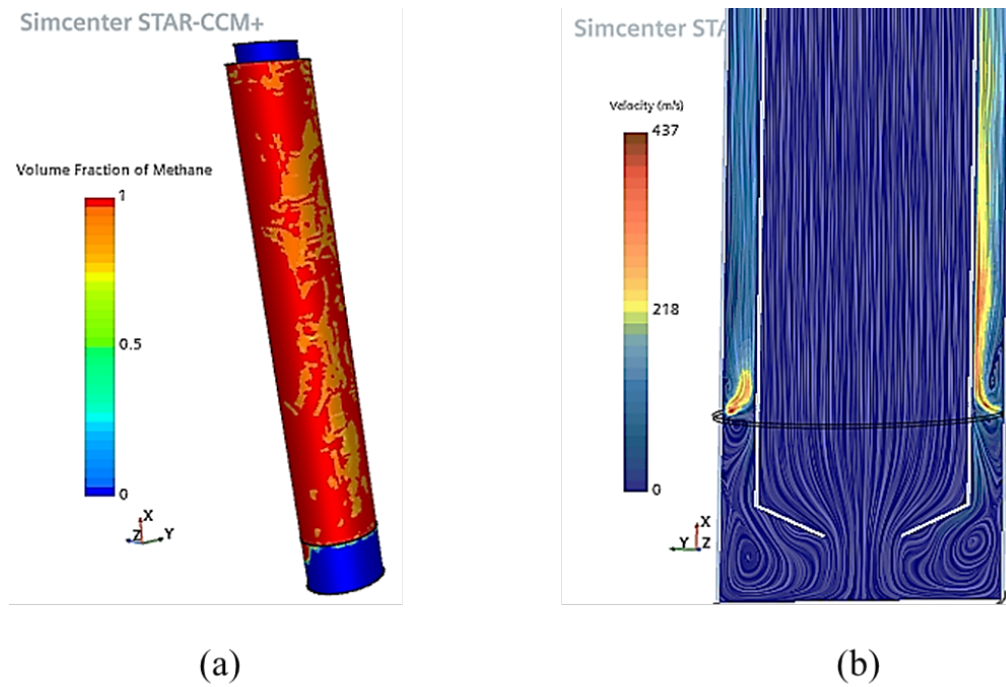
Changing from a 2D to a 3D solution could alter the results for identical geometry. The two-dimensional (2D) fluid dynamics simulation varies from the three-dimensional (3D) simulation in that the flow does not vary in the third dimension. In other words, we assume a zero or constant velocity component in the third coordinate axis. If this assumption is not valid, 3D simulation should be used. Even if the geometry is 2D, this does not guarantee that the flow is 2D. The flow can be 2D, but with a change regarding Reynolds number, it can become 3D.

The results of the 2D and 3D simulations were compared along the height of the well annulus. When the initial set of CFD simulations was compared to the actual experimental

data, it was discovered that the 2D simulation forecast did not represent the bottom dense zone at a higher circulation rate.

Meanwhile, a comparison of observed and simulated axial solid holdup distributions for increased gas velocity and liquid circulation rate indicated that the 2D simulation failed to forecast near the outlet region. Furthermore, as compared to the 3D simulation, the 2D simulation underpredicted the bottom holdup. Under secondary gas injection circumstances, 2D and 3D simulations revealed that 3D simulation predictions were more compatible with the experimentally observed particle build-up in the main zone.

Major forecast inequalities between both computing domains were detected at the bottom and top regions of the annulus, where 2D simulation significantly underpredicted the liquid holdup. Other than that, no significant difference was found between 2D and 3D simulation predictions in the fully formed (mid-section) area. To quantify the difference between the 2D and 3D simulation predictions, **Fig. 6.18** showing that the 3D simulation consistently provided good and reliable forecasts for all flow conditions. **Fig. 6.18a** showing that the phase distribution in the annulus is not having the same trend as 2-D simulations because of many factors such as rotation of drill string which reflects the reality during drilling. **Fig. 6.18b** showing asymmetry in the velocity vector during drill bit rotation as the ride side doesn't have the same velocity values as the left-hand side.



**Fig. 6.18** (3-D) model during gas kick (a) Phase distribution, (b) Velocity vector with drill bit rotation 100 rpm.

### 6.7. Turbulence models sensitivity analysis

In laminar flows, vectorial and scalar quantities have well-defined values within a space characterized by a characteristic length. Conversely, turbulent flows within the same space, defined by a characteristic length, exhibit continuous chaotic fluctuations in velocity, leading to variations in scalars such as density, temperature (T), and mixture composition. These turbulent flow fluctuations result from vortices generated by shear stresses within the flow. The growth of these vortices is determined by a dynamic interplay between nonlinear generation processes driven by the kinetic energy of the fluid and damping processes arising from viscous dissipation, which is proportional to the dynamic viscosity. The dominance of generation processes over damping processes occurs when a critical value of the Reynolds number (Re) is surpassed. This critical point marks the transition from laminar to turbulent behaviour in the flow.

The following models are available for modeling Reynolds-Averaged Navier Stokes turbulence in the multiphase mixture in STARCCM+ CFD simulator:

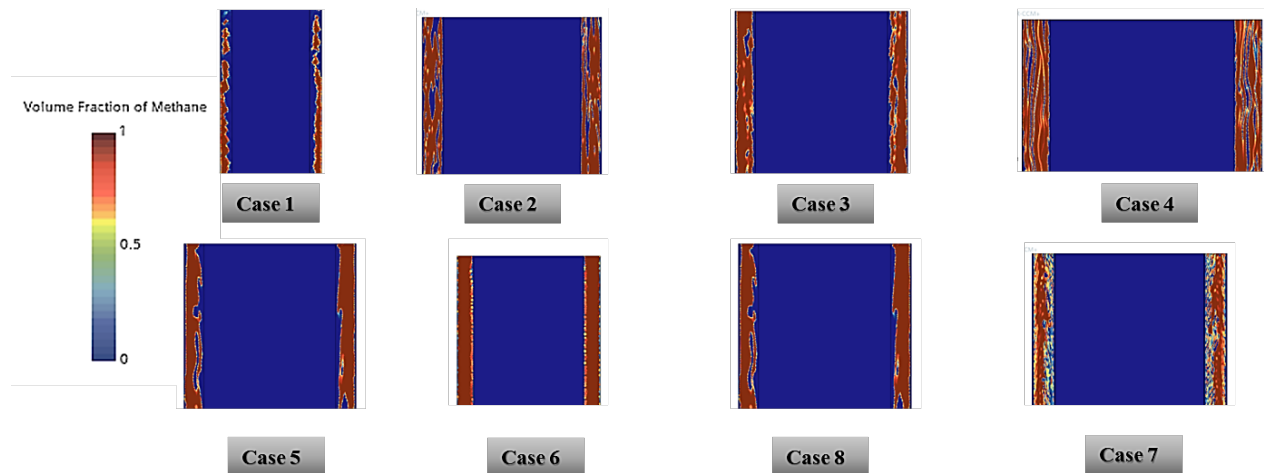
### **K-Epsilon Turbulence**

- ✓ EB K-Epsilon
- ✓ Lag EB K-Epsilon
- ✓ Realizable K-Epsilon
- ✓ Realizable K-Epsilon Two-Layer
- ✓ Standard K-Epsilon
- ✓ Standard K-Epsilon Low-Re
- ✓ Standard K-Epsilon Two-Layer
- ✓ V2F K-Epsilon

The realizable K-Epsilon Two-Layer model has proven to be most applicable for the simulation after sensitivity test based on the pressure drop, axial velocity, residuals, and Courant–Friedrichs–Lewy CFL to ensure a Courant number smaller or equal to 0.25, on the other hand models like EB K-Epsilon, Lag EB K-Epsilon, and V2F K-Epsilon did not continue till the end of the simulation (crash during running). The Standard K-Epsilon models having higher residuals during simulation running as well as producing higher (CFL) which indicate instability and loss of accuracy due to numerical errors. The realizable K-Epsilon Two-Layer model had improved performance over the Standard K-Epsilon model especially in the multiphase flow representation at boundary layers. **Table 6.2** comparing turbulence models available in STARCCM+ and other parameters used in sensitivity. **Fig.6.19**, **Fig.6.20** illustrate volume fraction of gas kick at top and bottom of model at different turbulent models respectively. **Fig.6.21** showing the residuals during simulation at different turbulent models, **Fig.6.22** demonstrating CFL results at the end of the simulation with different turbulent models.

**Table 6.2**  
Turbulence models sensitivity

File Name	Turbulence Model	Adaptive Time-Step	Multiphase Model	Gas Inlet Condition	Mud Inlet Flow rate	Gas type & Rotation	Time
1	EB K-Epsilon	<i>Convective CFL Condition (0.5)</i>	<i>Two Phase Flow Mud &amp; Gas</i>	<i>Stagnation inlet 2.339e7 pa</i>	<i>40 kg/sec</i>	<i>Ideal gas &amp; rotation</i>	<i>1 Sec</i>
2	Lag EB K-Epsilon						
3	Realizable K-Epsilon						
4	Realizable K-Epsilon Two-Layer						
5	Standard K-Epsilon						
6	Standard K-Epsilon Low-Re						
7	Standard K-Epsilon Two-Layer						
8	V2F K-Epsilon						



**Fig. 6.19** Volume fraction of gas kick at top of model at different turbulent models.



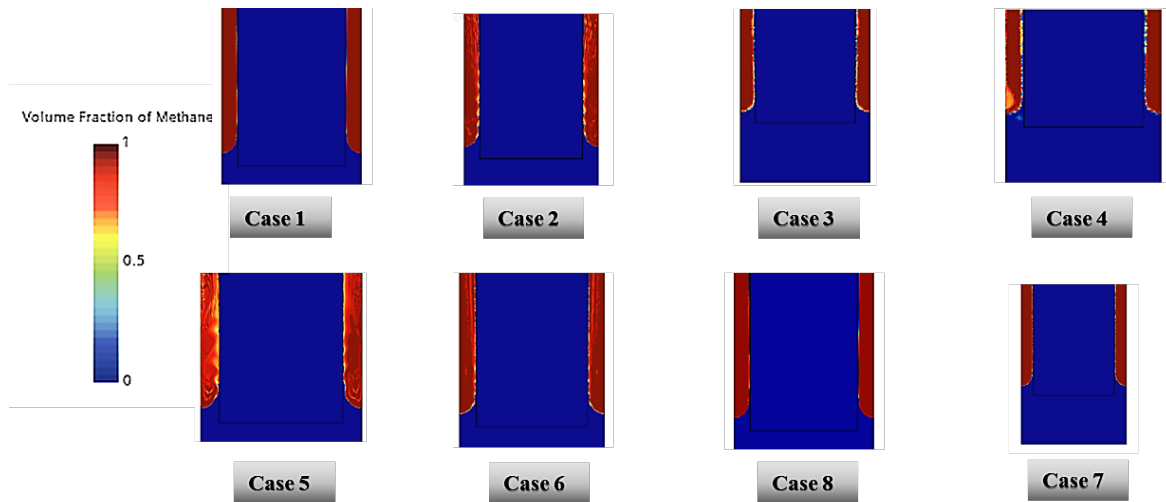


Fig. 6.20 Volume fraction of gas kick at bottom of model at different turbulent models.

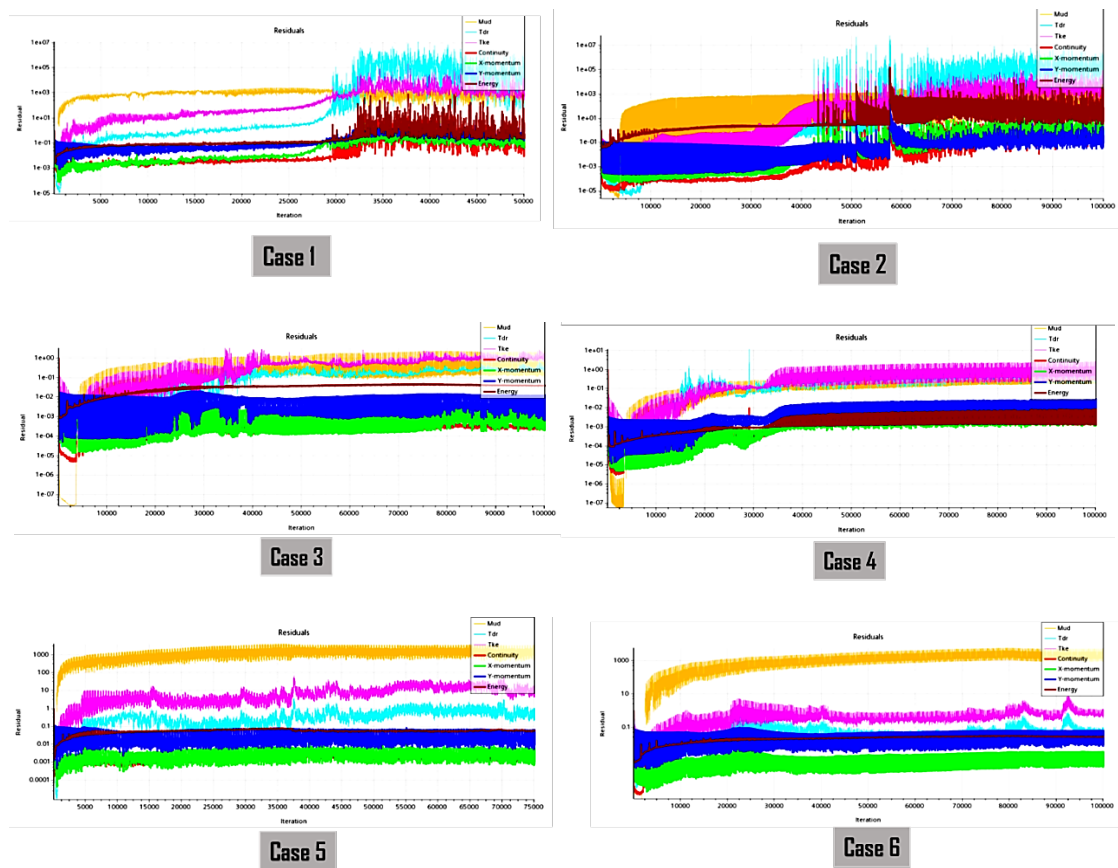


Fig. 6.21 Residuals during simulation at different turbulent models.

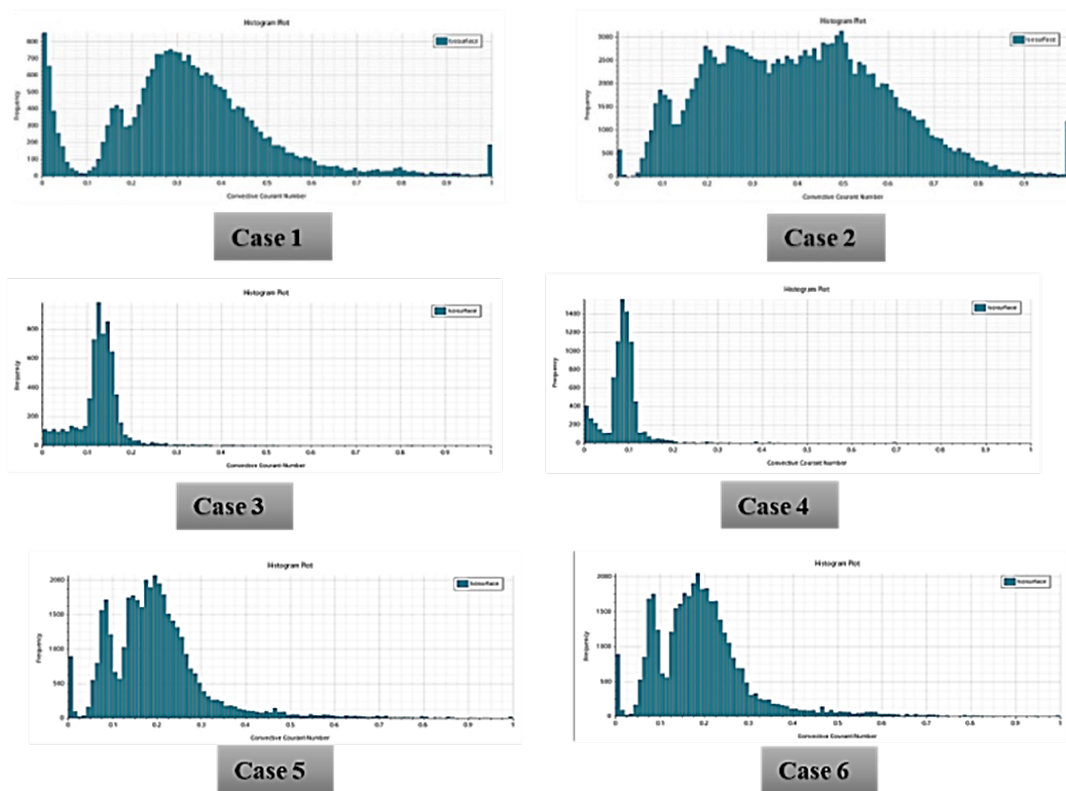


Fig. 6.22 CFL during simulation at different turbulent models (Frequency vs Courant Number).

## Brief conclusion

1. Introduction of real modelling methodology and configuration for simulating a gas-kick scenario, incorporating simplified assumptions for analysis.
2. Utilization of the Navier-Stokes solution considering non-Newtonian properties to determine the multiphase flow pattern during a gas kick.
3. In the provided configuration, characteristics like high injecting flow rate, small annular area, low rotation rate, and high mud viscosity inhibit radial flow development.
4. Negligible dissolved gas in simulations results in minimal changes in mud characteristics.
5. Entry point size and location significantly affect phase mixing.
6. Transitioning from 2D to 3D simulation can alter results.
7. Comparing 2D and 3D simulations along the well annulus height reveals discrepancies, particularly in representing the bottom dense zone at higher circulation rates.
8. The realizable K-Epsilon Two-Layer model proves most suitable, while other models like EB K-Epsilon, Lag EB K-Epsilon, and V2F K-Epsilon do not complete the simulation.

# CHAPTER 7

## Results and Discussion

### 7. Results and Discussion

In this chapter the techniques for analysing and interpreting data in the context of two-phase flow were covered in details, in addition to presenting the results of different kick scenarios.

#### *7.1. Two-Phase Flow Analysis*

Aside from model setup, boundary conditions, and beginning circumstances, the configuration of a simulation scenario for a multiphase flow issue necessitates decisions on how outcomes may be assessed, what values are typical, and where. To identify the appropriate values to monitor during computation, it is necessary to have a comprehensive knowledge of the flow problem beforehand, especially for a transient simulation.

Based on the literature parameters often utilized for two-phase flow analysis are as below:

- i. The void fraction prediction or liquid holdup is essential to the study of two-phase flow. In operations that entail the movement of mass and chemical reactions, it is the most important parameter.
- ii. Superficial phase velocity is frequently utilized as a parameter in flow pattern maps and is characterized as the volume flow rate divided by the total cross-sectional area of the tube.
- iii. The slip ratio is velocity ratio between the gas and liquid phases, which originated with the drift flux modelling technique, is frequently used to describe two-phase flow.

The distinctive flow characteristics could be expanded when adding variables that represent the fluctuations in flow over time and place, attributable to the richness of data obtained from

a transient CFD simulation. These methods aid in condensing the volume of data that may be obtained from a CFD simulation. The main objective is to condense and extract essential data that facilitates the comparison of simulated situations.

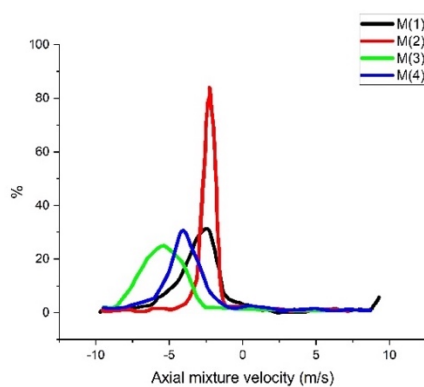
**Table 7.1**

Inlet condition for 4 compared cases.

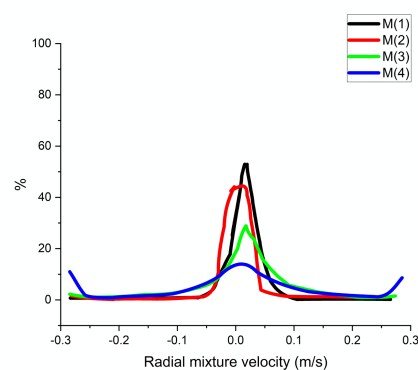
Case	Pressure at Gas Inlet	Pressure at Inlet	$\Delta p$ at kick
M (1)	2.336 E7 Pa	2.333 E7 Pa	3 E4 Pa
M (2)	2.336 E7 Pa	2.325 E7 Pa	1.1E4 Pa
M (3)	2.356 E7 Pa	2.333 E7 Pa	2.3 E4 Pa
M (4)	2.433 E7 Pa	233.3 E7 Pa	1E6 Pa

### 7.1.1. Velocity data

The velocity field predicted by the CFD simulation that models a two-phase flow using the volume of fluid approach can be examined. However, in cells that are entirely filled with a single fluid, mixing velocity can be assigned to a single phase with the aid of a high grid resolution. Examining the spatial changes in mixture velocity within the flow channel is another practical way to apply velocity data to characterize the flow. Graphs of velocity elements are therefore employed. The likelihood distribution of axial velocity may be estimated from the graphs by using time averaged mean velocity data. When flow has reached a steady state, denoted by the equilibrium of mass within the boundaries of the model, time averaging may be carried out.



(a)



(b)

**Fig. 7.1** Histogram of 4 constructed model simulating two phase flow in annulus (a) Axial mixture velocity, (b) Radial mixture velocity.

**Fig. 7.1 a** show the axial velocity histogram for each of the four simulated kick situations. Any positive velocity in the annulus indicates backward flow, whereas negative velocity accounts for upward flow. M (2) has the smallest axial velocity distribution, whereas M (3) has the widest range of axial velocities. **Fig. 7.1 b** illustrates the radial velocity distribution, which may be used to estimate the amount of radial fluid flow. Following the location of the gas influx, distinct phase segregation takes place, and the velocity of each phase deviate by twice. This leads to the broad axial velocity distribution of M (3). The velocities of the two phases have balanced, and the phases are currently distinctly differentiated after a distance equivalent to thirty times the annular clearance. From that point on, the gas phase accelerates, and the phase contact begins to erode more and more. Little ripples at the phase barrier give way to broad waves that eventually split apart to form many kinds of fluid ligaments and droplets. The gas phase's velocity rises and the mud phase's velocity falls with increasing distance from the gas entrance. There isn't any noticeable flow recirculation in this specific case. The simulation case has the most compact axial velocity distribution, where there is minimal distinction in axial velocity between the gas and mud. The pattern of the flow displays features exhibits characteristics found in both bubble/churn flow. Case M (2) in the simulation has the narrowest axial velocity distribution. Here, there is very little axial velocity difference between the gas and the mud. The flow morphology exhibits feature of both turbulent and bubble flows.

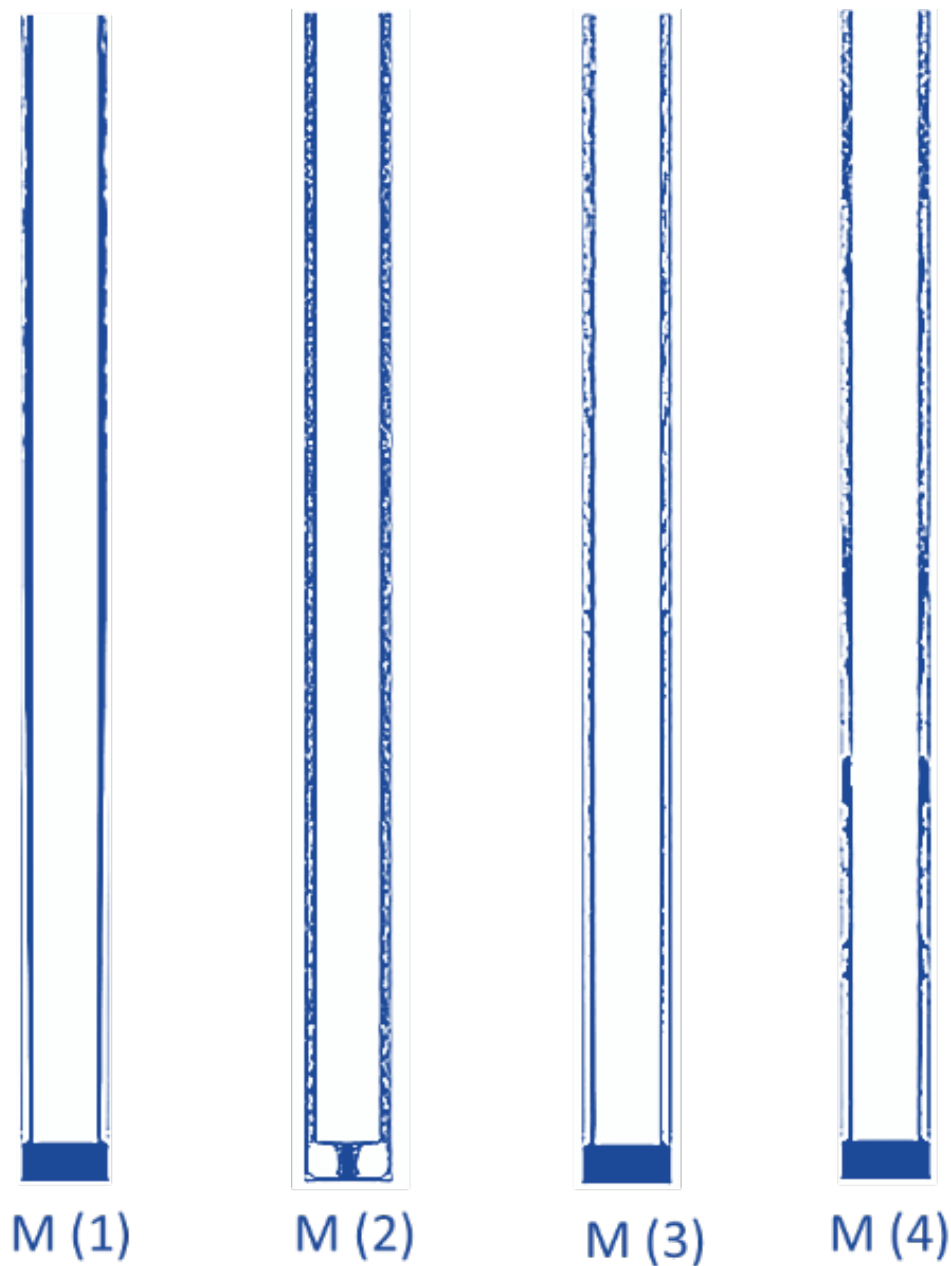
Larger bubbles moving through the annulus's core can be seen, as well as elongated fluid ligaments close to the annular walls. The slender streams of fluid serve as an indication of small bubbles of gas. that are left over when the annular channel's entry periodically produces Taylor bubbles.

The bubbles that are travelling through the core are about one-third the size of the annular gap and feature the characteristic deformed form of Taylor bubbles. The fluid structures maintain almost the same form throughout distance because of the small change in axial velocity. The broader distribution of radial values clearly signifies the rotational component in the flow. The wider variety of radial mixing velocities in **Fig. 7.1b** clearly indicates the rotating component in the flow. Simulation case M (1) shows similar behaviour like M (3). The velocities decrease when the differential pressure at the gas input decreases by around six times. The axial velocity distributions have a similar pattern. Nevertheless, in M (1), the annular channel is rotated in addition to the inner cylinder. The purpose of this configuration was to simulate the effect of stabilizers, like those seen near drill bit assemblies, which add rotational drag in comparison to smooth pipes. As seen in **Fig. 7.1b** the rotation around an axis, leads to a compact radial mixture velocity distribution because there is little fluid interaction between layers. Consequently, the phase interface's form is extremely smooth.

M (4) is the simulated scenario for the other end of the radial velocity variation. Intense interchange of radial momentum between phases takes place in this model, leading to an enlarged phase interface area and an extremely complicated phase distribution. M (2) showing that bubble flow regime has restricted radial fluid movement. The largest radial velocity dispersion is shown by the breakdown of flow in the annular phase and its shift into slug and churn flow regimes. This might also explain why fluid mechanical damage to pipe walls is strongest in flow regimes like churn and slug, as shown in research.

In conclusion, flow recirculation cells may be detected in the annulus using axial and radial velocities histograms. According to the flow regime, the profiles display common forms. As a result, flow patterns may be recognized without the need for eye inspection by using quantifiable factors. Once the flow has stabilized in the simulated channel segment, the data must be gathered. As such, the pictures don't tell us anything about how the flow changed

over time. **Fig. 7.2** shows the phase distribution of the simulated models that were described above.



**Fig. 7.2** Phase distribution of each model simulating two phase flow in annulus.

### 7.1.2. Void fraction

The void fraction, a common indicator of the transition from bubbly to slug flow, exhibits a notable influence from the gap size. The shift from bubbly to slug flow patterns is attributed



to an increased collision rate of gas bubbles, induced by the impact of channel walls on the flow's velocity profile. The formation of slugs is disrupted with a rise in gas flow rate, leading to a turbulent and oscillatory flow state. At exceedingly high gas flow rates, the flow ultimately adopts an annular configuration, featuring a gas core in the annular center and a liquid film coating on the walls. Analyzing the time series of the void fraction allows for the determination of slug frequency and provides geometric insights into flow structures. Subsequent sections of this thesis will illustrate this with an example.

The void fraction serves as a valuable tool in evaluating the adequacy of the model's grid resolution for accurately representing the morphology of two-phase flow in the current scenario. It acts as an indicator of the quality of the applied modeling approach. In most simulation scenarios, there is minimal smearing and effective phase separation, indicating that the grid resolution is satisfactory for resolving the emerging flow structures.

### *7.2. Analysis of dynamic behaviour of two-phase flow patterns in vertical wellbores during a gas kick*

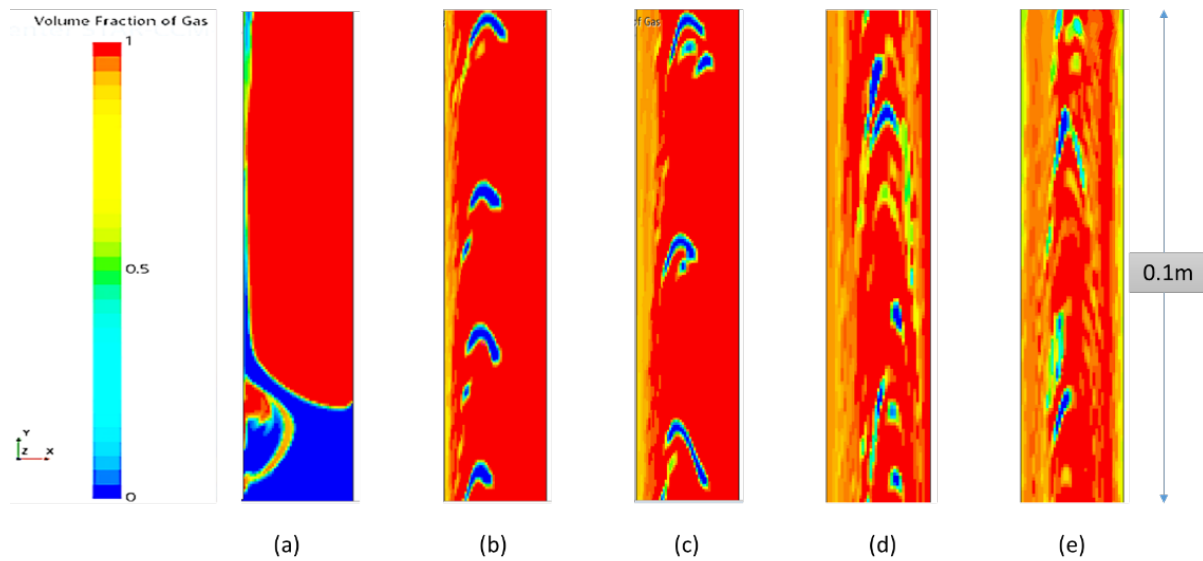
Considering the kick scenario, which is the consequence of the multiphase flow profile in which gas evolves and expands rapidly due to the reduced pressure, it is possible to perform the analysis on how quickly the kick evolves and expands occupying the annular channel. This is as such not so well monitored while the gas kick occurs and enter the annulus resulting in a blowout during the drilling operation.

**Fig. 7.3** show the phase distribution and their volume distribution for each individual segment, the wellbore measured from bottom to top in a positive direction. The colour line in the contour graphic represents the phase transition of the volume fraction in phases, with red and blue representing the gas and mud phases, respectively. Corresponding to **Fig. 7.3**, the volume fraction for each segment is shown in **Table 7.2**. A volume fraction of one represents

pure gas, while a volume fraction of zero represents pure mud, and the Volume fractions ranging from zero to one represent a mixed phase.

**Table 7.2** demonstrate the volume that each volume fraction represents for each individual segment and provide quantified details of the volume of fraction of each phase through the annulus. The proportions of gas and mud volumes, as well as the proportions of single-phase volume and transition volume, are also provided. It is shown that the gas void fraction changes with depth, in addition to the change of liquid fraction with respect to gas void fraction upward from the wellbore bottom. The liquid fraction decreases from around 25% to less than 9%, while the gas void fraction increases from 75% to reach more than 91% upward from the wellbore bottom.

The flow pattern appears to be changing from initially stratified to churn flow and eventually bubbly flow. However, the chosen model dimension is too short to cover the onset of bubbly flow, but the trend is clearly shown. First, a period from 0 to 0.2 second; the model exit did not receive any gas, but the gas flow starts to be induced by the entering gas bubbles. Second, from 0.2 to 0.35, the gas kick filled the annulus and reached the exit, and the gas became more dominant than the liquid phase (mud). At the end of the simulation (0.35 second), there is an increase in the gas phase when compared to the mud phase. The annulus is filled with gas, causing a high gas superficial velocity. Because of the gas kick, the mud obligated to move up as a thin film along the annulus; because of centrifugal forces, waves form and split at the peaks into more small fluid tendons; and the spreading of the interface between the phase increases with distance from the bottom hole. The more gas combined with the mud, the faster the fluid flow upward; as seen in a revolving motion right upper kick inlet in terms of gas velocity.



**Fig. 7.3** Comparison of volume of fraction in each contour individual segment position after the gas reach the outlet of the model (0.35 seconds).

**Table 7**

Volume of fraction analysis at each position across the annulus corresponding to **Fig.6.3**.

	(a)	(b)	(c)	(d)	(e)
<b>Segment position</b>	0.1 – 0.2 m	0.5-0.6m	1-1.1m	2-2.1m	2.9-3m
<b>Liquid fraction %</b>	Mud=25.1%	Mud=18%	Mud=13.1%	Mud=13.3%	Mud=8.8%
<b>Gas Void Fraction %</b>	Gas kick=74.9% (62.7% volume fraction1 & 12% volume fraction between 0-1)	Gas kick=82% (69.9% volume fraction1 & 12.1% volume fraction between 0-1)	Gas kick=86.9% (71.4% volume fraction1 & 15.5% volume fraction between 0-1)	Gas kick=86.7% (45.9% volume fraction1 & 40.8% volume fraction between 0-1)	Gas kick=91.2 (48.6% volume fraction1 & 42.6% volume fraction between 0-1)

The simulation results provide valuable insights into the dynamic behaviour of two-phase flow patterns in vertical wellbores during kick scenarios, shedding light on previously unexplored aspects of the process. These findings emphasize the critical role of flow rates,

well dimension, and fluid characteristics in determining these flow patterns. Notably, it was observed that as flow rates fluctuate during a kick, the two-phase flow pattern continuously evolves until a new steady state is established. Additionally, the expansion of gas due to the pressure drop along the vertical axis causes a gradual shift in the flow pattern within the wellbore. Importantly, the variation in gas velocity along the annulus, driven by gas expansion, creates transient flow conditions that disrupt the steady flow field generated by drilling fluid circulation. This unexpected influx of gas through the wellbore introduces a level of complexity, resulting in changing flow patterns both spatially and temporally. In essence, this research reveals that as wellbore depth decreases, the flow regimes transition towards annular flow, with distinct phases of flow patterns emerging in response to variations in superficial velocities. This comprehensive understanding of the evolving flow patterns during kick scenarios is crucial for enhancing well control strategies and ensuring the safety and efficiency of drilling operations in the oil and gas industry.

# CHAPTER 8

## Conclusions and recommendations for future work

### 8. Conclusion

The existing measurements and well control tools require advanced, customized modelling, and simulation software to enhance the utilization of information obtained from measurements, enabling direct control of the tools. This optimization aims to enhance the safety and cost-effectiveness of future well operations, making previously challenging operations feasible.

In the scope of this current dissertation, a meticulously validated model designed for simulating the flow of two-phase gas and liquid during the process of well drilling was developed through the application of computational fluid dynamics. The analysis carried out on the simulation data involved the consideration of gas kick solubility in drilling fluid in conjunction with advanced turbulence models and a model with dimensions of 2D and 3D, incorporating a simplified approach to multiphase flow. This examination, coupled with the consideration of a range of operational scenarios, ultimately led to the derivation of comprehensive and overarching findings:

- The evolving transformation of the flow pattern within vertical wellbores induced by the expansion of gas is a consequence of the declining pressure along the vertical axis. This gas expansion leads to a modification in the superficial gas velocity within the annulus.

- The outcomes of the simulation highlighted that the intensity of phase mixing is minimal in the vicinity of the kick inlet. Nevertheless, with an increase in distance from the entry point going upwards, the intensity of phase mixing amplifies predominantly due to the centrifugal spreading induced by the rotation of the drill pipe.
- During a kick, the pressure within the wellbore undergoes alterations, contrasting with the relatively constant fluid pressure observed in the formation. The magnitude of the gas inflow is contingent upon the variance in pressure between the pore pressure and the pressure designated for the wellbore at the kick inlet.
- The modelling approach adopted provides insights into the simulation outcomes, showcasing flow regimes with dynamic characteristics along the wellbore. Observable in the results are coherent waves resembling rings, progressing upward along the inner pipe, and ultimately bifurcating into smaller fluid tendons at their peaks.

#### *8.1. Outlook and recommendations for future work*

Subsequent research endeavours could focalize on the formulation of an all-encompassing wellbore model capable of simulating the dynamic characteristics of entire gas-kick occurrences, incorporating well control measures implemented by operators, such as the cessation of mud pumps and well closure. An improved model of this nature should also accommodate uncertainties in input parameters, enabling the application of stochastic analysis to kick events. This methodology lays the groundwork for accurate drilling calculations during well control operations.

The significance of gas solubility in oil-based muds (OBM) cannot be emphasized enough. Gas kicks in OBM are often smaller and reach the surface later, presenting challenges in timely detection. Unlike water-based muds (WBM), the pit volume in OBM does not visibly increase as the kick ascends to the surface due to the combined effects of gas solubility, pressure, and temperature on kick volume. This underscores the need for special precautions in early kick detection and flow check monitoring. Detecting a kick in OBM before dissolved gas degasses makes it more manageable, as bottom hole pressure (BHP) changes less rapidly. A proposed avenue for further exploration involves researching new methods for early detection of gas kicks in OBM before dissolved gas degassing occurs. Additionally, investigating the solubility of non-polar gases and acid gases in both OBM and WBM under specific pressure and temperature conditions could contribute to the development of a more precise calculation model.

The proposal suggests the necessity for further validation based on field data, encompassing various scenarios with diverse well geometries and mud properties, to underscore the significance of early kick detection in varying operational conditions. In general, computational fluid dynamics (CFD) simulations contribute to achieving a more profound comprehension and re-evaluation of assumptions pertaining to the flow conditions in a well undergoing a kick.

A probabilistic method is required for a suitable decision-making tool that allows assessments of the impacts of risk-reducing actions in real-time, accounting for all the uncertainties involved. A solid grasp of the underlying physical processes is necessary to perform random simulation of kick situations. With the aid of an extremely thorough CFD analysis, a step toward this basic knowledge of fluid mechanics was provided in this work.

## *8.2. Contribution to knowledge*

Upon a brief examination of the existing literature, it is evident that no prior research has presented Computational Fluid Dynamics (STARCCM+) validated model specifically addressing the transient flow subsequent to a gas kick in deep vertical wells. The study systematically illustrates the temporal evolution of the pressure profile within the annulus. Given that all parameters of the two-phase flow are intricately linked to the gas void fraction in the annulus, the mechanistic approach adopted in this research ensures a more scientific methodology when compared to empirical methods. Moreover, there is a notable absence of studies comparing two-phase liquid and gas, with the exception of investigations involving water and air.

This current study delves into the examination of the characteristics of two-phase flow within the annulus of a drilling well through the application of computational fluid dynamics. Several validation processes were conducted for single and two-phase (water-air) flow within pipes and annuli, serving as benchmarks for the reported results. Additionally, the newly acquired outcomes were systematically compared with two-phase drilling fluid and a gas kick scenario (involving methane gas) to comprehensively authenticate the reliability of the model. Consequently, this study stands as the pioneering endeavour in the realm of comparing two-phase liquid and gas flow under operational conditions through the utilization of a Computational Fluid Dynamics (STARCCM+) model.



# REFERENCES

1. Koyama, K., *2019 Global Energy Situation Indicated by BP Statistics*. 2020.
2. Augustine, C., et al. *A comparison of geothermal with oil and gas well drilling costs*. 2006. Curran Associates Inc New York, New York.
3. Paula, R.R., P.R. Ribeiro, and O.L.A. Santos. *HPHT drilling—new frontiers for well safety*. 2009 . SPE.
4. Shadravan, A. and M. Amani, *HPHT 101-What petroleum engineers and geoscientists should know about high pressure high temperature wells environment*. Energy Science and Technology, 2012. **4**(2): p. 36-60.
5. Yang, H., et al., *A new method for early gas kick detection based on the consistencies and differences of bottomhole pressures at two measured points*. Journal of Petroleum Science and Engineering, 2019. **176**: p. 1095-1105.
6. Huque, M.M., et al., *Kick detection and remedial action in managed pressure drilling: a review*. SN Applied Sciences, 2020. **2**: p. 1-29.
7. Elmore, R.J., G.H. Medley, and R.C. Goodwin. *MPD techniques optimize HPHT well control*. 2014. SPE.
8. Grace, R.D., *Blowout and well control handbook*. 2017: Gulf Professional Publishing.
9. J, A., et al., *Characterization of Dynamic Pressure Response in Vertical Two Phase Flow*. Journal of Petroleum & Environmental Biotechnology, 2017. **08**.
10. Brakel, J.D., et al., *SMART kick detection: First step on the well-control automation journey*. SPE Drilling & Completion, 2015. **30**(03): p. 233-242.
11. Grace, R.D., et al., *Blowout and well control handbook*. Blowout and Well Control Handbook, 2003: p. 1-469.
12. Raap, C., A.D. Craig, and R. Graham. *Drill pipe dynamic measurements provide valuable insight into drill string dysfunctions*. 2011. SPE.
13. Pinkston, F.W.M. and P.B. Flemings, *Overpressure at the Macondo Well and its impact on the Deepwater Horizon blowout*. Scientific reports, 2019. **9**(1): p. 7047.
14. Pouryoussefi, S.M. and Y. Zhang, *Identification of two-phase water–air flow patterns in a vertical pipe using fuzzy logic and genetic algorithm*. Applied Thermal Engineering, 2015. **85**: p. 195-206.
15. Hossain, M.E., *Fundamentals of Drilling Engineering: MCQs and Workout Examples for Beginners and Engineers*. 2016: John Wiley & Sons.
16. Jahanpeyma, Y. and S. Jamshidi, *Two-phase Simulation of Well Control Methods for Gas Kicks in Case of Water and Oil-based Muds*. Journal of Petroleum Science and Technology, 2018. **8**(4): p. 34.
17. Yamoah, S., et al., *Numerical investigation of models for drag, lift, wall lubrication and turbulent dispersion forces for the simulation of gas–liquid two-phase flow*. Chemical Engineering Research and Design, 2015. **98**: p. 17-35.
18. Burlutskii, E., *CFD study of oil-in-water two-phase flow in horizontal and vertical pipes*. Journal of Petroleum Science and Engineering, 2018. **162**: p. 524-531.
19. Hewitt, G.F., *Measurement of two phase flow parameters*. Nasa Sti/recon Technical Report A, 1978. **79**: p. 47262.
20. Sun, B., *Multiphase Flow in Oil and Gas Well Drilling*. 2016: John Wiley & Sons.
21. Ban, S., W. Pao, and M.S. Nasif, *Numerical simulation of two-phase flow regime in horizontal pipeline and its validation*. International Journal of Numerical Methods for Heat & Fluid Flow, 2018. **28**(6): p. 1279-1314.

22. Ma, Z., et al. *Multi-phase well control analysis during managed pressure drilling operations*. 2016. SPE.
23. White, E.T. and R.H. Beardmore, *The velocity of rise of single cylindrical air bubbles through liquids contained in vertical tubes*. Chemical Engineering Science, 1962. **17**(5): p. 351-361.
24. Taha, T. and Z.F. Cui, *CFD modelling of slug flow inside square capillaries*. Chemical Engineering Science, 2006. **61**(2): p. 665-675.
25. Ahmed, M.A., O.A. Hegab, and A. Sabry, *Early detection enhancement of the kick and near-balance drilling using mud logging warning sign*. Egyptian journal of basic and applied sciences, 2016. **3**(1): p. 85-93.
26. Rehman, S.R., et al., *Experimental investigation of volume fraction in an annulus using electrical resistance tomography*. SPE Journal, 2019. **24**(05): p. 1947-1956.
27. Zahid, A.A., et al., *Experimental investigation of multiphase flow behavior in drilling annuli using high speed visualization technique*. Frontiers in Energy, 2020. **14**: p. 635-643.
28. Pournazari, P., et al. *Enhanced kick detection with low-cost rig sensors through automated pattern recognition and real-time sensor calibration*. 2015. SPE.
29. Kocamustafaogullari, G. and Z. Wang, *An experimental study on local interfacial parameters in a horizontal bubbly two-phase flow*. International journal of multiphase flow, 1991. **17**(5): p. 553-572.
30. Sleiti, A.K., et al., *Early gas kick detection in vertical wells via transient multiphase flow modelling: A review*. Journal of Natural Gas Science and Engineering, 2020. **80**: p. 103391.
31. Sutkar, V.S., et al., *CFD-DEM model for coupled heat and mass transfer in a spout fluidized bed with liquid injection*. Chemical Engineering Journal, 2016. **288**: p. 185-197.
32. Guo, R., et al. *Numerical and experimental investigations of gas kick migration during casing while drilling*. 2017. SPE.
33. Jones, W.P. and B. Launder, *The calculation of low-Reynolds-number phenomena with a two-equation model of turbulence*. International Journal of Heat and Mass Transfer, 1973. **16**(6): p. 1119-1130.
34. Rodi, W. *Experience with two-layer models combining the k-epsilon model with a one-equation model near the wall*. 1991.
35. Kiran, R., R. Ahmed, and S. Salehi, *Experiments and CFD modelling for two phase flow in a vertical annulus*. Chemical Engineering Research and Design, 2020. **153**: p. 201-211.
36. Aarsnes, U.J.F., *Modeling of two-phase flow for estimation and control of drilling operations*. 2016.
37. Pilliod Jr, J.E. and E.G. Puckett, *Second-order accurate volume-of-fluid algorithms for tracking material interfaces*. Journal of Computational Physics, 2004. **199**(2): p. 465-502.
38. Sun, B., et al., *Multiphase flow modeling of gas intrusion in oil-based drilling mud*. Journal of Petroleum Science and Engineering, 2019. **174**: p. 1142-1151.
39. Sun, S., et al., *Research on gas bubble formation using CFD during gas kick*. Integrated Ferroelectrics, 2019. **199**(1): p. 179-192.
40. Waclawczyk, T. and T. Koronowicz, *Modeling of the flow in systems of immiscible fluids using Volume of Fluid method with CICSAM scheme*. Turbulence, 2005. **8**: p. 267-276.
41. Taitel, Y. and A.E. Dukler, *A model for predicting flow regime transitions in horizontal and near horizontal gas-liquid flow*. AIChE journal, 1976. **22**(1): p. 47-55.
42. Caetano, E.F., O. Shoham, and J.P. Brill, *Upward vertical two-phase flow through an annulus—Part II: Modeling bubble, slug, and annular flow*. 1992.
43. Ozar, B., et al., *Flow structure of gas-liquid two-phase flow in an annulus*. Chemical engineering science, 2008. **63**(15): p. 3998-4011.
44. Fjelde, K.K. and K.H. Karlsen, *High-resolution hybrid primitive-conservative upwind schemes for the drift flux model*. Computers & fluids, 2002. **31**(3): p. 335-367.
45. Solem, S., P. Aursand, and T. Flåtten, *The dispersive wave dynamics of a two-phase flow relaxation model*. ESAIM: Mathematical Modelling and Numerical Analysis, 2015. **49**(2): p. 601-619.

46. Stewart, H.B. and B. Wendroff, *Two-phase flow: models and methods*. Journal of Computational Physics, 1984. **56**(3): p. 363-409.
47. Shirdel, M. and K. Sepehrnoori, *Development of a transient mechanistic two-phase flow model for wellbores*. SPE Journal, 2012. **17**(03): p. 942-955.
48. Zuber, N. and J.A. Findlay, *Average volumetric concentration in two-phase flow systems*. 1965.
49. Wallis, G.B. and O.-D.T.-P. Flow, *McGraw-Hill*. New York, 1969. **265**.
50. Ishii, M. and K. Mishima, *Two-fluid model and hydrodynamic constitutive relations*. Nuclear Engineering and design, 1984. **82**(2-3): p. 107-126.
51. Rommetveit, R. and A. Blyberg, *Simulation of gas kicks during oil well drilling*. 1989.
52. Gavriluk, S.L. and J. Fabre, *Lagrangian coordinates for a drift-flux model of a gas-liquid mixture*. International journal of multiphase flow, 1996. **22**(3): p. 453-460.
53. Shi, H., et al., *Drift-flux modeling of two-phase flow in wellbores*. Spe Journal, 2005. **10**(01): p. 24-33.
54. Nickens, H.V., *A dynamic computer model of a kicking well*. SPE Drilling engineering, 1987. **2**(02): p. 159-173.
55. Podio, A.L. and A.P. Yang. *Well control simulator for IBM personal computer*. 1986. SPE.
56. Rommetveit, R. and E.H. Vefring. *Comparison of results from an advanced gas kick simulator with surface and downhole data from full scale gas kick experiments in an inclined well*. 1991. SPE.
57. Avelar, C.S., P.R. Ribeiro, and K. Sepehrnoori, *Deepwater gas kick simulation*. Journal of Petroleum Science and Engineering, 2009. **67**(1-2): p. 13-22.
58. Udegbumam, J.E., et al. *A simple transient flow model for mpd and ubd applications*. 2014. OnePetro.
59. Taitel, Y., O. Shoham, and J.P. Brill, *Simplified transient solution and simulation of two-phase flow in pipelines*. Chemical engineering science, 1989. **44**(6): p. 1353-1359.
60. Masella, J.M., et al., *Transient simulation of two-phase flows in pipes*. International Journal of Multiphase Flow, 1998. **24**(5): p. 739-755.
61. Choi, J., et al., *Development of a fast transient simulator for gas-liquid two-phase flow in pipes*. Journal of Petroleum science and engineering, 2013. **102**: p. 27-35.
62. Aarsnes, U.J.F., et al. *A simplified gas-liquid flow model for kick mitigation and control during drilling operations*. 2015. American Society of Mechanical Engineers.
63. Aarsnes, U.J.F., et al., *A simplified two-phase flow model using a quasi-equilibrium momentum balance*. International Journal of Multiphase Flow, 2016. **83**: p. 77-85.
64. Drew, D.A., *Averaged field equations for two-phase media*. Studies in Applied Mathematics, 1971. **50**(2): p. 133-166.
65. Ishii, M., *Thermo-fluid dynamic theory of two-phase flow*. NASA Sti/recon Technical Report A, 1975. **75**: p. 29657.
66. Ishii, M. and T. Hibiki, *Thermo-fluid dynamics of two-phase flow*. 2010: Springer Science & Business Media.
67. Bendiksen, O. *A new approach to computational aeroelasticity*. 1991.
68. Ishii, M., *One-dimensional drift-flux model and constitutive equations for relative motion between phases in various two-phase flow regimes*. 1977, Argonne National Lab., Ill.(USA).
69. Ekambara, K., et al., *CFD simulation of bubbly two-phase flow in horizontal pipes*. Chemical Engineering Journal, 2008. **144**(2): p. 277-288.
70. Ahmad, M.S., *CFD Simulation of Bubbly Two Phase Flow in Horizontal Pipes*. Bachelor of Chemical Engineering Thesis, 2009.
71. Xie, J., et al., *Numerical simulation of gas-liquid-solid three-phase flow in deep wells*. Advances in Mechanical Engineering, 2013. **5**: p. 951298.
72. Qi, F.S., et al., *Classification of bubbles in vertical gas-liquid flow: Part 1—An analysis of experimental data*. International journal of multiphase flow, 2012. **39**: p. 121-134.

73. Cheung, S.C.P., et al., *Classification of bubbles in vertical gas–liquid flow: part 2—a model evaluation*. International journal of multiphase flow, 2012. **39**: p. 135-147.
74. De Schepper, S.C.K., G.J. Heynderickx, and G.B. Marin, *CFD modeling of all gas–liquid and vapor–liquid flow regimes predicted by the Baker chart*. Chemical Engineering Journal, 2008. **138**(1-3): p. 349-357.
75. Yin, Q., et al. *Intelligent Early Kick Detection in Ultra-Deepwater High-Temperature High-Pressure (HPHT) Wells Based on Big Data Technology*. 2019. ISOPE.
76. Amin, A., et al., *Nonlinear model predictive control of a Hammerstein Weiner model based experimental managed pressure drilling setup*. ISA transactions, 2019. **88**: p. 225-232.
77. Rahman, M. and S. Imtiaz, *Characterization of Dynamic Pressure Response in Vertical Two Phase Flow*. Journal of Petroleum & Environmental Biotechnology, 2017: p. 08.
78. Mao, L., et al., *Dynamical simulation of high-pressure gas kick in ultra-deepwater riserless drilling*. Journal of Energy Resources Technology, 2021. **143**(6): p. 063001.
79. Sun, B., et al., *Effects of phase transition on gas kick migration in deepwater horizontal drilling*. Journal of Natural Gas Science and Engineering, 2017. **46**: p. 710-729.
80. Xu, Z., et al., *Gas kick simulation in oil-based drilling fluids with the gas solubility effect during high-temperature and high-pressure well drilling*. Applied Thermal Engineering, 2019. **149**: p. 1080-1097.
81. Toskey, E.D. *Kick detection at the subsea mudline*. 2015. OTC.
82. Nguyen, D. and S.S. Rahman, *A three-layer hydraulic program for effective cuttings transport and hole cleaning in highly deviated and horizontal wells*. SPE Drilling & Completion, 1998. **13**(03): p. 182-189.
83. Sorgun, M. and M.E. Ozbayoglu, *Predicting frictional pressure loss during horizontal drilling for non-Newtonian fluids*. Energy Sources, Part A: Recovery, Utilization, and Environmental Effects, 2011. **33**(7): p. 631-640.
84. Fjelde, K.K., et al. *Improvements in dynamic modeling of underbalanced drilling*. 2003. OnePetro.
85. Zhou, J., et al., *Switched control for pressure regulation and kick attenuation in a managed pressure drilling system*. IEEE Transactions on Control Systems Technology, 2010. **19**(2): p. 337-350.
86. O'Bryan, P.L., et al., *An experimental study of gas solubility in oil-based drilling fluids*. SPE drilling engineering, 1988. **3**(01): p. 33-42.
87. White, D.B. and I.C. Walton. *A Computer Model for kicks in Water-and oil-based muds*. 1990. SPE.
88. Podryabinkin, E., et al. *Detailed modeling of drilling fluid flow in a wellbore annulus while drilling*. 2013. American Society of Mechanical Engineers.
89. Loyseau, X.F., P.G. Verdin, and L.D. Brown, *Scale-up and turbulence modelling in pipes*. Journal of Petroleum Science and Engineering, 2018. **162**: p. 1-11.
90. Lote, D.A., V. Vinod, and A.W. Patwardhan, *Computational fluid dynamics simulations of the air–water two-phase vertically upward bubbly flow in pipes*. Industrial & Engineering Chemistry Research, 2018. **57**(31): p. 10609-10627.
91. Spoerker, H.F., C. Gruber, and W. Brandstaetter. *Dynamic modelling of gas distribution in the wellbore during kick situations*. 2012. OnePetro.
92. Sultan, R.A., et al., *CFD and experimental approach on three phase gas-liquid-solid Newtonian fluid flow in horizontal pipes*. International Journal of Computational Methods and Experimental Measurements, 2018. **7**(1): p. 33-44.
93. Sultan, R.A., et al., *Validation of CFD model of multiphase flow through pipeline and annular geometries*. Particulate Science and Technology, 2019. **37**(6): p. 685-697.
94. Sultan, R.A., et al., *CFD analysis of pressure losses and deposition velocities in horizontal annuli*. International Journal of Chemical Engineering, 2019. **2019**.
95. Sleiti, A., M. Salehi, and S. Idem, *Detailed velocity profiles in close-coupled elbows—Measurements and computational fluid dynamics predictions (RP-1682)*. Science and Technology for the Built Environment, 2017. **23**(8): p. 1212-1223.

96. Bacon, W., et al. *An improved dynamic well control response to a gas influx in managed pressure drilling operations*. 2012. SPE.
97. Denney, D., *Dynamic Well-Control Response to Gas Influx in Managed-Pressure Drilling*. Journal of Petroleum Technology, 2013. **65**(01): p. 111-114.
98. Lage, A.C.V.M. and R.W. Time. *Mechanistic model for upward two-phase flow in annuli*. 2000. SPE.
99. Ambrus, A., et al. *A simplified transient multi-phase model for automated well control applications*. 2015. IPTC.
100. Nygaard, G. and G. Nævdal. *Modelling two-phase flow for control design in oil well drilling*. 2005. IEEE.
101. Kaasa, G.-O., et al., *Simplified hydraulics model used for intelligent estimation of downhole pressure for a managed-pressure-drilling control system*. SPE Drilling & Completion, 2012. **27**(01): p. 127-138.
102. Hauge, E., et al., *A novel model-based scheme for kick and loss mitigation during drilling*. Journal of Process Control, 2013. **23**(4): p. 463-472.
103. Xu, Y., Z. Guan, and W. Chen. *Methods of early gas kick detection and well control risk assessment in deepwater drilling*. 2018. SPE.
104. Petersen, J., et al. *A general dynamic model for single and multi-phase flow operations during drilling, completion, well control and intervention*. 2008. SPE.
105. Ghobadpouri, S., E. Hajidavalloo, and A.R. Noghrehabadi, *Modeling and simulation of gas-liquid-solid three-phase flow in under-balanced drilling operation*. Journal of Petroleum Science and Engineering, 2017. **156**: p. 348-355.
106. Dabiri Atashbeyk, M., K. Shahbazi, and M. Fattahi, *Pressure profile estimation through CFD in UBD operation considering with influx to wellbore*. Iranian Journal of Chemistry and Chemical Engineering (IJCCE), 2018. **37**(6): p. 271-283.
107. Liao, Y., et al., *Wellhead backpressure control strategies and outflow response characteristics for gas kick during managed pressure drilling*. Journal of Natural Gas Science and Engineering, 2020. **75**: p. 103164.
108. Vajargah, A.K. and E. van Oort, *Early kick detection and well control decision-making for managed pressure drilling automation*. Journal of Natural Gas Science and Engineering, 2015. **27**: p. 354-366.
109. Thiago, P.d., et al. *Bridging the gap between MPD and Well Control*. 2016. OnePetro.
110. Quoc, B.T., et al. *A Well Control Approach with Managed Pressure Drilling MPD on HPHT Wells in Vietnam-Case History*. 2016. SPE.
111. Ma, Z., et al. *Gas kicks in non-aqueous drilling fluids: a well control challenge*. 2018. OnePetro.
112. Patrício, R.V., et al., *Dynamic gas kick regulation through control reconfiguration under MPD scenario—Two-phase flow validation*. Journal of Petroleum Science and Engineering, 2019. **172**: p. 806-818.
113. Chen, X., et al., *Early gas kick detection-inversion-control integrated system: The significance of applications of managed pressure drilling: A review*. Geoenergy Science and Engineering, 2023: p. 212134.
114. Khezrian, M., E. Hajidavalloo, and Y. Shekari, *Modeling and simulation of under-balanced drilling operation using two-fluid model of two-phase flow*. Chemical Engineering Research and Design, 2015. **93**: p. 30-37.
115. An, J., K. Lee, and J. Choe. *Well control simulation model of oil-based muds for HPHT wells*. 2015. SPE.
116. Linga, H., A. Torsvik, and A. Saasen. *Kick detection capability of oil-based muds in well control situations*. 2016. OnePetro.
117. Chen, X., et al. *Well Control for Offshore High-Pressure/High-Temperature Highly Deviated Gas Wells Drilling: How to Determine the Kick Tolerance?* 2018. SPE.
118. O'Bryan, P.L. and A.T. Bourgoyne, *Methods for handling drilled gas in oil-based drilling fluids*. SPE drilling engineering, 1989. **4**(03): p. 237-246.

119. Omrani, A.E., M.A. Franchek, and Y. Tang. *BOP pressure and flowrate conditions during high pressure gas kick control*. 2019. OTC.
120. He, H., et al., *A constitutive model for predicting the solubility of gases in water at high temperature and pressure*. Journal of Petroleum Science and Engineering, 2020. **192**: p. 107337.
121. Sun, B., et al., *Multiphase flow behavior for acid-gas mixture and drilling fluid flow in vertical wellbore*. Journal of Petroleum Science and Engineering, 2018. **165**: p. 388-396.
122. Noh, W. and P. Woodward. *Simple line interface method*. 1976.
123. Skudarnov, P.V., C.X. Lin, and M.A. Ebadian, *Double-species slurry flow in a horizontal pipeline*. J. Fluids Eng., 2004. **126**(1): p. 125-132.
124. Kelessidis, V.C., P. Dalamarinis, and R. Maglione, *Experimental study and predictions of pressure losses of fluids modeled as Herschel–Bulkley in concentric and eccentric annuli in laminar, transitional and turbulent flows*. Journal of Petroleum Science and Engineering, 2011. **77**(3): p. 305-312.
125. Kocamustafaogullari, G. and W.D. Huang, *Internal structure and interfacial velocity development for bubbly two-phase flow*. Nuclear Engineering and Design, 1994. **151**(1): p. 79-101.
126. Iskandrani, A. and G. Kojasoy, *Local void fraction and velocity field description in horizontal bubbly flow*. Nuclear Engineering and Design, 2001. **204**(1): p. 117-128.
127. Dewangan, S.K. and S.L. Sinha, *Exploring the hole cleaning parameters of horizontal wellbore using two-phase Eulerian CFD approach*. The Journal of Computational Multiphase Flows, 2016. **8**(1): p. 15-39.
128. Chen, L., et al., *CFD simulation of coal-water slurry flowing in horizontal pipelines*. Korean journal of chemical engineering, 2009. **26**: p. 1144-1154.
129. Gopaliya, M.K. and D.R. Kaushal, *Modeling of sand-water slurry flow through horizontal pipe using CFD*. Journal of Hydrology and Hydromechanics, 2016. **64**(3): p. 261.
130. Goel, S., et al., *Horizons of modern molecular dynamics simulation in digitalized solid freeform fabrication with advanced materials*. Materials Today Chemistry, 2020. **18**: p. 100356.
131. Spoerker, H.F., C. Gruber, and W. Brandstaetter. *Dynamic Modelling of Gas Distribution in the Wellbore During Kick Situations*. in *IADC/SPE Drilling Conference and Exhibition*. 2012.
132. Zhang, J.J., *Applied petroleum geomechanics*. Vol. 1. 2019: Gulf Professional Publishing Houston, TX, USA.